

NPS ARCHIVE
1961
PORTER, W.

PRESSURE DISTRIBUTIONS, ADDED-MASS, AND
DAMPING COEFFICIENTS FOR CYLINDERS
OSCILLATING IN A FREE SURFACE.

William Robert Porter

thesis
748

Library
U. S. Naval Postgraduate School
Monterey, California



Pressure Distributions, Added-Mass, and Damping Coefficients
for Cylinders Oscillating in a Free Surface

By

William Robert Porter

B.S. (United States Naval Academy) 1946
B.S. (Massachusetts Institute of Technology) 1948
M.S. (Massachusetts Institute of Technology) 1954
Nav. E. (Massachusetts Institute of Technology) 1955

DISSERTATION

Submitted in partial satisfaction of the requirements for the degree of

DOCTOR OF PHILOSOPHY

in

Engineering Science

in the

GRADUATE DIVISION

of the

UNIVERSITY OF CALIFORNIA

[Berkeley, Calif.]

Approved:

J. V. Wehausen
.....
J. R. Paulling
.....
E. Pinney
.....

Committee in Charge

Deposited in the University Library.....

Date

Librarian

AS AFFATIVE

961

ORTER, W.

~~THIS~~
~~P-148~~
~~C. 11~~

ABSTRACT

Pressure Distributions, Added-Mass, and Damping Coefficients for Cylinders Oscillating in a Free Surface

A linearized theory is developed for the pressure distributions, added-mass and damping coefficients for horizontal cylinders oscillating vertically with small amplitude while semi-immersed in the free surface of a fluid of uniform depth. The results of sample calculations made by digital computer are presented. The calculations of the pressure distribution and the total vertical force for the case of a circular cylinder in fluid of infinite depth are compared with values measured in an experiment.

The problem is formulated as a linearized boundary-value problem in the theory of infinitesimal surface waves. A velocity potential is synthesized from appropriate functions. The boundary conditions on the free surface and on the bottom and that the surface takes the form of outgoing waves far from the body are satisfied exactly. The boundary condition on the surface of the cylinder is satisfied at the rest position of the cylinder by an expansion in non-orthogonal functions. Convergence in the general case is assumed.

The expansion coefficients for the case of a circular cylinder in fluid of infinite depth were calculated by two different numerical procedures. One of these methods was chosen for further development to provide sample calculations for elliptic and more general cylinders of approximately ship-like cross-section.

The pressure fluctuation at several locations on the surface of a circular cylinder and the total vertical force required to sustain vertical oscillations were measured. Two-dimensional conditions were simulated. The measured values and values based on the sample calculations show similar distinctive behavior.

The results of a general study of instrumentation for the measurement of pressure fluctuations in similar experiments are presented.

TABLE OF CONTENTS

	Page
PART A. Theoretical Development.	
I. Introduction.	1
II. Formulation of the Problem.	5
2.1 Description.	5
2.2 The Cylinders.	6
2.3 Infinitesimal Surface Wave Theory.	7
2.4 The Boundary Value Problem in Potential Theory.	7
III. Problem Solution.	9
3.1 Description	9
3.2 Notation of the Geometry.	10
3.3 The Component Potential Functions.	10
3.31 The Multipole Potential φ_{2m} .	11
3.32 The Combined Multipole and Standing-Wave Potentials.	14
3.33 The Source Potential.	17
3.34 The Combined Source and Standing-Wave Potentials.	19
3.4 The Potential Solution.	21
3.5 Evaluating the Expansion Coefficients.	23
3.6 The Ratio of Waveheight to Oscillation Amplitude.	25
3.7 The Pressure on the Cylinder Surface.	26
3.8 The Vertical Force Required to Sustain Oscillations.	28
3.9 The Added-Mass and Damping Coefficients.	30
3.91 The Added Mass and the Added-Mass Coefficient.	30

	Page
3.92 The Radiated Energy and the Damping Coefficient.	31
IV. The Special Case of Infinite Fluid-Depth.	33
4.1 Special Definition of the Multipole Potential $\bar{\varphi}_{2m}$.	33
4.2 The Source Potential and the Complete Potential Solution.	34
4.3 Evaluating the Expansion Coefficients.	35
4.4 Asymptotic Value for the Added Mass and Definition of the Free-Surface Correction.	36
PART B. Numerical Analysis and Results of Sample Calculations.	
V. The Circular Cylinder in Infinite-Depth Fluid.	39
5.1 Calculation of the Expansion Coefficients.	39
5.11 Choice of Method.	39
5.12 Form of the Equations for Calculation.	42
5.2 The Principal Dependent Variables.	43
5.21 The Results for $A(\delta)$, $B(\delta)$.	43
5.22 The Quantities $M(\delta, \theta)$, $N(\delta, \theta)$, and $M_0(\delta)$, $N_0(\delta)$.	44
5.3 Hydrodynamic Pressure Distribution on the Cylinder Surface.	48
5.4 The Added-Mass and Damping Coefficients.	50
VI. Elliptic and More General Cylinders in Infinitely Deep Fluid.	57
6.1 Description of the Method.	57
6.11 Numerical Procedures.	57
6.12 The Selection of Mapping Parameters a_{2n+1} .	58

	Page
6.2 Results for Examples from the One-Parameter (Elliptic) Family of Cylinders.	60
6.3 Results for Examples from the Two-Parameter (Lewis Form) Family of Cylinders.	67
6.4 Results for Examples from a Three-Parameter (Landweber-Macagno) Family of Cylinders.	74
 PART C. The Experiment, Results, and General Study of Pressure Fluctuation Measurements.	
 VII. Experiment and Results.	 82
7.1 Purpose and Direction.	82
7.2 Results of Measurements of the Pressure Fluctuation.	83
7.3 Results of Measurements of the Vertical Force Acting on the Cylinder.	84
7.4 The Cylinder and the Experiment Arrangement.	88
7.41 The Cylinder and the Motion Generator.	88
7.42 The Simulation of Two-Dimensional Conditions.	92
7.43 Electrical Instrumentation.	95
 VIII. General Study of Instrumentation for Measurement of Pressure Fluctuations.	 96
8.1 General Characteristics of the Pressure Measurement.	96
8.2 Piezoelectric Transducers.	98
8.21 Open Circuit Operation; the Piezo-electric Crystal Wafer.	98
8.22 Low Frequency Response of Piezo-electric Transducer and Amplifier.	99
8.23 Extending Low Frequency Response by Capacitive Loading.	103

	Page
8.24 Extending Low Frequency Response by Feedback Amplifier Technique.	104
8.3 The Pressure Sensitivity of Diaphragm-Type Transducers.	106
8.31 Definition of Sensitivity.	106
8.32 Small Deflections of Clamped-Edge Flat Circular Plates; Kirchhoff Theory.	109
8.33 Pressure Sensitivity of Flat Circular Plates with Deflection not Infinitesimal.	110
8.34 The Large Deflections of a Thin Dia- phragm with Zero Initial Tension; Solution of Hencky.	115
8.35 The Small Deflection of a Thin Mem- brane with Initial Tension.	118
8.36 The Large Deflection of a Thin Dia- phragm with Initial Tension.	120
8.37 Composite Approximate Solution for the Finite Deflection of a Clamped Edge Diaphragm under Uniform Load.	123
8.4 Dynamic Response of Flat Circular Diaphragms.	124
8.41 Error Due to Dynamic Response Charac- teristics of the Diaphragm.	124
8.42 The Lowest Natural Mode Frequency of Circular Diaphragms.	125
8.5 Pressure Gauges Mounted Internally.	128
8.51 Advantages and Disadvantages.	128
8.52 The Effect of Acceleration of the En- closed Fluid on the Indicated Pressure.	128
8.53 The Dynamic Response of the Internally Mounted Gauge.	130

ACKNOWLEDGMENT	Page 136
REFERENCES	137
APPENDICES	
Appendix A. Mathematical Notes Referenced in the Text.	141
A-1 Asymptotic Behavior of $\varphi_{2m}''(x,y,h)$ for $ x \rightarrow \infty$, $y = 0$.	142
A-2 Asymptotic Behavior of $\varphi_s(K,h)$ for $ x \rightarrow \infty$, $y = 0$.	145
A-3 Expanded Forms Useful in Numerical Calculation of Certain Definite Integrals.	146
A-3.1 The Coefficients of $p_{2m}(\delta)$, $q_{2m}(\delta)$ in Ex- pansion Equations for the Method of Inte- gration.	146
A-3.2 Two Special Forms.	147
A-3.3 Expressions in the Right-Hand Side of the $p_{2m}(\delta)$ Expansion Equations.	148
A-3.4 Alternate Forms for $\varphi_{sa}(\delta,0)$, $\gamma_{sa}(\delta,0)$.	148
A-3.5 Expressions in the Right-Hand Side of the $q_{2m}(\delta)$ Expansion Equations.	149
Appendix B. The Finite Deflection of Circular Plates with Initial Twisting.	152
B-1 Introduction.	153
B-2 Governing Differential Equations.	154
B-3 Series Assumed for Solution.	155
B-4 Evaluation of Coefficients b_{2n} in Terms of b_0 and Definition of the Function ϕ_1 .	156
B-5 Evaluation of Coefficients c_{2n} in Terms of b_0 and Definition of the Function ϕ_2 .	158
B-6 Evaluation of b_0 by the Boundary Condition.	160
B-7 Graphical Solution.	161

	Page
B-8 Special Cases.	163
a. Zero Initial Strain. (The Solution of Hencky).	163
b. Lightly Loaded Plates.	163
c. Comparison with the Membrane Solution.	165
Appendix C. The Attenuation of Oscillatory Pressure Fluctuations Travelling in a Viscous Fluid Through a Connecting Tube to an Instrument Cavity with Resilient Walls.	166
C-1 Description.	167
C-2 The Navier-Stokes (Momentum) Equations.	168
C-3 The Equation of Continuity.	171
C-4 The Equation of State and Effect on Tube Wall Elasticity.	171
C-5 Boundary Conditions and the Effect of Diaphragm Elasticity.	173
C-6 The Solution of the Governing Equation.	175
C-7 The Short Tube Approximations.	176
C-8 Approximation Valid for Small Values of $\omega^2 a / \nu$.	177
C-9 Approximation Valid for Moderate Damping Values.	178
C-10 Approximation Valid for Small Damping Values.	181

ILLUSTRATIONS

	Page
Figure 1. The Functions $A(\delta)$ and $B(\delta)$.	45
Figure 2. The Function $\tan^{-1} (B(\delta)/A(\delta))$.	46
Figure 3. Calculation Error Index vs Frequency.	49
Figure 4. $p_a(\delta, \theta)$ for the Circular Cylinder.	51
Figure 5. The Trend of p_a/δ for Large δ .	52
Figure 6. $p_v(\delta, \theta)$ for the Circular Cylinder.	53
Table I-A. $p_a(\delta, \theta)$ for the Circular Cylinder.	53 A
Table I-B. $p_v(\delta, \theta)$ for the Circular Cylinder.	53 B
Figure 7. The Added-Mass and Damping Coefficients for the Circular Cylinder.	55
Figure 8. The Amplitude Ratio \bar{A} for the Circular Cylinder.	56
Figure 9. $p_a(\delta, \theta)$ for the Ellipse $H = 3/2$.	62
Figure 10. $p_a(\delta, \theta)$ for the Ellipse $H = 1/5$.	63
Figure 11. $p_v(\delta, \theta)$ for the Ellipse $H = 3/2$.	64
Figure 12. $p_v(\delta, \theta)$ for the Ellipse $H = 1/5$.	64
Figure 13. k_4 for the Elliptic Cylinders $H = 1/5, 3/2$.	65
Figure 14. \bar{A} for Three Elliptic Cylinders.	66
Figure 15. $p_a(\delta, \theta)$ for the Full Section, $H = 1$.	69
Figure 16. $p_a(\delta, \theta)$ for the Cusped Section, $H = 1$.	70
Figure 17. $p_v(\delta, \theta)$ for the Full Section, $H = 1$.	71
Figure 18. $p_v(\delta, \theta)$ for the Cusped Section, $H = 1$.	71
Figure 19. k_4 for Three Cylinders, $H = 1$.	72
Figure 20. The Damping Coefficient $\frac{2\pi}{A^2 + B^2}$ for Three Cylinders, $H = 1$.	73
Figure 21. Three Cylinders, $H = 1/5$.	75
Figure 22. $p_a(\delta, \theta)$ for the Full Form, $H = 1/5$.	76

	Page
Figure 23. $p_v(\delta, \theta)$ for the Full Form, $H = 1/5$.	76
Figure 24. $p_a(\delta, \theta)$ for the Bulbous Section, $H = 1/5$.	78
Figure 25. The Trend of p_a/δ for Large δ , Bulbous Section, $H = 1/5$.	79
Figure 26. $p_v(\delta, \theta)$ for the Bulbous Section $H = 1/5$.	80
Figure 27. k_4 and \bar{A} for Three Cylinders, $H = 1/5$.	81
Figure 28. The Calculated and Measured Amplitude of Total Pressure Fluctuation.	85
Figure 29. Calculated and Measured Total Vertical Force.	87
Figure 30. The Model.	89
Figure 31. The Vertical Motion Dynamometer.	90
Figure 32. Top View of Arrangements.	94
Figure 33. Fractional Amplitude Response of a Piezoelectric Transducer and D.C. Amplifier as a Function of Frequency.	102
Figure 34. Fractional Response as a Function of (Added/Internal) Capacitance.	107
Figure 35. Non-dimensional Deflection of Flat Circular Diaphragms with Clamped Edges and No Initial Tension.	111
Figure 36. Non-dimensional Pressure Sensitivity of a Flat Circular Plate.	112
Figure 37. Deflection Coefficient K as a Function of Initial Strain and Load.	122
Figure 38. Graphical Solution for the Fundamental Natural Frequency of a Clamped, Circular, Flat Diaphragm.	127
Figure 39. An Instrument Cavity in an Oscillating Wall.	129
Figure 40. Fractional Response and Phase Lag of Indicated Pressure, Viscous Regime.	132
Figure 41. Fractional Response and Phase Lag of Indicated Pressure, Moderate Damping.	134
Figure 42. The Functions $f_{17}(b_o)$ and $K(b_o)$.	162

1. Introduction

The study of the hydrodynamics of cylinders oscillating in a free surface is of interest for several reasons and has therefore received attention for some years. Ursell [1949]* formulated the problem of the horizontal circular cylinder, semi-submerged and undergoing forced periodic heaving oscillations, as a boundary-value problem in the theory of infinitesimal gravity waves. He completed the rigorous solution in principle and presented the results of a numerical calculation that leads to added-mass and damping coefficients. One might say the modern history of the problem begins with this solution by Ursell.

Grim [1953] follows a somewhat different procedure in synthesizing a potential solution but with a restricted number of coefficients so that the results are approximate. He compares his circular-cylinder results with Ursell's calculation. Grim extended his method to present approximate results for certain elliptic cylinders and for certain cylinders of somewhat ship-like cross-section called "Lewis Forms" in the field of naval architecture.

Tasai [1959] returned to the method of Ursell, using in principle an unlimited number of expansion coefficients, and, by a mapping procedure, extended the results of Ursell to include elliptic and Lewis-form cylinders. He presents the results of numerical calculations for the added-mass coefficient and waveheight ratio (equivalent to damping factor) for certain elliptic and Lewis-form cylinders. Tasai compares his results for an elliptic cylinder (horizontal-to-vertical-axes ratio of 1.5) to the results of Grim. Grim's approximate

*References identified in the text by author and date are collected at the end.

results are markedly low for the added-mass coefficient. There is closer agreement for waveheight ratio.

The work of Ursell, Grim, and Tasai cited above is restricted to water of infinite depth. Yu [1960] added the condition of uniform finite-depth to the problem as formulated by Ursell. The potential functions used by Yu are those appropriate to infinitesimal gravity-waves in water of finite depth. Yu completes the solution in principle following the method of Ursell for a circular cylinder. He presents the results of a numerical calculation for the added-mass coefficient and for the waveheight ratio. His result recovers the solution of Ursell as the water depth approaches infinity; practically speaking, the numerical results are essentially the same when the water depth is equal to ten radius-lengths.

Yu also reported an experiment with a semi-submerged cylinder in simulated two-dimensional conditions. He measured the waveheight ratio and shows substantial agreement with his calculated results. The few other reported experiments simulating two-dimensional conditions are not readily compared. Holstein [1936] used a prismatic cylinder of somewhat ship-like cross-section, nearly rectangular. Schuler [1936] used a similar form but in free oscillation, a very different hydrodynamic problem. Dimpker [1934] used several prismatic forms, including a circular cylinder, but again reports measurements for free oscillations.

There exists work on the similar problem in three dimensions, on approximate methods for solving the three-dimensional problem by drawing on two-dimensional results, and experimental work with models

not simulating two-dimensional conditions. Including the third dimension is a sufficient departure from the objective of this work that pursuit of that worthy problem is not undertaken here.

The present paper considers the case of the more general cylinders in a fluid that may be of uniform finite depth. The problem is formulated as a boundary-value problem in the theory of infinitesimal gravity waves. Within this framework the problem is linear and the solution is obtained by superposition of appropriate velocity potentials. Following Ursell, the solution is obtained in principle employing an unlimited number of expansion coefficients. For the special case of the circular cylinder, one recovers the solution of Yu. For the special case of infinite water depth, a solution is obtained which includes that of Tasai and is also explicit for more general cylinders than he treated (for example, the three-parameter cross-section family of Landweber and Macagno [1959]). Finally, for the special case of infinite depth and a circular cylinder, the parent solution of Ursell is recovered.

The hydrodynamic pressure distribution for the cases of the previous solutions can be derived from the work of the authors cited. However, none state this result or present sample calculations for their cases. The pressure distribution is considered here in order to provide possible insight into similar problems of naval architectural interest and to provide calculations for comparison with experimental measurements.

The results of numerical calculations for the case of a circular cylinder in fluid of infinite depth are presented. The numerical

procedure differs from that of Ursell for the same case. The force and waveheight ratio results are in agreement. The pressure distribution was not previously reported.

In order to compare the theoretical results with experimental values, measurements were made on a circular cylinder in simulated two-dimensional conditions. Total vertical force and water pressure fluctuation on the model surface were measured. The measured values compare favorably with the predicted values. Over a small part of the frequency range used, a distinct departure from two-dimensional conditions was observed and was due to the particular experimental arrangement. In this small range, measured values consistently deviate from predicted two-dimensional values.

The results of numerical calculations for elliptic cylinders and certain cylinders of ship-like cross-section in fluid of infinite depth are presented. Certain added-mass and waveheight ratios of this group can be compared with those of Tasai, who used a different numerical procedure. The pressure distributions and the results for certain cross-sections have not been previously reported.

Numerical calculations following this procedure for circular, elliptic and more general cylinders in fluid of finite depth are to be done at the Computer Center, University of California. The calculations reported here were done at this facility.

II. Formulation of the Problem

2.1 Description.

We consider cylinders of a certain class to be defined more precisely in the next section. The cylinder is immersed in a previously-undisturbed fluid which may be of uniform finite or infinite depth. The axis of the cylinder is in the plane of the still free surface. Consider now that the cylinder is forced in vertical simple harmonic motion and that steady-state conditions are attained. We assume two-dimensional conditions, and that the amplitude of oscillation is small compared with the cylinder beam. In the steady state, the forced vertical motion generates a surface disturbance that at a distance from the cylinder takes the form of uniform progressive gravity waves whose amplitude is proportional to the oscillation amplitude.

We require the pressure distribution on the surface of the cylinder, the vertical force required to sustain the oscillations, and the ratio of the waveheight far from the body to the oscillation amplitude.

The total vertical force in the steady-state is periodic and includes two components of particular interest. Because of steady-state periodic conditions it is possible to resolve the vertical force into components in phase with the motion acceleration and velocity. These components do not depend on the previous history of motion, given steady-state. It is possible therefore to define added-mass and damping coefficients as ratios of the appropriate force component to the mass of the displaced fluid that are functions

of body geometry and oscillation frequency only. Expressions for the added-mass and damping coefficients are required.

2.2 The Cylinders.

The cylinders admitted are those mapped by conformal transformation of circles by

$$\frac{z}{a} = \zeta + \sum_{n=0}^N a_{2n+1} \zeta^{-(2n+1)}$$

where* $\zeta = i\rho e^{-i\theta}$

$$z = x + iy = i r e^{-i\beta}$$

The elementary case $a_{2n+1} = 0$ provides a circular cylinder. The case $N = 0$ yields elliptic cylinders. Lewis

[1929] introduced the use of this transform

with $N = 1$ for a two-parameter family with a_1, a_3 selected to provide cylinders of more or less ship-like cross-section. The solution of Tasai [1959] employs this two-parameter family. Landweber and Macagno [1959] use this transform with $N = 2$ and select a_1, a_3, a_5 to provide a more general selection of ship-like cross-sections. Prohaska [1947] treated sections derived by transformations employing a_1, a_5 and a_1, a_7 and a_3, a_7 .

In this work we leave N unspecified in the solution of the problem, and select various a_{2n+1} for sample numerical calculations.

* The η - and y -axes are chosen positive down from the free surface and the angular coordinates θ, β are measured from the vertical to facilitate reference to related work cited.

2.3 Infinitesimal Surface Wave Theory.

The problem is solved within the framework of infinitesimal surface wave theory. We may apply this theory if we assume that the fluid is incompressible, that the flow is irrotational, and that the motion amplitudes and velocities are all sufficiently small to reject all but linear terms. In this problem we also neglect surface tension.

The process of linearization is specifically employed three times: First, in linearization of the free-surface boundary condition; second, in satisfying the boundary condition on the surface of the cylinder at the rest-position; third, in the approximation of the hydrodynamic pressure by using the linearized form of Bernoulli's equation. These are well-established elements of the general theory within which we work. For a more complete discussion see Wehausen [1960] or Stoker [1957].

2.4 The Boundary-Value Problem in Potential Theory.

Given the assumptions above, we can state the boundary-value problem in potential theory. We seek a velocity potential ϕ which is a solution of the Laplace equation $\nabla^2\phi = 0$ in the fluid domain and which satisfies the following boundary conditions.

(i) The linearized free-surface condition:

$$K\phi + \frac{\partial\phi}{\partial y} = 0$$

on the surface $y = 0$ outside the body of the cylinder. Here $K = \omega^2/g$.

(ii) The normal velocity at the lower boundary of the fluid vanishes:

$$\frac{\partial \varphi}{\partial y} = 0$$

on the bottom $y = h$.

(iii) The radiation condition: The disturbed surface takes the form of regular progressive outgoing gravity waves at large distance from the cylinder.

(iv) The normal velocity of the fluid at the surface of the cylinder is equal to the component of the cylinder's forced velocity in that direction.

III. Solution of the Problem

3.1 Description.

The problem has been stated in Chapter II. The solution is described in this section and outlined in this chapter. The complete velocity potential φ (and the corresponding stream function γ) describing the fluid motion will be synthesized as the sum of appropriate potential functions. Each component function individually satisfies the Laplace equation and the boundary conditions on the free surface and on the bottom. The asymptotic behavior of the component functions for large distance from the cylinder correctly contributes to a potential appropriate to outgoing surface waves, and thus the radiation condition is satisfied. In order to satisfy the last boundary condition, concerning the normal velocity of the fluid at the cylinder boundary, an expansion in non-orthogonal functions is required. It is shown that an unlimited number of coefficients can, in principle, be determined. Convergence of the expansion, proved for the circular cylinder by Ursell [1949, 1953], is assumed for the general case. Thus the complete potential and stream function are known and the problem is solved. Having the potential, we determine the pressure distribution and, by integration, the vertical force required to sustain the oscillation. The vertical force is resolved into components in phase with the acceleration and velocity to give added-mass and damping coefficients. The ratio of waveheight to oscillation amplitude is available from the asymptotic behavior (progressive surface waves) of the potential and from the damping coefficient.

3.2 Notation of the Geometry.

The z - or physical-plane geometry is conformally mapped from the reference ζ -plane by the transform

$$\frac{z}{a} = \zeta + \sum_{n=0}^N a_{2n+1} \zeta^{-(2n+1)}$$

where a and a_{2n+1} are real so that the z -plane coordinates mapped from $\zeta = i\rho e^{-i\theta}$ are

$$z = x + iy = i r e^{-i\beta},$$

$$x = a \left[\rho \sin \theta + \sum_{n=0}^N (-1)^n \frac{a_{2n+1}}{\rho^{2n+1}} \sin(2n+1)\theta \right],$$

$$y = a \left[\rho \cos \theta + \sum_{n=0}^N (-1)^{n+1} \frac{a_{2n+1}}{\rho^{2n+1}} \cos(2n+1)\theta \right].$$

Special notation will be convenient for coordinate values on the cylinder surface mapped from the reference circle $\rho = \rho_0$.

$$x(\text{body}) = aX, \quad X = X(\rho_0, \theta)$$

$$x(\text{body}, \theta = \pi/2) = aG, \quad G = X(\rho_0, \pi/2)$$

$$y(\text{body}) = aY, \quad Y = Y(\rho_0, \theta)$$

The product aG is the half-beam, b , of the cylinder at the free surface. The fluid depth is uniform at $y = h$.

3.3 The Component Potential Functions.

In the following sections we shall develop the complete velocity potential ϕ and stream function γ in the form

$$\begin{aligned} \frac{\phi_s}{\gamma_s} \sin \omega t + \frac{\phi_c}{\gamma_c} \cos \omega t + \sum_{m=1}^{\infty} p_{2m} \left(\frac{\phi_{2m}}{\gamma_{2m}} \cos \omega t + \frac{\phi_{2m}^w}{\gamma_{2m}^w} \sin \omega t \right) + \\ + \sum_{m=1}^{\infty} q_{2m} \left(\frac{\phi_{2m}}{\gamma_{2m}} \sin \omega t - \frac{\phi_{2m}^w}{\gamma_{2m}^w} \cos \omega t \right). \end{aligned}$$

Components are named as follows:

- ϕ_s source potential;
- ϕ_c standing-wave potential;
- p_{2m}, q_{2m} expansion coefficients;
- ϕ_{2m} multipole potential;
- ϕ_{2m}^w associated standing-wave potential.

The combined components $\left(\frac{\phi_s}{\gamma_s} \sin \omega t + \frac{\phi_c}{\gamma_c} \cos \omega t \right)$ and the combined components $\left(\frac{\phi_{2m}}{\gamma_{2m}} \cos \omega t + \frac{\phi_{2m}^w}{\gamma_{2m}^w} \sin \omega t \right)$ display asymptotic behavior appropriate to outgoing surface waves. The multipole $\frac{\phi_{2m}}{\gamma_{2m}}$ in turn consists of two parts, each with several terms.

3.31 The Multipole Potential ϕ_{2m} .

The multipole potential is written in two parts

$$\phi_{2m} = \phi'_{2m}(x, \beta) + \phi''_{2m}(x, y, h), \quad m=1, 2, 3, \dots$$

The part $\phi'_{2m}(x, \beta)$ satisfies the free-surface condition and the bottom condition for infinite depth but does not satisfy the bottom condition for finite depth. The part $\phi''_{2m}(x, y, h)$ is added

to make the total satisfy the finite-depth boundary condition, following Thorne [1953]. The function $\varphi''_{2m}(x,y,h)$ independently satisfies the free-surface condition and for $h \rightarrow \infty$, $\varphi''_{2m}(x,y,h) \rightarrow 0$.

The index $\underline{2m}$ will be understood when it is dropped from the symbols φ'_{2m} and φ''_{2m} .

(a) Part $\varphi'_{2m}(r,\beta)$:

$$\begin{aligned} \varphi'(r,\beta) = & \frac{a^{2m} \cos 2m\beta}{r^{2m}} + \sum_{n=0}^N (-1)^n a_{2n+1} \frac{a^{(2m+2n+2)} \cos(2m+2n+2)\beta}{r^{2m+2n+2}} + \\ & + \frac{K}{2m-1} \frac{a^{2m} \cos(2m-1)\beta}{r^{2m-1}} + K \sum_{n=0}^N (-1)^n \frac{a_{2n+1}}{2m+2n+1} \frac{a^{2m+2n+2} \cos(2m+2n+1)\beta}{r^{2m+2n+1}}. \end{aligned}$$

To show that $\varphi'(r,\beta)$ satisfies the free-surface condition, it is convenient to express that boundary condition in another form:

$$K\varphi_{2m} + \frac{\partial \varphi_{2m}}{\partial y} = K\varphi' + \frac{\partial \varphi'}{\partial y} + K\varphi'' + \frac{\partial \varphi''}{\partial y} = 0, \quad \beta = \theta = \pi/2.$$

The part $K\varphi' + \partial \varphi'/\partial y$, independently zero, is written

$$K\varphi' - \frac{1}{r} \frac{\partial \varphi'}{\partial \beta} = 0, \quad \beta = \pi/2.$$

When the substitution is made and evaluated at $\beta = \pi/2$, the remaining terms are

$$\begin{aligned} a^{2m} [\cos m\pi + \sin(2m-1)\pi/2]/r^{2m} + \sum_{n=0}^N (-1)^n a_{2n+1} a^{2s} [\cos s\pi + \\ + \sin(2s-1)\pi/2]/r^{2s}. \end{aligned}$$

We have introduced $2s = 2m+2n+2$. Now, using the identities $\cos m\pi = (-1)^m$ and $\sin(2m-1)\pi/2 = (-1)^{m+1}$, it is clear this sum is identically zero; therefore, $\varphi'(r,\beta)$ satisfies the free-surface condition.

The function $\varphi'_{2m}(x, \beta)$ satisfies the bottom condition only in the case of infinite depth. The total $\varphi_{2m} = \varphi'_{2m} + \varphi''_{2m}$ will be adjusted to satisfy the bottom condition at finite depth in (c) below.

(b) Part $\varphi''_{2m}(x, y, h)$:

$$\varphi''(x, y, h) = \int_0^{\infty} [c_3(k) \sinh ky + c_4(k) \cosh k(h-y)] \cos kx \, dk,$$

where $c_3(k)$, $c_4(k)$ are found below and assure convergence.

Carrying out the operation $(K + \partial/\partial y)\varphi''$ leads to the definition

$$c_4(k) = -c_3(k) \frac{k}{K \cosh kh - k \sinh kh}$$

to assure that $\varphi''(x, y, h)$ satisfies the free-surface condition at $y = 0$.

(c) The Finite-Depth Boundary Condition for the Multipole.

The coefficient $c_3(k)$ in the integral term $\varphi''(x, y, h)$ is determined by using the bottom condition,

$$\frac{\partial \varphi_{2m}}{\partial y} = \frac{\partial \varphi'}{\partial y} + \frac{\partial \varphi''}{\partial y} = 0, \quad y = h.$$

To find the first term, use the expansion (for $y > 0$)

$$\frac{\cos n\beta}{r^n} = \frac{1}{(n-1)!} \int_0^{\infty} k^{n-1} e^{-ky} \cos kx \, dk.$$

[Whittaker and Watson, A Course of Modern Analysis, Cambridge 1927. para. 12.2 Ex.2]. With this expansion, one may write for φ' , when $y > 0$,

$$\varphi' = \int_0^{\infty} L(k) e^{-ky} \cos kx \, dk$$

where

$$L(k) = \frac{k^{2m-2} a^{2m} (K+k)}{(2m-1)!} + \sum_{n=0}^N (-1)^n \frac{k^{2s-2} a^{2s} (K+k)}{(2s-1)!}.$$

The bottom condition is satisfied when

$$\left. \frac{\partial \varphi_{2m}}{\partial y} \right|_{y=h} = \int_0^{\infty} [-kL e^{-kh} + c_3(k) k \cosh kh] \cos kx \, dk$$

vanishes. The definition $c_3(k) = L e^{-kh} / \cosh kh$ assures this.

With $c_3(k)$ determined, $\varphi_2''(x, y, h)$ is written as a Cauchy Principal Value integral (\mathcal{P}).

$$\begin{aligned} \varphi_2(x, y, h) &= \mathcal{P} \int_0^{\infty} L e^{-ky} \frac{K \sinh ky - k \cosh ky}{K \cosh kh - k \sinh kh} \cos kx \, dk \\ &= \mathcal{P} \int_0^{\infty} \frac{s^{-kh} (K+k) k^{2m-2} a^{2m}}{(2m-1)!} \frac{K \sinh ky - k \cosh ky}{K \cosh kh - k \cosh kh} \cos kx \, dk + \\ &+ \sum_{n=0}^N (-1)^n a_{2n+1} \mathcal{P} \int_0^{\infty} \frac{s^{-kh} (K+k) k^{2s-2} a^{2s}}{(2s-1)!} \frac{K \sinh ky - k \cosh ky}{K \cosh kh - k \cosh kh} \cos kx \, dk. \end{aligned}$$

3.32 The Combined Multipole and Associated Standing-Wave Potentials.

The radiation condition [2.4(iii)] requires that the asymptotic behavior of the potential for large x and $y = 0$ be appropriate to outwardly progressing surface waves. The part φ' of the multipole tends to zero for $|x| \rightarrow \infty$. However, the part φ'' of the multipole does not tend to zero for $|x| \rightarrow \infty, y = 0$. The associated standing-wave potential φ_{2m}^w is shown below to combine with the multipole to form a total which satisfies the radiation condition.

Since $\varphi'(r, \beta) \rightarrow 0$ for $|x| \rightarrow \infty$, $\varphi_{2m}(x, 0, h) \rightarrow \varphi''(x, 0, h)$ for $|x| \rightarrow \infty$. It is shown in Appendix A-1 that the following asymptotic expansion holds:

$$\varphi_2''(x, y, h) \sim -E_{2m} \frac{\cosh K_0(h-y)}{\cosh K_0 h} \sin K_0 |x| \quad \text{as } |x| \rightarrow \infty,$$

and

$$\varphi_2''(x, 0, h) \sim -E_{2m} \sin K_0 |x| \quad \text{as } |x| \rightarrow \infty,$$

where

$$E_{2m}(K_0 a, K_0 h) = \frac{2\pi}{2K_0 h + \sinh 2K_0 h} \left[\frac{K_0^{2m} a^{2m}}{(2m-1)!} + \sum_{n=0}^N (-1)^n \frac{a_{2n+1} K_0^{2s} a^{2s}}{(2s-1)!} \right]$$

and $K_0(K, h)$ is defined as the positive real root of

$$K = K_0 \tanh K_0 h.$$

For finite $h > 0$ the asymptotic behavior of $\varphi''(x, 0, h)$ as $|x| \rightarrow \infty$ with an appropriate harmonic function of time, is identified as typical of a standing wave in a fluid of depth h . We add a standing-wave potential consisting of the function

$$\varphi_{2m}^w = c_{2m} \cosh K_0(h-y) \cos K_0 x \quad m=1, 2, 3, \dots$$

multiplied by a harmonic function of time. The coefficients c_{2m} are chosen in the following so that the combined potential represents progressive waves and the radiation condition is satisfied.

To determine c_{2m} , consider

$$\varphi_{2m} \cos \omega t + \varphi_{2m}^w \sin \omega t \Big|_{y=0} \sim \varphi_{2m}''(x, 0, h) \cos \omega t + \varphi_{2m}^w(x, 0, h) \sin \omega t \quad \text{as } |x| \rightarrow \infty.$$

The right-hand side is asymptotically equal to

$$-E_{2m} \sin K_0 |x| \cos \omega t + c_{2m} \cosh K_0 h \cos K_0 x \sin \omega t \quad \text{as } |x| \rightarrow \infty.$$

By defining

$$\phi_{2m} = E_{2m} / \cosh K_0 h$$

the asymptotic behavior of the combined functions is

$$= E_{2m} \sin (K_0 |x| - \omega t) ,$$

which displays the required behavior.

We also form the sum with conjugate harmonic time functions,

$$\phi_{2m} \sin \omega t - \phi_{2m}^w \cos \omega t ,$$

which for $|x| \rightarrow \infty$, $y = 0$, tends asymptotically to

$$= E_{2m} \cos (K_0 |x| - \omega t) .$$

A linear combination of multipole potentials, adjusted as above to be progressive-wave producing, is

$$\sum_{m=1}^{\infty} p_{2m} (\phi_{2m} \cos \omega t + \phi_{2m}^w \sin \omega t) + \sum_{m=1}^{\infty} q_{2m} (\phi_{2m} \sin \omega t - \phi_{2m}^w \cos \omega t) .$$

The coefficients $p_{2m}(Ka)$ and $q_{2m}(Ka)$ are to be determined, and are assumed to behave so that convergence is assured.

The asymptotic form of the free surface $y = 0$ for large $x > 0$ is

$$\eta = \frac{1}{g} \frac{\partial \phi}{\partial t} \sim \frac{\omega}{g} \sum_{m=1}^{\infty} p_{2m} E \cos (K_0 x - \omega t) - \frac{\omega}{g} \sum_{m=1}^{\infty} q_{2m} E \sin (K_0 x - \omega t) .$$

In complex notation, if we reserve the operator i for geometric variables and introduce the operator j for functions of time t , this sum is

$$\operatorname{Re}_j \sum_{m=1}^{\infty} (p_{2m} + j q_{2m})(\varphi_{2m} + j \varphi_{2m}^w) e^{-j\omega t}.$$

We will later make use of the corresponding stream functions γ_{2m} and γ_{2m}^w , which may be found from

$$f_{2m}(z) = \varphi_{2m} + i\gamma_{2m}$$

$$\begin{aligned} &= (-1)^m a^{2m} z^{-2m} + \sum_{n=0}^N (-1)^n a_{2n+1} (-1)^s z^{-2s} - (-1)^m \frac{iK}{2m-1} a^{2m} z^{-(2m-1)} - \\ &- \sum_{n=0}^N (-1)^n a_{2n+1} (-1)^s \frac{iK}{2s-1} a^{2s} z^{-(2s-1)} - \\ &- \int_0^{\infty} \frac{L e^{-kh} [iK \sin kz + k \cos kz]}{K \cosh kh - k \sinh kh} dk \end{aligned}$$

$$\text{and } f_{2m}^w(z) = \varphi_{2m}^w + i \gamma_{2m}^w.$$

$$= c_{2m} \cosh K_0 (h + iz).$$

With these definitions, the complete wave-producing multipole is

$$\operatorname{Re}_j \sum_{m=1}^{\infty} (p_{2m} + j q_{2m})(f_{2m}(z) + j f_{2m}^w(z)) e^{-j\omega t}.$$

3.33 The Source Potential.

The potential function that represents a source at the origin and that satisfies the free-surface boundary condition is

$$\int_0^{\infty} \frac{e^{-ky} \cos kx}{K-k} dk = \pi e^{-Ky} \sin Kx = \int_0^{\infty} \frac{e^{-mx} (m \cos my - K \sin my)}{m^2 + K^2} dm.$$

It is easily seen from the form on the right that this satisfies

the free-surface condition. The bottom condition, however, is not satisfied in the case of fluid of finite depth. To satisfy the finite-depth bottom condition, we add a term in the manner of Thorne [1953],

$$\int_0^{\infty} [c_1(k) \sinh ky + c_2(k) \cosh k(h-y)] \cos kx \, dk .$$

The coefficients $c_1(k)$, $c_2(k)$ are determined below and assure convergence.

This integral term satisfies the free-surface condition given that

$$c_2(k) = -c_1(k) \frac{k}{K \cosh kh - k \sinh kh} .$$

The coefficient $c_1(k)$ is determined so that the combined term

$$\int_0^{\infty} \frac{\varepsilon^{-ky} \cos kx}{K-k} \, dk + \int_0^{\infty} c_1(k) \left[\sinh ky - \frac{K \cosh k(h-y)}{K \cosh kh - k \sinh kh} \right] \cos kx \, dk$$

satisfies the finite-depth boundary condition. This boundary condition, $\partial\phi/\partial y = 0$, $y = h$, leads to

$$c_1(k) = \frac{\varepsilon^{-kh}}{K-k} \frac{1}{\cosh kh} .$$

With this coefficient, the source potential is

$$\varphi_s = \int_0^{\infty} \frac{\cosh k(h-y) \cos kx}{K \cosh kh - k \sinh kh} \, dk .$$

When $h \rightarrow \infty$, this simplifies to the source potential given first.

3.34 The Combined Source and Standing-Wave Potentials.

The radiation condition is satisfied by adding a standing-wave potential to the source potential, with the necessary harmonic functions of time, to form the term

$$\varphi_c \cos \omega t + \varphi_s \sin \omega t .$$

The standing-wave potential function is

$$\varphi_c = a_o \cosh K_o(h-y) \cos K_o x ,$$

with a_o defined as given below.

Appendix A-2 shows that the asymptotic behavior of the source-function φ_s for $|x| \rightarrow \infty$, $y = 0$ is

$$E_s \sin K_o |x|$$

where

$$E_s(K_o h) = \frac{2\pi(\cosh K_o h)^2}{2K_o h + \sinh 2K_o h} .$$

Now a_o is defined as

$$a_o = \frac{E_s}{\cosh K_o h}$$

so that the asymptotic form, as $|x| \rightarrow \infty$,

$$\begin{aligned} (\varphi_c \cos \omega t + \varphi_s \sin \omega t) \Big|_{y=0} &\sim a_o \cosh K_o h \cos K_o |x| \cos \omega t + \\ &+ E_s \sin K_o |x| \sin \omega t \end{aligned}$$

may be written

$$E_s \cos (K_o |x| - \omega t) .$$

The source potential and its associated standing-wave potential

$$\oint_0^{\infty} \frac{\cosh k(h-y) \cos kx}{K \cosh kh - k \sinh kh} dk \sin \omega t + \frac{E_s}{\cosh K_0 h} \cosh K_0(h-y) \cos K_0 x \cos \omega t$$

therefore satisfy the free-surface, finite-depth, and radiation boundary conditions.

In the special case $h \rightarrow \infty$ this may be written

$$\left[\pi \varepsilon^{-Ky} \sin Kx - \int_0^{\infty} \frac{e^{-mx} (m \cos my - K \sin my)}{m^2 + K^2} dm \right] \sin \omega t + \pi \varepsilon^{-Ky} \cos Kx \cos \omega t,$$

which is the form used by Ursell [1949] and Tasai [1959].

The form of the free surface for large $x > 0$ for either case is

$$\eta = \frac{1}{g} \frac{\partial \varphi}{\partial t} \sim \frac{\omega E_s}{g} \sin(K_0 x - \omega t).$$

For the special case $h \rightarrow \infty$, $E_s \rightarrow \pi$.

The stream function corresponding to this potential may be found from

$$\operatorname{Re}_j (f_c(z) + j f_s(z)) \varepsilon^{-j\omega t}$$

where

$$f_c(z) = \varphi_c + i\gamma_c$$

$$= \frac{2\pi \cosh K_0 h}{2K_0 h + \sinh 2K_0 h} \cosh K_0(h+iz)$$

$$f_s(z) = \varphi_s + i\gamma_s$$

$$= \oint_0^{\infty} \frac{\cosh K_0(h+iz)}{K \cosh kh - k \sinh kh} dk.$$

3.4 The Potential Solution.

The potential solution written as a function of the complex variable $z = x + iy$ is

$$\varphi + iy = \frac{gh_w}{\pi\omega J} \operatorname{Re}_j [f_c(z) + jf_s(z) + \sum_{m=1}^{\infty} (p_{2m} + jq_{2m})(f_{2m}(z) + jf_{2m}^w(z))e^{-j\omega t}] .$$

The coefficients $p_{2m}(Ka)$, $q_{2m}(Ka)$ are determined later by use of the normal-velocity boundary condition. The right-hand side has been normalized by the coefficient $J(K_0 h)$ in order to display the surface waveheight h_w at large distance from the cylinder.

The function $J(K_0 h)$ may be determined as follows, for example, from the asymptotic development of the potential for large $x > 0$, $y = 0$.

$$\begin{aligned} \varphi(x, 0, h) \sim \frac{gh_w}{\pi\omega J} \left[E_s \cos(K_0 x - \omega t) + \sum_{m=1}^{\infty} p_{2m} E_{2m} \sin(K_0 x - \omega t) - \right. \\ \left. - \sum_{m=1}^{\infty} q_{2m} E_{2m} \cos(K_0 x - \omega t) \right] . \end{aligned}$$

The corresponding asymptotic surface waveheight as $x \rightarrow \infty$ is

$$\begin{aligned} \eta &= \frac{1}{g} \frac{\partial \varphi}{\partial t} \\ &\sim \frac{h_w}{\pi J} \left[(E_s - \sum_{m=1}^{\infty} q_{2m} E_{2m}) \sin(K_0 x - \omega t) + \right. \\ &\quad \left. + \sum_{m=1}^{\infty} p_{2m} E_{2m} \cos(K_0 x - \omega t) \right] . \end{aligned}$$

This may be written

$$h_w \sin(K_0 x - \omega t + \tau)$$

when we define

$$\pi^2 J(K_0 h)^2 = [E_s(K_0 h) - \sum_{m=1}^{\infty} q_{2m}(Ka) E_{2m}(K_0 h)]^2 + [\sum_{m=1}^{\infty} p_{2m}(Ka) E_{2m}(K_0 h)]^2$$

$$\tan \tau = \sum_{m=1}^{\infty} p_{2m} E_{2m} / (E_s - \sum_{m=1}^{\infty} q_{2m} E_{2m}) .$$

For $h \rightarrow \infty$, we recall that $E_{2m} \rightarrow 0$, $E_s \rightarrow \pi$, so that $J \rightarrow 1$.

All quantities in the potential and stream function

$$\begin{aligned} \frac{\varphi}{\gamma} = \frac{gh_w}{\pi\omega J} & \left[\frac{\varphi_s}{\gamma_s} \sin \omega t + \frac{\varphi_c}{\gamma_c} \cos \omega t + \sum_{m=1}^{\infty} p_{2m} \left(\frac{\varphi_{2m}}{\gamma_{2m}} \cos \omega t + \frac{\varphi_{2m}^w}{\gamma_{2m}^w} \sin \omega t \right) + \right. \\ & \left. + \sum_{m=1}^{\infty} q_{2m} \left(\frac{\varphi_{2m}}{\gamma_{2m}} \sin \omega t - \frac{\varphi_{2m}^w}{\gamma_{2m}^w} \cos \omega t \right) \right] , \end{aligned}$$

except the expansion coefficients for a given cylinder, water-depth, and heaving oscillation have been determined. When the expansion coefficients are determined in the next section it will be convenient to have the following notation. The subscript a designates evaluation on the cylinder boundary.

$$\varphi]_{\text{body}} = \frac{gh_w}{\pi\omega J} (M \sin \omega t + N \cos \omega t)$$

$$M(Ka, \Theta) = \varphi_{sa} + \sum_{m=1}^{\infty} p_{2m} \varphi_{2ma}^w + \sum_{m=1}^{\infty} q_{2m} \varphi_{2ma}$$

$$N(Ka, \Theta) = \varphi_{ca} - \sum_{m=1}^{\infty} q_{2m} \varphi_{2ma}^w + \sum_{m=1}^{\infty} p_{2m} \varphi_{2ma}$$

$$\gamma]_{\text{body}} = \frac{gh_w}{\pi\omega J} (D \sin \omega t + C \cos \omega t)$$

$$D(Ka, \theta) = \gamma_{sa} + \sum_{m=1}^{\infty} p_{2m} \gamma_{2ma}^w + \sum_{m=1}^{\infty} q_{2m} \gamma_{2ma}$$

$$C(Ka, \theta) = \gamma_{ca} + \sum_{m=1}^{\infty} p_{2m} \gamma_{2ma} - \sum_{m=1}^{\infty} q_{2m} \gamma_{2ma}^w .$$

In addition we designate the evaluation of $\gamma]_{\text{body}}$ for $\theta = \beta = \pi/2$ by

$$\gamma]_{\text{body}, \pi/2} = \frac{gh_w}{\pi\omega J} (B \sin \omega t + A \cos \omega t)$$

$$B(Ka) = D(Ka, \pi/2) = \gamma_{sa} \pi/2 + \sum_{m=1}^{\infty} p_{2m} \gamma_{2ma}^w \pi/2 + \sum_{m=1}^{\infty} q_{2m} \gamma_{2ma} \pi/2$$

$$A(Ka) = C(Ka, \pi/2) = \gamma_{ca} \pi/2 + \sum_{m=1}^{\infty} p_{2m} \gamma_{2ma} \pi/2 - \sum_{m=1}^{\infty} q_{2m} \gamma_{2ma}^w \pi/2 .$$

The apparent redundancy of notation has the purpose of facilitating reference to related solutions previously mentioned.

3.5 Evaluating the Expansion Coefficients.

The vertical velocity component that is perpendicular to the cylinder surface must equal the normal velocity of the fluid at that point. This boundary condition is to be satisfied at the rest position of the cylinder by suitable choice of expansion coefficients $p_{2m}(Ka)$, $q_{2m}(Ka)$.

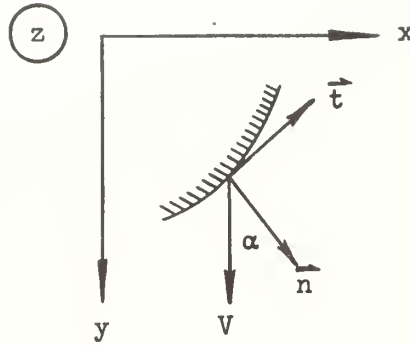
The vertical motion is $y = h_0 \cos(\omega t + \varepsilon)$. After using the substitutions

$$\frac{\partial x}{\partial s} = \frac{\partial y}{\partial n} = \cos \alpha$$

$$\frac{\partial \varphi}{\partial n} = - \left[\frac{\partial \gamma}{\partial s} \right]_{\text{body}}$$

the boundary condition is

$$- \frac{\partial \gamma}{\partial s} = \frac{dy}{dt} \frac{\partial x}{\partial s} \Big|_{\text{body}} .$$



After integrating and setting the integration constant equal to zero,

$$\gamma = - \left[\frac{dy}{dt} x \right]_{\text{body}} .$$

We evaluate this expression at the special location $\beta = \theta = \pi/2$, using the notation of the preceding section:

$$\gamma \Big|_{\text{body}, \pi/2} = \frac{gh_w}{\pi \omega J} (A \cos \omega t + B \sin \omega t) = - \frac{dy}{dt} aG .$$

Then we may use

$$\frac{dy}{dt} = - \frac{gh_w}{\pi \omega a G J} (A \cos \omega t + B \sin \omega t)$$

to evaluate the same expression in general locations on the cylinder:

$$\begin{aligned} \gamma \Big|_{\text{body}} &= \frac{gh_w}{\pi \omega J} (C \cos \omega t + D \sin \omega t) = - \left[\frac{dy}{dt} x \right]_{\text{body}} \\ &= \frac{gh_w}{\pi \omega a G J} (A \cos \omega t + B \sin \omega t) aX . \end{aligned}$$

Equating the coefficients of $\sin \omega t$ and of $\cos \omega t$, we obtain

$$C(Ka, \theta) - \frac{X(\theta)}{G} A(Ka) = 0 ,$$

$$D(Ka, \theta) - \frac{X(\theta)}{G} B(Ka) = 0 .$$

Substitution of the definitions of A, B, C, and D and introduction, for convenience, of the notation

$$f_{2m}(Ka, \theta) = \frac{X}{G} \gamma_{2m\pi/2} - \gamma_{2ma}, \quad m=1,2,3,\dots,$$

$$g_{2m}(Ka, \theta) = \frac{X}{G} \gamma_{2m\pi/2}^w - \gamma_{2ma}^w, \quad m=1,2,3,\dots,$$

leads to the two equations

$$+ \sum_{m=1}^{\infty} p_{2m} f_{2m} - \sum_{m=1}^{\infty} q_{2m} g_{2m} = \gamma_{ca} - \frac{X}{G} \gamma_{c\pi/2},$$

$$+ \sum_{m=1}^{\infty} p_{2m} g_{2m} + \sum_{m=1}^{\infty} q_{2m} f_{2m} = \gamma_{sa} - \frac{X}{G} \gamma_{s\pi/2}.$$

These two equations display the roles of $p_{2m}(ka)$ and $q_{2m}(Ka)$ as expansion coefficients. In a given example the coefficients can in principle be evaluated. In practical calculations some sufficient finite number of coefficients can be found by the approximation methods employed for expansions in non-orthogonal functions, as in the sample calculations given later.

In the special case of fluid of infinite depth, $g_{2m}(Ka, \theta)$ is identically zero.

3.6 The Ratio of Waveheight to Oscillation Amplitude.

We return to the expression for the normal velocity condition evaluated at $\beta = \theta = \pi/2$ given above.

$$\frac{gh_w}{\pi\omega J} (A \cos \omega t + B \sin \omega t) = - \frac{dy}{dt} (aG)$$

$$= \omega h_0 b \sin(\omega t + \epsilon).$$

The trigonometric expansion for $\sin(\omega t + \epsilon)$ leads to

$$A = \frac{\omega^2 b}{g} \frac{h_o}{h_w} \pi J \sin \epsilon .$$

$$B = \frac{\omega^2 b}{g} \frac{h_o}{h_w} \pi J \cos \epsilon .$$

These give, respectively, by division and addition after squaring,

$$\epsilon = \tan^{-1} \frac{A}{B} ,$$

$$\frac{h_w}{h_o} = \frac{Kb \pi J}{\sqrt{A^2 + B^2}} .$$

The first result defines the previously-unspecified phase angle ϵ of the motion. The second gives the ratio of the height at infinity of the generated progressive waves to the oscillation amplitude.

3.7 Pressure on the Cylinder Surface.

Gauge pressure at a point on the cylinder surface with reference to the constant pressure p_o on the free surface is

$$(P - p_o) = \rho g y - \rho \frac{\partial \phi}{\partial t}$$

from the linearized form of Bernoulli's equation. The first term on the right contributes a hydrostatic pressure due to the location of the point at rest,

$$y = aY ,$$

and a fluctuation of the hydrostatic pressure due to vertical motion

$$\rho g h_o \cos(\omega t + \epsilon) .$$

The hydrodynamic pressure is

$$p(Ka, \theta, t) = -\rho \frac{\partial \varphi}{\partial t}$$

$$= \frac{\rho g h_w}{\pi F} [-M \cos \omega t + N \sin \omega t]$$

where we have used the notation for the potential φ introduced in Section 3.4 and $M(Ka, \theta)$, $N(Ka, \theta)$ are to be evaluated at the point on the cylinder of interest.

The acceleration of the given motion

$$y = h_0 \cos(\omega t + \varepsilon)$$

$$= \frac{h_0}{\sqrt{A^2 + B^2}} (B \cos \omega t - A \sin \omega t)$$

is

$$\frac{dy}{dt} = \frac{\omega^2 h_0}{\sqrt{A^2 + B^2}} (A \sin \omega t - B \cos \omega t).$$

The hydrodynamic pressure p is resolved into components in phase with the acceleration and with the vertical velocity:

$$p(Ka, \theta, t) = \frac{\rho g h_w}{\pi F} \frac{MB + NA}{A^2 + B^2} (A \sin \omega t - B \cos \omega t) +$$

$$+ \frac{\rho g h_w}{\pi F} \frac{MA - NB}{A^2 + B^2} (-A \cos \omega t - B \sin \omega t).$$

After substituting for the waveheight h_w , this may be written

$$p = \rho b \frac{MB + NA}{A^2 + B^2} \ddot{y} + \rho b \frac{MA - NB}{A^2 + B^2} \omega \dot{y}$$

or in units of the hydrostatic fluctuation $\rho g h_0$,

$$\frac{p}{\rho g h_0} = K_b \frac{MB + NA}{A^2 + B^2} \frac{\frac{y}{h_0}}{\omega^2 h_0} + K_b \frac{MA - NB}{A^2 + B^2} \frac{\frac{y}{h_0}}{\omega h_0},$$

where $M(Ka, \theta)$, $N(Ka, \theta)$ are evaluated for the location of interest.

The total change in fluid pressure must include the fluctuation in hydrostatic pressure due to vertical motion. This may be added in normalized form y/h_0 to the above expression to give the total. Examples for specific cylinders are given later.

3.8 The Vertical Force Required to Sustain Oscillations.

One part of the vertical force is that opposing the resultant of the hydrodynamic pressure. This is called the hydrodynamic force. The hydrodynamic force per unit cylinder length is found by integrating the vertical component of the hydrodynamic pressure acting on an element of area.

$$dF = p(Ka, \theta, t) \cos \alpha ds.$$

After substituting $\cos \alpha = \partial x / \partial s$ and also

$$\begin{aligned} \frac{\partial x}{\partial s} ds &= dx = a \left[\rho_0 \cos \theta + \sum_{n=0}^N (-1)^n \frac{(2n+1)a_{2n+1}}{\rho_0} \cos (2n+1)\theta \right] d\theta \\ &= aW(\theta)d\theta \end{aligned}$$

in the form

$$dx = b \frac{W(\theta)}{G} d\theta$$

where $b = aG$ is the half-beam at the free surface, the force becomes

$$F = 2b \int_0^{\pi/2} p(Ka, \theta, t) \frac{W(\theta)}{G} d\theta .$$

Recalling the notation for the pressure introduced in the last section, one may express this in the form

$$F = \frac{2\rho g h_w b}{\pi J} (N_0 \sin \omega t - M_0 \cos \omega t)$$

where

$$M_0(Ka) = \int_0^{\pi/2} M(Ka, \theta) \frac{W(\theta)}{G} d\theta ,$$

$$N_0(Ka) = \int_0^{\pi/2} N(Ka, \theta) \frac{W(\theta)}{G} d\theta .$$

The hydrodynamic force is resolved following the procedure of the preceding section,

$$F(Ka, t) = \frac{2\rho g h_w b}{\pi J} \frac{M_0 B + N_0 A}{A^2 + B^2} (A \sin \omega t - B \cos \omega t) \\ + \frac{2\rho g h_w b}{\pi J} \frac{M_0 A - N_0 B}{A^2 + B^2} (-A \cos \omega t - B \sin \omega t) .$$

Substituting for the waveheight h_w , one finds

$$F = 2\rho b^2 \frac{M_0 B + N_0 A}{A^2 + B^2} \eta + 2\rho b^2 \frac{M_0 A - N_0 B}{A^2 + B^2} \omega \eta' .$$

It is convenient to normalize the hydrodynamic force in units of the change of hydrostatic force (naval architectural "tons-per-inch immersion").

$$\frac{F}{2\rho g b h_0} = Kb \frac{M_0 B + N_0 A}{A^2 + B^2} \left(\frac{\eta'}{\omega h_0} \right) + Kb \frac{M_0 A - N_0 B}{A^2 + B^2} \left(\frac{\eta}{\omega h_0} \right) .$$

The total force fluctuation is found by adding the normalized buoyancy change, y/h_0 , and of course account must be taken of the inertia of the mass of the body and net buoyancy at the rest position.

3.9 The Added-Mass and Damping Coefficients.

Since the fluid motion, and thus the pressure on the cylinder surface and the vertical force, is periodic, it is meaningful to define added-mass and damping coefficients and they will not be functions of time, i.e. of the past history of the motion.

3.9.1 The Added Mass and Added-Mass Coefficient.

The added mass is the ratio of the hydrodynamic force in phase with the acceleration to the acceleration

$$m = \frac{\pi}{2} b^2 \rho \frac{4}{\pi} \frac{M_0 B + N_0 A}{A^2 + B^2} .$$

The asymptotic value of the added mass for large Kb in the special case of infinitely deep fluid is given in Section 4.4.

It is convenient in this problem to define an added-mass coefficient as the ratio of the added mass m to the mass of the fluid displaced by a circular cylinder of equal beam.

$$\frac{m}{\frac{\pi}{2} b^2 \rho} = \frac{4}{\pi} \frac{M_0 B + N_0 A}{A^2 + B^2} .$$

To normalize the added mass with units of the actual displaced fluid mass, one may use the volume of the cylinder per unit length,

$$V = \frac{\pi}{2} \frac{b^2}{g^2} \left[\rho_0^2 - \sum_{n=0}^N \frac{(2n+1) (a_{2n+1})^2}{\rho_0 (2n+1)^2} \right],$$

so that the ratio of the added mass to the mass of the displaced fluid is

$$\frac{m}{\rho V} = \frac{\frac{\pi b^2}{2}}{V} \frac{1}{\pi} \frac{M_c B + N_o A}{A^2 + B^2}.$$

The coefficient defined in this manner is inconvenient for the case of a flat plate oriented perpendicular to the motion. In this case $V = 0$; however, the added mass is still defined and finite.

3.92 The Radiated Energy and the Damping Coefficient.

An energy balance must exist between the average rate of work done in one cycle of vertical motion and the average energy flux radiated by the outward-going surface waves. The average rate of work done over one period T is

$$c \omega h_0^2 / T$$

where c is the factor of proportionality for the component of hydrodynamic force in phase with the velocity,

$$F_y = c(dy/dt).$$

The average energy flux per unit width of periodic outgoing waves on two sides is

$$\frac{1}{2} h_0^2 \rho g \frac{\omega}{K}.$$

Therefore,

$$c = \left(\frac{h_w}{h_o} \right)^2 \frac{\rho g^2}{\omega^3} = \pi b^2 \rho \frac{2\pi J^2}{A^2 + B^2} \omega .$$

When this is compared with the results in Section 3.8,

$$M_o A - N_o B = \pi^2 J^2 / 2 .$$

This is useful for checking numerical calculations and simplifies the expression for the component of vertical force in phase with the motion velocity,

$$F_v = 2\rho b^2 \frac{(\pi^2 J^2 / 2)}{A^2 + B^2} \omega y' .$$

The ratio

$$\frac{F_v}{\frac{\pi}{2} b^2 \rho} = \frac{2\pi J^2}{A^2 + B^2} \omega y'$$

leads to the convenient use of

$$\frac{2\pi J^2}{A^2 + B^2}$$

as a damping-force coefficient. If the added-mass coefficient is referred to the actual mass of fluid displaced by the volume V , the corresponding definition of the damping-force coefficient is

$$\frac{F_v}{\rho V \cdot \omega y'} = \frac{\frac{\pi}{2} b^2}{V} \frac{2\pi J^2}{A^2 + B^2} .$$

IV. The Special Case of Infinite Fluid-Depth

The case of a fluid of infinite depth deserves special mention. An important reason is that the expansion to satisfy the normal-velocity boundary condition on the cylinder can be done with different functions. A second purpose is to summarize the simplified definitions. Finally, with respect to the added-mass coefficient, a correction factor accounting for free surface effects is readily defined. For practical calculations, this case is simpler and is of interest since the infinite-depth results are approached rapidly with increasing depth ratio.

4.1 Special Definition of the Multipole Potential $\bar{\varphi}_{2m}$.

The multipole potential which may be used in case $h = \infty$ is designated by $\bar{\varphi}_{2m}$ and defined by

$$\bar{\varphi}_{2m} = \frac{\cos 2m\theta}{\rho^{2m}} + Ka \left[\frac{\cos(2m-1)\theta}{(2m-1)\rho^{(2m-1)}} + \sum_{n=0}^N (-1)^n \frac{(2n+1)a_{2n+1} \cos(2m+2n+1)\theta}{(2m+2n+1)\rho^{(2m+2n+1)}} \right].$$

This replaces $\varphi_{2m}^i(r, \beta)$ and since $\bar{\varphi}_{2m} \rightarrow 0$ as $h \rightarrow \infty$, there need be no counterpart to $\varphi_{2m}''(x, y, h)$. It is evident that $\bar{\varphi}_{2m}$ vanishes for $|x| \rightarrow \infty$ and thus has no role in satisfying the radiation boundary condition. It is consistent that $\varphi_{2m}^w = 0$ for this case. It is shown below that $\bar{\varphi}_{2m}$ satisfies the free-surface condition.

The free-surface condition

$$K\varphi + \frac{\partial \varphi}{\partial y} = 0, \quad \theta = \pm \pi/2, \quad |x| \geq b,$$

can be written

$$K\varphi + \frac{1}{(\partial y / \partial \theta)} \frac{\partial \varphi}{\partial \theta} = 0$$

by noting that $\partial x / \partial \theta = 0$ when $\theta = \pm \pi/2$. With

$$\begin{aligned} \frac{\partial y}{\partial \theta} &= -a \left[\rho \sin \theta + \sum_{n=0}^N (-1)^{n+1} \frac{(2n+1)a_{2n+1}}{\rho^{2n+1}} \sin(2n+1)\theta \right] \\ &= \mp \left[\rho - \sum_{n=0}^N (2n+1)a_{2n+1} \frac{1}{\rho^{2n+1}} \right], \quad \theta = \pm \pi/2 \end{aligned}$$

the free-surface condition is

$$Ka \left[\rho - \sum_{n=0}^N (2n+1) \frac{a_{2n+1}}{\rho^{2n+1}} \right] \varphi + \frac{\partial \varphi}{\partial \theta} = 0, \quad \theta = \pm \pi/2, |x| \geq b.$$

Simple substitution paralleling Section 3.31(a) demonstrates that

$\bar{\varphi}_{2m}$, like $\varphi'_{2m}(r, \beta)$, satisfies the free-surface condition for all m, n .

The corresponding stream function is

$$\bar{\gamma}_{2m} = \frac{\sin 2m\theta}{\rho^{2m}} + Ka \left[\frac{\sin(2m-1)\theta}{(2m-1)\rho^{2m-1}} + \sum_{n=0}^N (-1)^n \frac{(2n+1)a_{2n+1}}{(2m+2n+1)} \frac{\sin(2m+2n+1)\theta}{\rho^{2m+2n+1}} \right].$$

The stream function evaluated on the cylinder is used in satisfying the normal velocity condition. The part $\bar{\gamma}_{2m}^{\text{body}}$ is designated $\bar{\gamma}_{2ma}$, as before, and at $\theta = \pi/2$,

$$\bar{\gamma}_{2ma, \pi/2} = Ka(-1)^{m-1} \left[\frac{1}{(2m-1)\rho_0^{2m-1}} - \sum_{n=0}^N \frac{(2n+1)a_{2n+1}}{(2m+2n+1)\rho_0^{2m+2n+1}} \right].$$

4.2 The Source Potential and the Complete Potential Solution.

The definition of the combined source and standing wave

potential $(\varphi_c \cos \omega t + \varphi_s \sin \omega t)$ remains as in Sections 3.33, 3.34, where it was written for the special case as

$$\left[\pi \varepsilon^{-Ky} \sin Kx - \int_0^{\infty} \frac{\varepsilon^{-mx} (m \cos my - K \sin my)}{m^2 + K^2} dm \right] \sin \omega t + \\ + \pi \varepsilon^{-Ky} \cos Kx \cos \omega t .$$

The conjugate stream function $\gamma_s \sin \omega t + \gamma_c \cos \omega t$ is

$$\left[-\pi \varepsilon^{-Ky} \cos Kx + \int_0^{\infty} \frac{\varepsilon^{-mx} (m \sin my + K \cos my)}{m^2 + K^2} dm \right] \sin \omega t + \\ + \pi \varepsilon^{-Ky} \sin Kx \cos \omega t .$$

For this case the potential and stream functions equivalent to those given in Section 3.4 are

$$\frac{\varphi}{\gamma} = \frac{h_w g}{\pi \omega} \left[\left(\frac{\varphi_c}{\gamma_c} + \sum_{m=1}^{\infty} p_{2m} \frac{\bar{\varphi}_{2m}}{\gamma_{2m}} \right) \cos \omega t + \left(\frac{\varphi_s}{\gamma_s} + \sum_{m=1}^{\infty} q_{2m} \frac{\bar{\varphi}_{2m}}{\gamma_{2m}} \right) \sin \omega t \right] .$$

The expansion coefficients $p_{2m}(Ka)$, $q_{2m}(Ka)$ are to be evaluated below following the procedure of Section 3.5.

4.3 Evaluating the Expansion Coefficients.

The normal-velocity boundary condition on the cylinder surface is used to evaluate the expansion coefficients. Since $\gamma(\rho_0) = - (dy/dt)x(\rho_0)$, the two equations

$$C(Ka, \Theta) - \frac{X(\Theta)}{G} A(Ka) = 0 ,$$

$$D(Ka, \Theta) - \frac{X(\Theta)}{G} B(Ka) = 0$$

are found as before, but now with

$$A(Ka) = \gamma_{ca\pi/2} + \sum_{m=1}^{\infty} p_{2m} \bar{\gamma}_{2m\pi/2} = C(Ka, \pi/2) ,$$

$$B(Ka) = \gamma_{sa\pi/2} + \sum_{m=1}^{\infty} q_{2m} \bar{\gamma}_{2m\pi/2} = D(Ka, \pi/2) ,$$

$$C(Ka, \theta) = \gamma_{ca} + \sum_{m=1}^{\infty} p_{2m} \bar{\gamma}_{2ma} ,$$

$$D(Ka, \theta) = \gamma_{sa} + \sum_{m=1}^{\infty} q_{2m} \bar{\gamma}_{2ma} .$$

With these definitions, the expansion equations are

$$\sum_{m=1}^{\infty} p_{2m} \bar{f}_{2m} = \gamma_{ca} - \frac{X(\theta)}{G} \gamma_{ca\pi/2} ,$$

$$\sum_{m=1}^{\infty} q_{2m} \bar{f}_{2m} = \gamma_{sa} - \frac{X(\theta)}{G} \gamma_{sa\pi/2} ,$$

where \bar{f}_{2m} is now given by

$$\bar{f}_{2m}(Ka, \theta) = \frac{X(\theta)}{G} \bar{\gamma}_{2m\pi/2} - \bar{\gamma}_{2ma}(Ka, \theta) .$$

This is the set of expansion functions which may be used in the infinite-depth case to replace the equivalent unbarred set.

Completion of the problem and the results are identical in form with the corresponding steps in the general case.

4.4 Asymptotic Value for the Added Mass and Definition of the Free-Surface Correction.

The added mass is the same as in Section 3.91,

$$m = \frac{\pi}{2} b^2 \rho \frac{4}{\pi} \frac{M_c B + N_c A}{A^2 + B^2} .$$

The asymptotic value of the added mass for large Kb (in this case of infinitely deep fluid) is

$$m_{\infty} = \frac{\pi b^2 \rho}{2 G^2} \left[\left(\rho_0 + \frac{a_1^2}{\rho_0} \right) + \sum_{n=1}^N \frac{(2n+1)(a_{2n+1})^2}{\rho_0 (2n+1)^2} \right],$$

which may be found in a manner following Landweber and Macagno [1957].

We recall that the origin of the result called m_{∞} here is in the work of Lewis [1929]. The ratio of the asymptotic value m_{∞} to the mass of the fluid displaced by a circular cylinder of equal beam, $\pi b^2 \rho / 2$, is the inertia-coefficient C of Lewis [1929] or the added-mass coefficient C_v of Landweber and Macagno [1957, 1959].

The ratio of the added mass m to its asymptotic value m_{∞} defines a free-surface correction factor that is a function of the non-dimensional frequency Kb only.

$$k_4 = \frac{m}{m_{\infty}} \frac{(\pi b^2 \rho / 2)}{m_{\infty}} \frac{4}{\pi} \frac{M_0 B + N_0 A}{A^2 + B^2}.$$

The value of m_{∞} for an elliptic cylinder is $\pi b^2 \rho / 2$, from the definition above. Therefore, in the special case of elliptic cylinders (including the circular cylinder), the free-surface correction factor k_4 is numerically equal to the added-mass coefficient defined as the ratio of the added mass to the mass of the fluid displaced by a circular cylinder of equal beam.

Examples of the free-surface correction factor k_4 were calculated for various cylinders and are presented in Part B of this work.

The approach used to define k_4 could be used to define a correction factor for the free-surface effect on the added mass of cylinders in fluid of finite depth but the asymptotic value m_∞ for the case of finite depth is not yet simply expressed.

A first-order approximation of the added mass m for elliptic cylinders valid for $Kb \Rightarrow 0$ is given by Ursell [1949] for the infinite-depth case:

$$m = \frac{4}{\pi} \rho b^2 \left[-\log_e Kb - \log_e \left(1 + \frac{d}{b} \right) + 0.23 \right] .$$

Here d is the draft, $y(\beta=0)$, and b remains the half-beam, $x(\beta=\pi/2)$. It appears from various calculations that this is a useful approximation for other than elliptic cylinders, but this is not established as a theorem.

PART B. Numerical Analysis and Results of Sample Calculations.

V. The Circular Cylinder in Infinitely Deep Fluid

The principle objective of the first sample calculations was to provide the calculated pressure distribution on the surface of a circular cylinder in fluid of infinite depth. In addition, the added-mass and damping coefficients were calculated. These coefficients were calculated by Ursell and the present calculation confirms his results and extends the range of the frequency variable. Our method of calculating the expansion coefficients $p_{2m}(Ka)$, $q_{2m}(Ka)$ and of finding the added mass coefficients is notably different.

The calculations were done on the IBM 704 digital computer at the Computer Center, University of California, Berkeley.

5.1 Calculation of the Expansion Coefficients.

5.11 Choice of Method.

The definitions of most of the functions required in the calculation of this case are simplified. The mapping is trivial: all a_{2n+1} are zero, and $\rho_0 = 1$ is convenient in that the unit circle in the reference plane corresponds to a cylinder of radius a . The angular coordinates are equal, $\beta = \theta$. The specially defined $\bar{\varphi}_{2m}$ of Chapter IV is identical with the general case φ_{2m} of Chapter III.

We will use δ for the frequency parameter (here Ka) in all numerical calculations.

The expansion equations of Section 4.3 become in this case

$$\sum_{m=1}^{\infty} p_{2m}(\delta) f_{2m}(\delta, \theta) = \gamma_{ca}(\delta, \theta) - \sin \theta \gamma_{ca}(\delta, \pi/2)$$

$$\sum_{m=1}^{\infty} q_{2m}(\delta) f_{2m}(\delta, \theta) = \gamma_{sa}(\delta, \theta) - \sin \theta \gamma_{sa}(\delta, \pi/2),$$

where

$$X(\theta) = \sin \theta, \quad Y(\theta) = \cos \theta,$$

$$X(\pi/2) = G = 1,$$

$$\gamma_{ca}(\delta, \theta) = \pi \varepsilon^{-\delta \cos \theta} \sin(\delta \sin \theta),$$

$$\gamma_{sa}(\delta, \theta) = \varepsilon^{-\delta \cos \theta} \left[(\underline{\gamma} + \log_{\varepsilon} \delta + \sum_{n=1}^{\infty} \frac{\delta^n}{n!n} \cos n\theta) \sin(\delta \sin \theta) - \right. \\ \left. (\theta + \sum_{n=1}^{\infty} \frac{\delta^n}{n!n} \sin n\theta) \cos(\delta \sin \theta) \right],$$

$$f_{2m}(\delta, \theta) = -\sin 2m\theta - \frac{\delta}{(2m-1)} [\sin(2m-1)\theta - (-1)^{m-1} \sin \theta].$$

We have substituted a form of $\gamma_{sa}(\delta, \theta)$ from Appendix A-3.4. A method must be chosen to find $p_{2m}(\delta)$, $q_{2m}(\delta)$ from the expansion equations for $m=1, 2, 3, \dots$, their computation being terminated in practice at some finite \bar{m} . The first method chosen was to generate \bar{m} simultaneous linear equations each for $p_{2m}(m=1, 2, \dots, \bar{m})$ and $q_{2m}(m=1, 2, \dots, \bar{m})$ by proceeding as follows. Each expansion equation was multiplied by $\sin k\theta d\theta$ and $\cos j\theta d\theta$ with $k=1, 2, 3, \dots$ and $j=0, 1, 2, \dots$ terminating at \bar{k} , $(\bar{j}-1)$ so that $\bar{m} = \bar{k} + \bar{j}$. The \bar{m} equations (each for p_{2m} , q_{2m}) were integrated over the interval $0 \leq \theta \leq \pi/2$. This will be called the "method of integration." The \bar{m} equations were solved for \bar{m} values p_{2m} , q_{2m} by the Gauss elimination procedure. Yu [1960] used the method of integration but with $\cos r\theta$, $r=1, 2, 3, \dots, \bar{m}$ as the only multiplier in his calculations.

The second method used for sample calculations was to generate \bar{m} simultaneous linear equations from each expansion equation by evaluating each at more-or-less arbitrarily chosen angles θ_i in the range $0 < \theta_i < \pi/2$ with $i=1,2,3,\dots,\bar{m}$. Ursell [1949] and Tasai [1960] chose to take values $m=1,2,3,\dots,m_0$ with $m_0 < \bar{m}$ so that m_0 values of p_{2m} , q_{2m} could be found from \bar{m} simultaneous equations by the method of least squares to satisfy the truncated expansion equations at $\theta = \theta_i$ in the least-squares sense. In the sample calculations reported here the \bar{m} equations were solved directly by the Gauss elimination process for \bar{m} expansion coefficients. This will be called the "discrete-angle" method.

In all cases the calculated expansion coefficients were tested by substituting them in the left-hand side of the basic expansion equations (Section 5.11) and comparing this result with the calculated right-hand side at various values of $\theta = \theta_t$. This calculation was printed from the computer with five significant figures. In the case of the calculations by the discrete-angle method, test values $\theta = \theta_t$ that equal the discrete-angles θ_i lead to exact agreement and gave proof the matrix was properly inverted. For interstitial θ_t , the difference in right- and left-hand sides is an accuracy index not generally zero. This index would not, in general, be zero for any $0 < \theta_t < \pi/2$ in the case of expansion coefficients calculated by the method of integration from integrated equations and substituted into the basic expansion equations.

An example of this index for various calculations at $\delta = 1$ and $\theta_t = 20^\circ, 80^\circ$ follows. In these calculations by the discrete-angle method the nearest θ_i differed from θ_t by at least five degrees.

The tabular entry is $\frac{|RHS - LHS|}{RHS} \times 100\%$

Method: Discrete-angle. Integration.

\bar{m} : 6 9 6 8

for $p_{2m}(1)$:

$\theta_t = 20^\circ$ 1.52% 0.045 0.49 0.24

80° 0.75 0.51 0.83 0.89

for $q_{2m}(1)$:

$\theta_t = 20^\circ$ 4.37% 0.13 1.38 0.60

80° 1.6 1.1 1.79 0.42

Another index used to test the calculations is reported in Section 5.22.

5.12 Form of the Equations for Calculation.

The expansion equations used in the method of integration are as follows:

for p_{2m} :

$$\sum_{m=1}^{\bar{m}} p_{2m}(\delta) \int_0^{\pi/2} f_{2m}(\delta, \theta) \frac{\sin k\theta}{\cos j\theta} d\theta = \int_0^{\pi/2} \gamma_{ca}(\delta, \theta) \frac{\sin k\theta}{\cos j\theta} d\theta$$

$$= \int_0^{\pi/2} \gamma_{ca}(\delta, \pi/2) \sin \theta \frac{\sin k\theta}{\cos j\theta} d\theta$$

$$k=1, 2, 3, \dots, \bar{k}$$

$$j=0, 1, 2, \dots, (\bar{j}-1)$$

$$\bar{m} = \bar{k} + \bar{j}.$$

for q_{2m} :

$$\sum_{m=1}^{\overline{m}} q_{2m}(\delta) \int_0^{\pi/2} f_{2m}(\delta, \theta) \frac{\sin k\theta}{\cos j\theta} d\theta = \int_0^{\pi/2} \gamma_{sa}(\delta, \theta) \frac{\sin k\theta}{\cos j\theta} d\theta -$$

$$- \int_0^{\pi/2} \gamma_{sa}(\delta, \pi/2) \frac{\sin \theta}{\cos j\theta} d\theta$$

$$k=1, 2, 3, \dots, \overline{k}$$

$$j=0, 1, 2, \dots, (\overline{j}-1)$$

$$\overline{m} = \overline{k} + \overline{j}.$$

All integrations in these equations were reduced to the form of rapidly converging series or to algebraic results, before doing machine calculations. The forms used are given in Appendix A-3; the integrals on the right-hand side are not widely published.

The expansion equations used in the discrete-angle method are given in Section 5.11, above.

5.2 The Principal Dependent Variables.

5.21 The Results for $A(\delta)$, $B(\delta)$.

The dependent variables $A(\delta)$ and $B(\delta)$ are calculated from:

$$A(\delta) = \sum_{m=1}^{\overline{m}} p_{2m}(\delta) \gamma_{2ma}(\delta, \pi/2) + \gamma_{ca}(\delta, \pi/2)$$

$$= \delta \sum_{m=1}^{\overline{m}} \frac{(-1)^{m-1}}{2^{m-1}} p_{2m}(\delta) + \pi \sin \delta$$

$$B(\delta) = \sum_{m=1}^{\overline{m}} q_{2m}(\delta) \gamma_{2ma}(\delta, \pi/2) + \gamma_{sa}(\delta, \pi/2)$$

$$= \delta \sum_{m=1}^{\overline{m}} \frac{(-1)^{m-1}}{2^{m-1}} q_{2m}(\delta) - \left[\frac{\pi}{2} + Si(\delta) \right] \cos(\delta) + Ci(\delta) \sin(\delta).$$

The substitution for $\gamma_{sa}(\delta, \pi/2)$ employs the identity

$$\int_0^{\infty} \frac{\delta e^{-x}}{\delta^2 + x^2} dx = \left[\frac{\pi}{2} - Si(\delta) \right] \cos(\delta) + Ci(\delta) \sin(\delta),$$

where $Si(\delta)$ and $Ci(\delta)$ are the sine and cosine integrals and are available in tabulated or series form.

The quantities $A(\delta)$ and $B(\delta)$ in the form $A^2 + B^2$ are useful for interpolation of the added-mass and damping coefficients, as pointed out by Ursell [1957]. The phase angle of the motion $\epsilon = \tan^{-1} B(\delta)/A(\delta)$ is smoothly varying and nearly linear in δ . The results of this calculation and that of Ursell [1949] for $A(\delta)$, $B(\delta)$ are given graphically in Figures 1 and 2.

5.22 The Quantities $M(\delta, \theta)$, $N(\delta, \theta)$, and $M_0(\delta)$, $N_0(\delta)$.

The dependent variables $M(\delta, \theta)$ and $N(\delta, \theta)$ are required for the calculation of the hydrodynamic pressure distribution. They may be calculated from their definitions in Section 3.4, which in this case become:

$$\begin{aligned} M(\delta, \theta) &= \sum_{n=1}^{\infty} q_{2n}(\delta) \psi_{2na}(\delta - \theta) + \psi_{sa}(\delta - \theta) \\ &= \sum_{n=1}^{\infty} q_{2n} \left[\cos 2n\theta + \frac{\delta}{2n-1} \cos (2n-1)\theta \right] + \\ &+ \epsilon^{-\delta} \cos \theta \left[(\theta + \sum_{n=1}^{\infty} \frac{\delta^n}{n!n} \sin n\theta) \sin(\delta \sin \theta) + (\gamma + \log_e \delta + \right. \\ &\quad \left. + \sum_{n=1}^{\infty} \frac{\delta^n}{n!n} \cos n\theta) \cos(\delta \sin \theta) \right], \end{aligned}$$

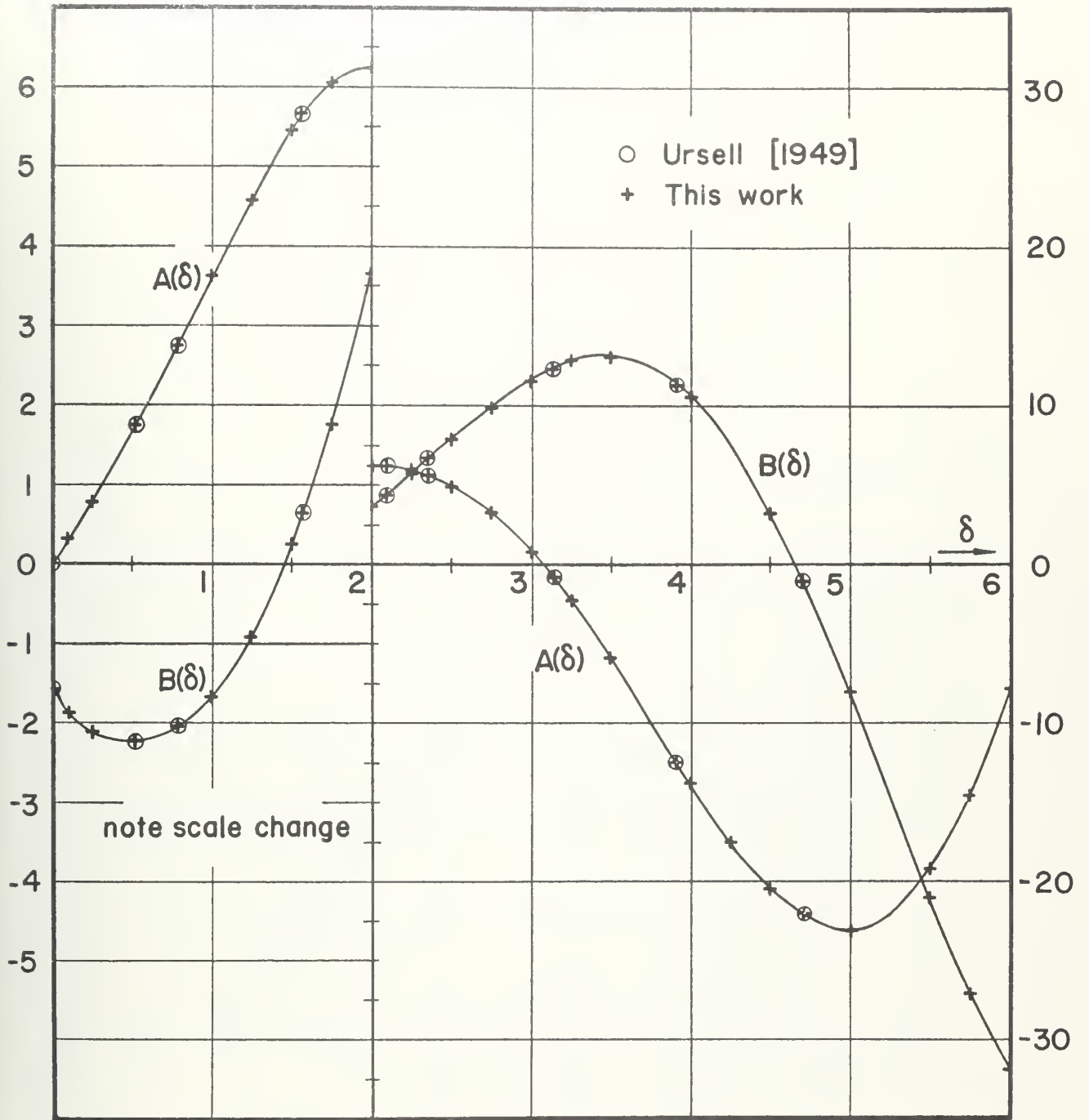


FIGURE 1. THE FUNCTIONS $A(\delta)$ and $B(\delta)$

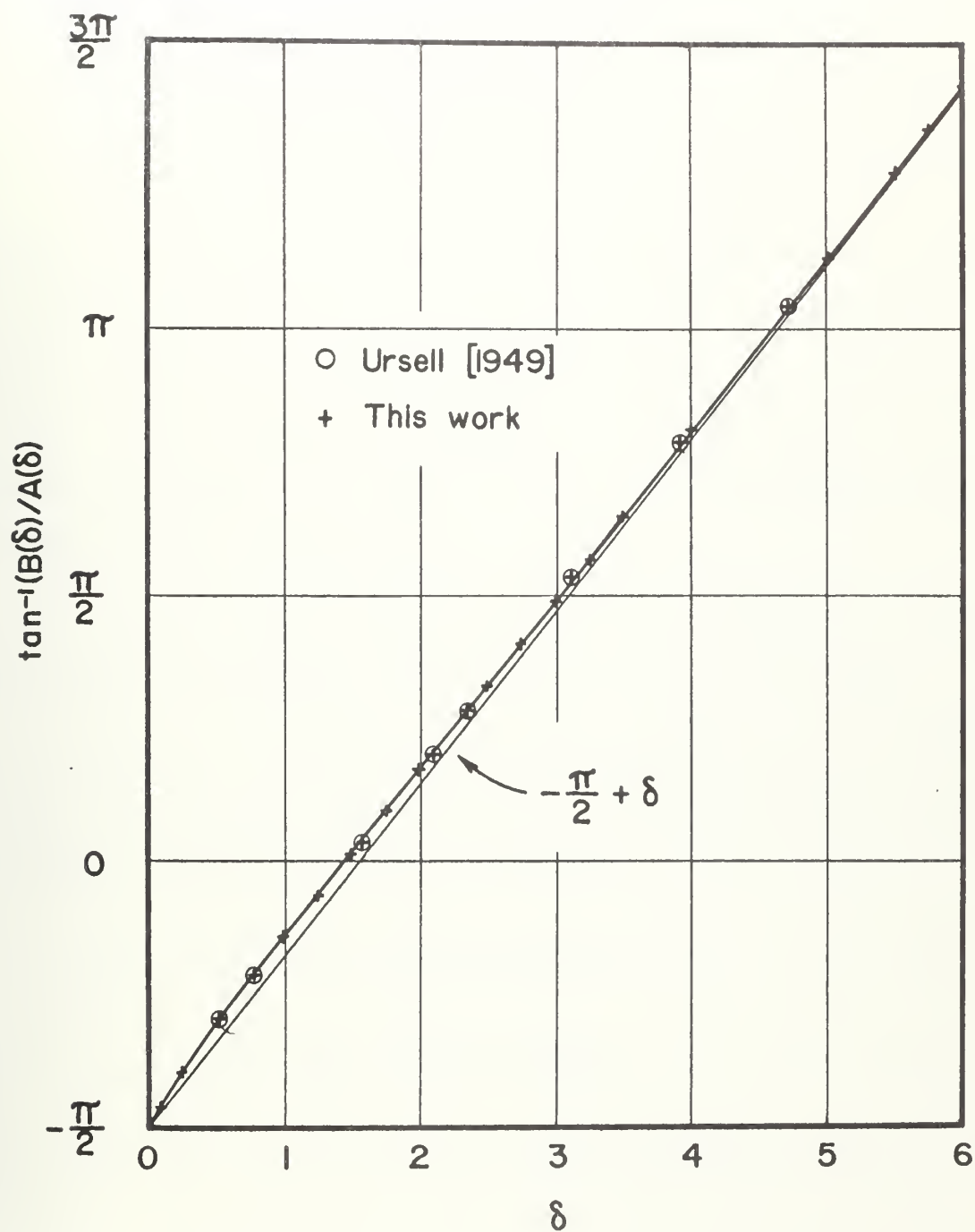


FIGURE 2. THE FUNCTION $\tan^{-1}(B(\delta)/A(\delta))$

$$\begin{aligned}
 N(\delta, \theta) &= \sum_{m=1}^{\infty} p_{2m}(\delta) \varphi_{2ma}(\delta, \theta) + \varphi_{ca} \\
 &= \sum_{m=1}^{\infty} p_{2m} \left[\cos 2m\theta + \frac{\delta}{2m-1} \cos (2m-1)\theta \right] + \pi e^{-\delta \cos \theta} \cos(\delta \sin \theta).
 \end{aligned}$$

Here we have substituted the definitions of $\varphi_{ca}(\delta, \theta)$ and $\varphi_{sa}(\delta, \theta)$ from Section 4.2 and a form suitable for numerical calculation of $\varphi_{sa}(\delta, \theta)$ from Appendix A-3.4. The open-ended summations over the index n in $M(\delta, \theta)$ were automatically run to "convergence" on the digital computer, where "convergence" means the least significant digit in the floating-point calculation.

The $M(\delta, \theta)$ and $N(\delta, \theta)$ were calculated for each δ at intervals on the cylinder surface never larger than $\theta = 0^\circ(10^\circ)90^\circ$.

The values of $M(\delta, \theta)$ and $N(\delta, \theta)$ available at $\theta = 0^\circ(10^\circ)90^\circ$ were used to calculate $M_0(\delta)$ and $N_0(\delta)$ by a numerical quadrature. The defining equations are, from Section 3.8,

$$\begin{aligned}
 M_0(\delta) &= \frac{1}{G} \int_0^{\pi/2} M(\delta, \theta) W(\theta) d\theta \\
 N_0(\delta) &= \frac{1}{G} \int_0^{\pi/2} N(\delta, \theta) W(\theta) d\theta.
 \end{aligned}$$

In this case $G=1$ and $W(\theta) = \cos \theta$. It is possible in the case of the circular cylinder in infinitely deep fluid, as shown by Ursell [1949], to substitute the defining equations for $M(\delta, \theta)$, $N(\delta, \theta)$ and to simplify before calculating M_0 , N_0 . Here, however, we are concerned with the values of $M(\delta, \theta)$, $N(\delta, \theta)$ which other calculators bypassed. Using the calculated values of $M(\delta, \theta)$, $N(\delta, \theta)$ in a numerical calculation of $M_0(\delta)$, $N_0(\delta)$ gives an important check since (Section 3.92)

$$M_0 A - N_0 B = \pi^2/2 .$$

The procedure employed was to perform a Lagrangian interpolation based on the calculated values of $M(\delta, \theta)$, $N(\delta, \theta)$ at $\theta = 0^\circ(10^\circ)90^\circ$ and then to use Simpson's Rule for approximate integration of $M(\delta, \theta) W(\theta)$ and $N(\delta, \theta) W(\theta)$ with a convenient interval of θ .

The calculations were tested at each δ by computing $M_0(\delta)A(\delta) - N_0(\delta)B(\delta)$ and observing the percentage deviation of the calculated value from $\pi^2/2$. Curves plotted through error index points are shown in Figure 3 as a function of the frequency parameter for sample calculations with six and nine expansion coefficients (each) $p_{2m}(\delta)$, $q_{2m}(\delta)$. At higher values of δ , seventeen expansion coefficients were calculated by the discrete-angle method.

5.3 Hydrodynamic Pressure Distribution on the Cylinder Surface.

The hydrodynamic pressure at the location θ on the cylinder surface in units of the hydrostatic fluctuation is (Section 3.7)

$$\begin{aligned} \frac{p(\delta, \theta)}{\rho g h_0} = & \delta \frac{M(\delta, \theta)B(\delta) + N(\delta, \theta)A(\delta)}{A(\delta)^2 + B(\delta)^2} (\text{unit acceleration}) + \\ & + \delta \frac{M(\delta, \theta)A(\delta) - N(\delta, \theta)B(\delta)}{A(\delta)^2 + B(\delta)^2} (\text{unit velocity}) . \end{aligned}$$

This is a simple, but repetitive, algebraic calculation using the principal dependent variables. The pressure fluctuation in phase with acceleration,

$$p_a = \delta \frac{MB + NA}{A^2 + B^2} ,$$

and the pressure fluctuation in phase with the velocity,

$$p_v = \delta \frac{MA - NB}{A^2 + B^2}$$

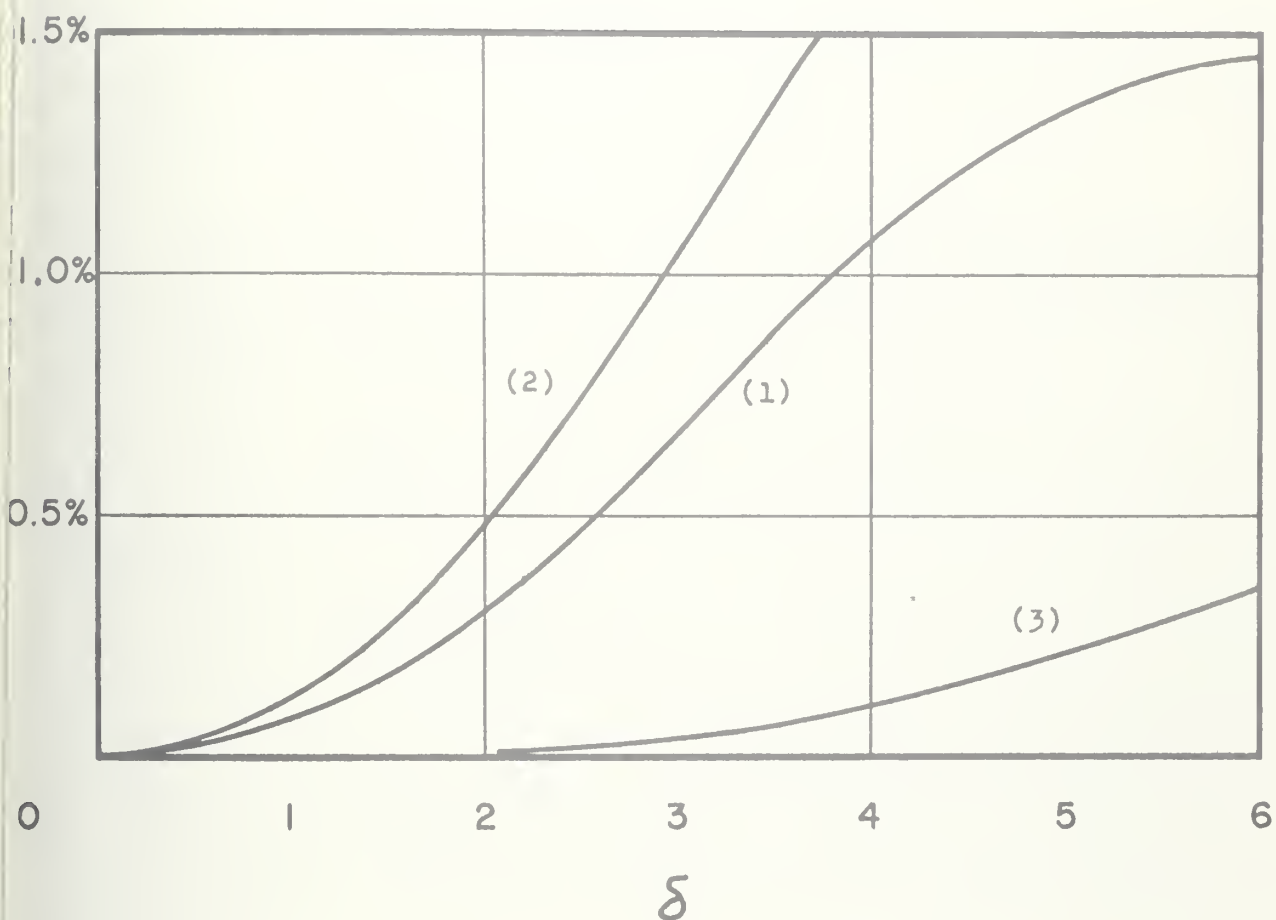


FIGURE 3. CALCULATION ERROR INDEX vs FREQUENCY.

$$\text{Index} = \frac{(M_o A - N_o B) - \pi^2/2}{\pi^2/2} \times 100\%$$

- (1) Six expansion coefficients. Method of integration.
- (2) Six expansion coefficients. Discrete angle method.
- (3) Nine expansion coefficients. Discrete angle method.

were calculated for given δ and $\theta = 0^\circ(10^\circ)90^\circ$.

Curves through calculated points of $p_a(\delta, \theta)$ and $p_v(\delta, \theta)$ are shown for example and Table I lists calculated values.

These computed values are used for a prediction of the total pressure fluctuation on the cylinder used in the experimental work reported in Part C.

It can be shown by deriving the velocity potential appropriate to the case of large δ that the angular dependence of the hydrodynamic pressure approaches $\cos \theta$, that is, for large δ

$$\frac{p(\delta, \theta)}{\rho g h_o} = \delta \cos \theta \quad (\text{unit acceleration}).$$

Therefore

$$\frac{p_a}{\delta} = \frac{MB + NA}{A^2 + B^2} \sim \cos \theta \quad \text{as } \delta \rightarrow \infty.$$

The sample calculations illustrate this since it is seen from Figure 6 p_v tends to zero and from Figure 5 that p_a/δ tends to $\cos \theta$ for large values of δ . The same result holds for any cylinder of the elliptic family.

5.4 The Added-Mass and Damping Coefficients.

The ratio of the added mass to the mass of fluid displaced by the cylinder (Section 3.91)

$$\frac{m}{\pi a^2 \rho / 2} = \frac{4}{\pi} \frac{M_o B + N_o A}{A^2 + B^2}$$

and the damping-force coefficient (Section 3.92)

$$\frac{F_v}{\pi a^2 \rho / 2} = \frac{2\pi}{A^2 + B^2}$$

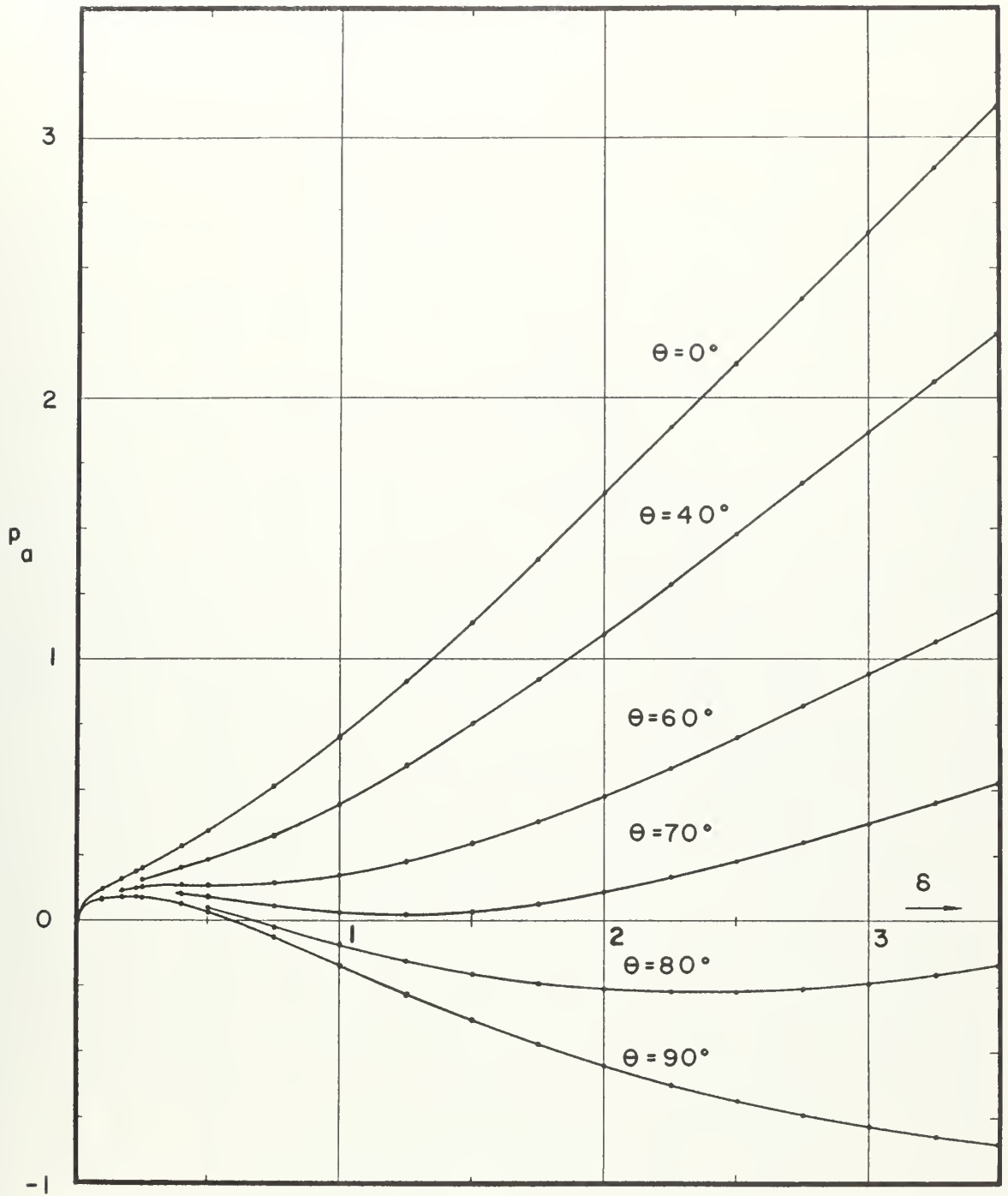


FIGURE 4. $p_a(\delta, \theta)$ FOR THE CIRCULAR CYLINDER.

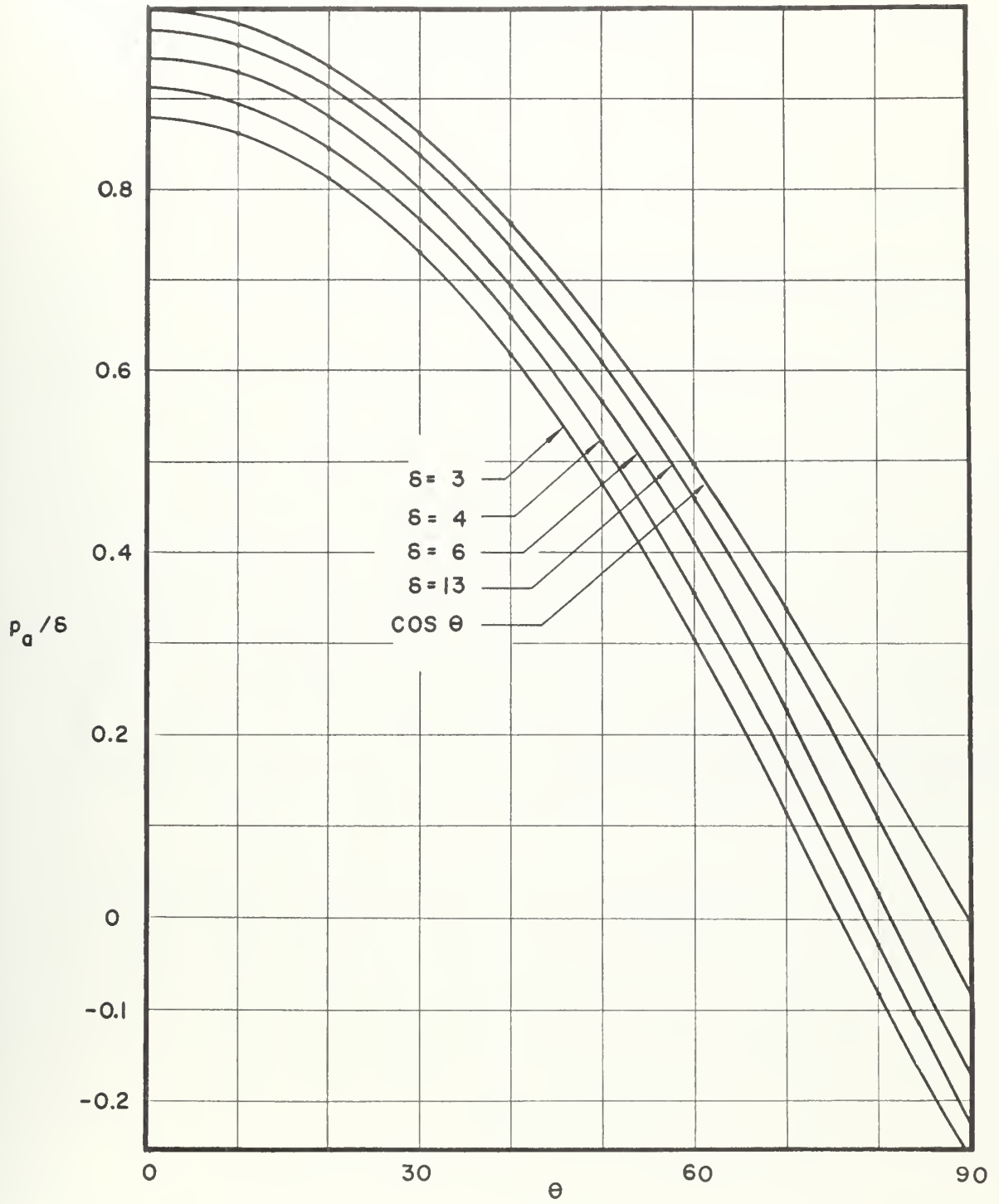


FIGURE 5. THE TREND OF p_d/s FOR LARGE s .

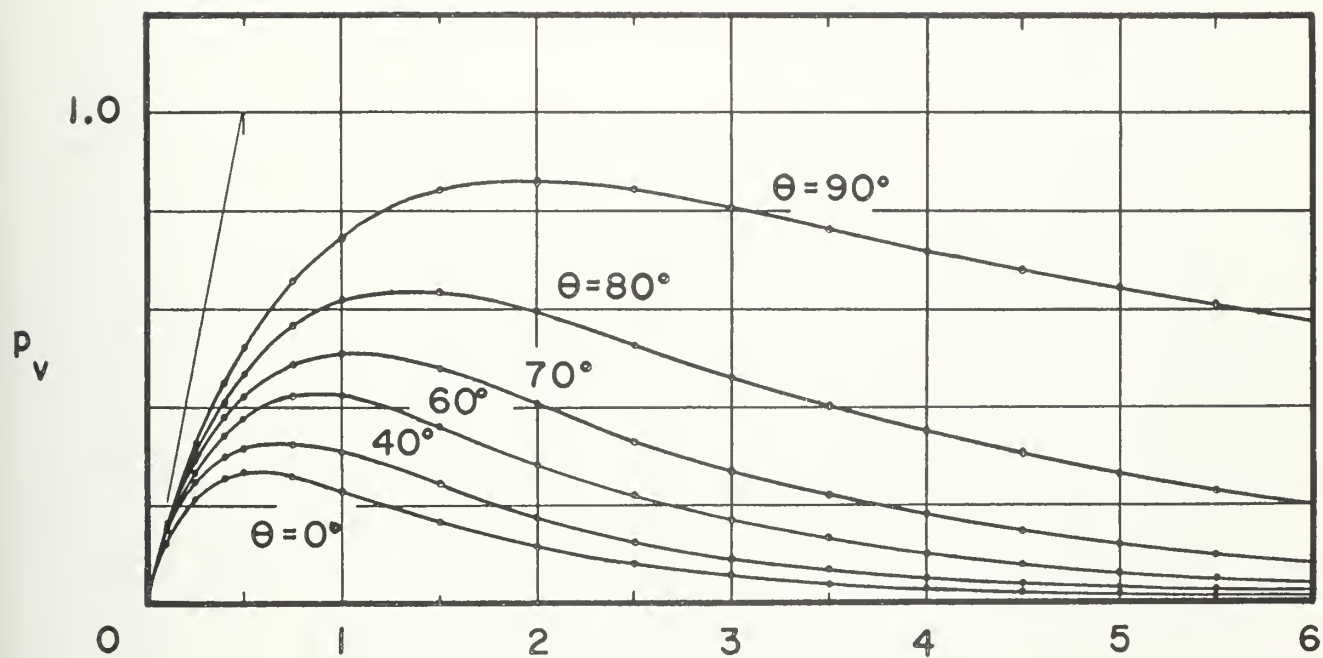


FIGURE 6. $p_v(\delta, \theta)$ FOR THE CIRCULAR CYLINDER.

TABLE I-A $p_0(6, \theta)$ FOR THE CIRCULAR CYLINDER.

$\delta \backslash \theta$	0	10	20	30	40	50	60	70	80	90
0.100	0.12	0.12	0.12	0.11	0.11	0.10	0.096	0.089	0.085	0.084
0.175	.17	.17	.16	.15	.14	.13	.12	0.11	.097	.095
0.250	.21	.20	.20	.18	.17	.15	.13	.11	.096	.092
0.400	.28	.28	.26	.24	.21	.17	.13	.10	+ .073	+ .064
0.500	.34	.33	.31	.28	.24	.19	.14	0.087	+ .049	+ .033
0.750	.51	.49	.46	.40	.33	.24	.15	+ .053	- .024	- .064
1.00	.70	.68	.63	.55	.45	.32	.17	+ .030	- .097	- .18
1.25	.92	.90	.83	.73	.59	.42	.22	+ .023	- .16	- .28
1.50	1.15	1.12	1.04	.92	.75	.53	.29	+ .036	- .21	- .38
1.75	1.39	1.36	1.27	1.12	.92	.67	.38	+ .064	- .24	- .47
2.00	1.64	1.60	1.50	1.33	1.10	.81	.48	+0.11	- .26	- .55
2.25	1.88	1.85	1.73	1.54	1.29	.96	.58	+ .16	- .27	- .62
2.50	2.14	2.10	1.97	1.76	1.48	1.12	.70	+ .22	- .27	- .68
2.75	2.39	2.34	2.21	1.98	1.67	1.28	.82	+ .29	- .26	- .74
3.00	2.64	2.60	2.45	2.20	1.86	1.44	.94	+ .37	- .24	- .78
3.25	2.90	2.85	2.69	2.42	2.06	1.61	1.06	+ .45	- .22	- .82
3.50	3.15	3.10	2.93	2.64	2.26	1.77	1.19	+ .53	- .19	- .86
3.75	3.41	3.35	3.16	2.86	2.46	1.94	1.31	+ .62	- .16	- .89
4.00	3.66	3.60	3.40	3.09	2.65	2.10	1.45	+ .70	- .13	- .92
4.50	4.17	4.10	3.88	3.53	3.04	2.43	1.71	+ .88	- .052	- .96
5.00	4.67	4.59	4.36	3.97	3.43	2.76	1.97	1.05	+ .030	- 1.00
5.50	5.17	5.09	4.83	4.41	3.82	3.09	2.23	1.23	+ .12	- 1.03
6.00	5.68	5.59	5.31	4.84	4.21	3.42	2.49	1.42	.21	- 1.05
7.00	6.69	6.58	6.25	5.72	4.99	4.08	3.00	1.78	.39	- 1.08
8.50	8.20	8.06	7.67	7.03	6.15	5.05	3.77	2.31	.67	- 1.10
10.00	9.70	9.55	9.10	8.33	7.30	6.03	4.53	2.84	.95	- 1.12
13.00	12.7	12.5	11.9	10.9	9.61	7.97	6.05	3.89	1.51	- 1.12

TABLE I-B $p_v(s, \theta)$ FOR THE CIRCULAR CYLINDER.

$s \backslash \theta$	0	10	20	30	40	50	60	70	80	90
0.100	.013	.013	.013	.013	.014	.014	.014	.015	.015	.015
0.175	.19	.19	.19	.20	.20	.21	.21	.22	.23	.24
0.250	.23	.23	.23	.24	.25	.26	.27	.29	.30	.32
0.400	.26	.27	.27	.28	.30	.32	.35	.38	.41	.45
0.500	.27	.28	.28	.30	.32	.35	.39	.42	.47	.52
0.750	.26	.27	.28	.30	.33	.37	.42	.49	.57	.66
1.00	.23	.24	.25	.27	.31	.35	.42	.51	.62	.75
1.25	.20	.20	.21	.24	.27	.32	.40	.50	.64	.81
1.50	.17	.17	.18	.20	.24	.29	.36	.48	.63	.84
1.75	.14	.14	.15	.17	.20	.25	.33	.44	.62	.86
2.00	.11	.12	.13	.14	.17	.22	.29	.41	.59	.86
2.25	0.096	0.098	.11	.12	.15	.19	.26	.37	.56	.85
2.50	.080	.082	0.088	.10	.12	.16	.22	.34	.53	.84
2.75	.067	.069	.074	0.085	.10	.14	.20	.30	.49	.82
3.00	.057	.058	.063	.072	0.089	.12	.17	.27	.46	.80
3.25	.048	.049	.053	.061	.076	.10	.15	.24	.43	.78
3.50	.041	.042	.045	.052	.065	0.087	.13	.22	.40	.76
3.75	.036	.035	.040	.047	.052	.076	.12	.19	.37	.74
4.00	.030	.031	.034	.039	.048	.066	.10	.18	.35	.72
4.50	.023	.024	.025	.029	.036	.050	0.078	.14	.30	.68
5.00	.018	.018	.020	.022	.028	.038	.061	.12	.26	.64
5.50	.014	.014	.015	.018	.022	.030	.048	0.095	.23	.60
6.00	.011	.011	.012	.014	.017	.023	.038	.077	.20	.57
7.00	0.0074	0.0076	0.0081	0.0091	.011	.015	.025	.052	.15	.51
8.50	.0043	.0044	.0047	.0053	0.0063	0.0084	.014	.030	.10	.44
10.00	.0027	.0028	.0030	.0033	.0039	.0051	0.0080	.018	0.070	.39
13.00	.0013	.0013	.0014	.0015	.0018	.0023	.0034	0.0074	.035	.31

were previously reported by Ursell [1949] for certain $0 \leq \delta \leq 3\pi/2$. His values are confirmed and the range of frequency parameter is extended. The values of $M_0(\delta)$, $N_0(\delta)$ used here were calculated from the values of $M(\delta, \theta)$, $N(\delta, \theta)$ used in the hydrodynamic pressure calculation as discussed in Section 5.22. The results are shown graphically in Figure 7.

The results for the damping coefficient can be converted to amplitude ratio by

$$\left(\frac{h_w}{h_o}\right)^2 = \frac{\delta^2 \pi}{2} \left(\frac{2\pi}{A^2 + B^2}\right) .$$

Ursell [1953,1954] derived the asymptotic result

$$\frac{h_w}{h_o} \sim \frac{4}{\delta} \text{ as } \delta \rightarrow \infty .$$

He pointed out in [1957] that although this asymptotic form is correct, it may be hazardous to interpolate with this result since earlier theories predicted distinct minima. He suggested extended calculations could help settle the matter. The present calculations for the amplitude ratio tend distinctly to the asymptotic value as given by Ursell and shown in Figure 8.

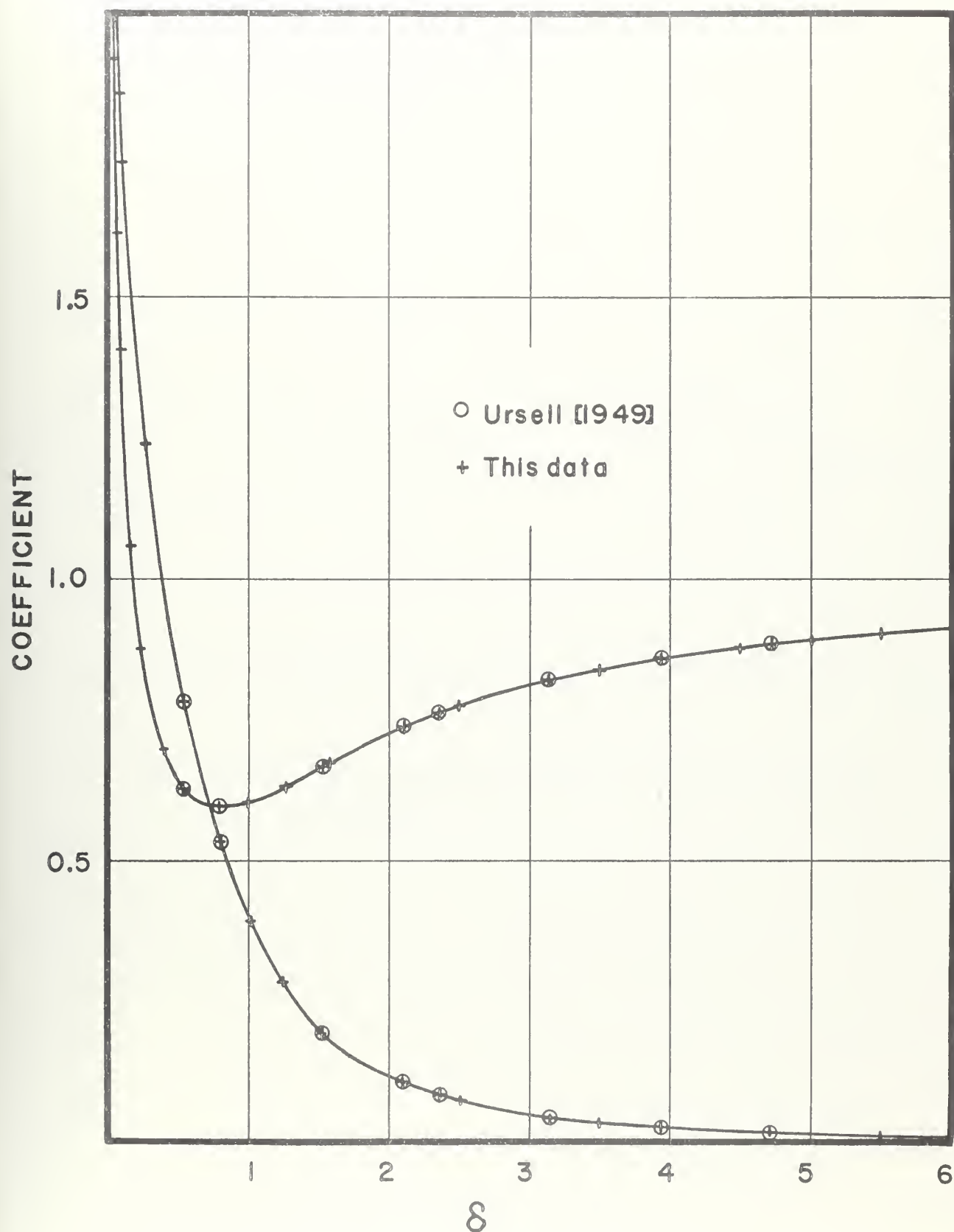


FIGURE 7. THE ADDED-MASS AND DAMPING COEFFICIENTS FOR THE CIRCULAR CYLINDER.

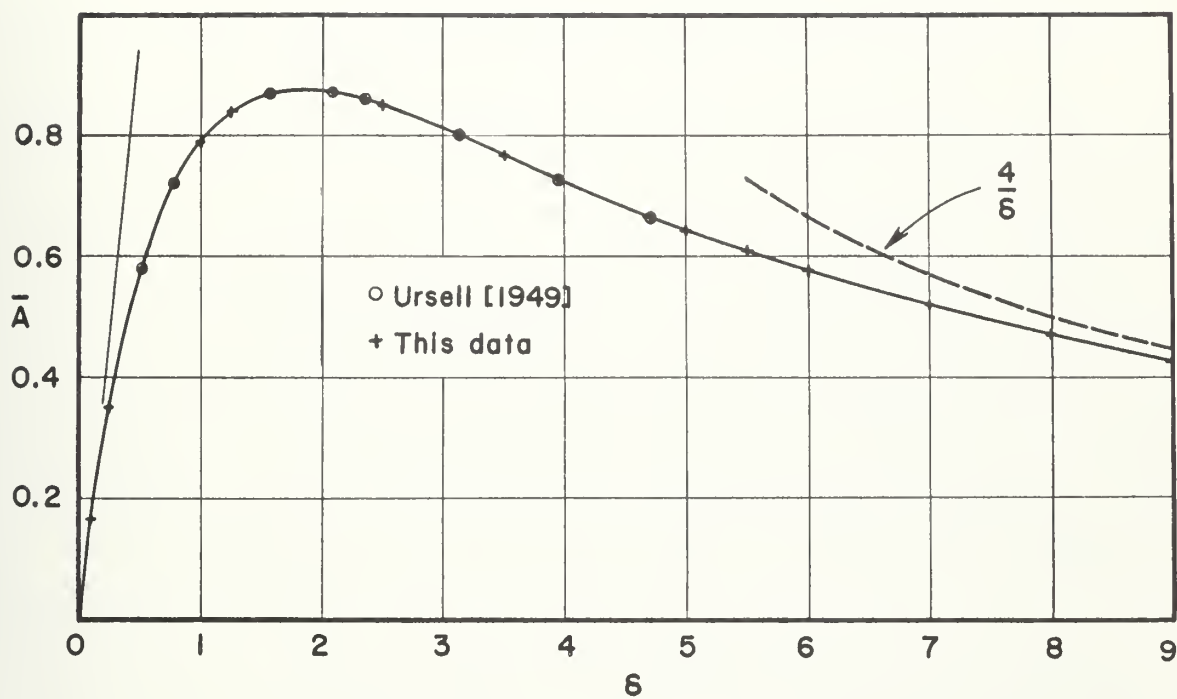


FIGURE 8. THE AMPLITUDE RATIO \bar{A} FOR THE CIRCULAR CYLINDER.

VI. Elliptic and More General Cylinders in Infinitely Deep Fluid

6.1 Description of the Method.

Sample calculations were made for the hydrodynamic pressure distribution, added-mass and damping coefficients of elliptic and more general cylinders in infinitely deep fluid. An important objective of the sample calculations, in addition to that of obtaining the hydrodynamic quantities of interest, was to test the flexibility of the program written for control of the automatic digital computer. The program was successfully tested over a wide range of cylindrical shapes generally encompassing those of naval architectural interest. Some of these sample calculations are reported here. It is intended that a more comprehensive atlas will be separately reported later.

The calculations were done on the IBM 704 digital computer at the Computer Center, University of California, Berkeley.

6.11 Numerical Procedures.

The expansion coefficients $p_{2m}(\delta)$, $q_{2m}(\delta)$ were calculated by the discrete-angle method described in Section 5.11. The expansion equations are given in Section 4.3. The forms of $\gamma_{sa}(\delta, \theta)$ and $\gamma_{sa}(\delta, \pi/2)$ suitable to numerical calculation are given in Appendix A-3.4. The number of expansion equations \bar{m} and the discrete angles θ_i were varied. The least number \bar{m} in the calculations reported here was nine so that the hydrodynamic pressure could be calculated at ten degree intervals with expansion

coefficients known to satisfy the truncated expansion equations exactly at ten degree intervals. More often in these calculations $\bar{m} = 17$. In every case the expansion coefficients were tested at arbitrary $\theta = \theta_t \neq \theta_i$ to provide the accuracy index described in Section 5.11.

The principal dependent variables $A(\delta)$, $B(\delta)$, $M(\delta, \theta)$, and $N(\delta, \theta)$ were calculated in the same manner as for the case of the circular cylinder but with appropriate definitions of $\bar{\gamma}_{2ma}(\delta, \pi/2)$ and $\bar{\varphi}_{2ma}(\delta, \theta)$ as given in Section 4.1. The dependent variables $M_o(\delta)$, $N_o(\delta)$ were calculated by numerical quadrature from the calculated values of $M(\delta, \theta)$, $N(\delta, \theta)$ as described in Section 5.22 and the result was tested by comparing $M_o A - N_o B$ with $\pi^2/2$.

6.12 The Selection of Mapping Parameters a_{2n+1} .

The number $N + 1$ of mapping parameters a_{2n+1} , $n=0,1,2,\dots,N$ (Sections 2.2, 3.2) has been left unspecified in the problem solution. It is convenient here to classify the cylinders by the number $N + 1$. The naval architect is more accustomed to classifying ship sections by other parameters so some of this nomenclature is introduced.

The ratio of the half-breadth of the cylinder at the free surface to the depth of the cylinder at the centerline is designated H :

$$H = x(\pi/2) / y(0) = b/d.$$

The ratio of the cross-sectional area of the cylinder to the area

$$2x(\pi/2)y(0) = 2bd,$$

$$S = \frac{\pi}{2} \frac{b^2}{G^2} \rho_o^2 - \left[\sum_{n=0}^N \frac{(2n+1)(a_{2n+1})^2}{\rho_o^{2n+1}} \right] / 2bd,$$

is designated S and called the "area coefficient."

The one-parameter cylinders generated by assigning $N = 0$ suitable values to $a_1 \geq 0$ are members of the elliptic family. The special case $a_1 = 0$ is the circular cylinder. The ratio $H = (1 + a_1) / (1 - a_1)$ is uniquely determined. The area coefficient for any elliptic cylinder is constant; $S = \pi/4$. Thus in naval architectural terms the one-parameter family of cylinders offers a choice of beam-draft ratio but constant area-coefficients.

The two-parameter cylinders generated by assigning $N = 1$ and suitable values to $a_1 \geq 0, a_3 \geq 0$, to provide more-or-less ship-like cross-sections are commonly called Lewis forms, the ratio H and the area coefficient S ,

$$H = \frac{1 + a_1 + a_3}{1 - a_1 + a_3}$$

$$S = \frac{\pi}{4} \frac{1 - a_1^2 - 3a_3^2}{(1 + a_3)^2 - a_1^2},$$

are determined by a_1, a_3 and conversely for ship-like forms. Thus the two-parameter family of Lewis forms permits some selection of area coefficient at fixed beam-draft ratio.

Still greater flexibility in selecting a geometric form with given beam-draft ratio and area coefficient is possible in the

three-parameter family. Here $N = 2$ and appropriate values are assigned a_1, a_3, a_5 . L. Landweber and M. Macagno [1959] introduced a systematic treatment of these forms and present a convenient method for finding the asymptotic value of the added mass m_∞ (Section 4.4). The introduction of the third parameter specifically permits a variation in the vertical distribution of the cross-section area at given beam-draft ratio and area-coefficient. This, in naval-architectural terms, is a two-dimensional interpretation of the vertical prismatic coefficient. Ship-like forms with higher area coefficient are also possible.

Prohaska [1947] considered two special cases from the four parameter family, $N = 3$. He selected non-zero values for a_1, a_7 and for a_3, a_7 . The examples he illustrates of the case a_3, a_7 not zero are cusped, while several in the group a_1, a_7 not zero may be called ship-like.

The program for the control of the automatic computations permits the selection of any foreseeable number of coefficients. Coefficients are stated consecutively up to the highest non-zero value and the summations over N terminate at that number. Many sample calculations have been done with various combinations of coefficients through a_7 . The results of sample calculations of examples from the one-, two-, and three-parameter families are presented here.

6.2 Results for Examples from the One-Parameter (Elliptic) Family of Cylinders.

The sample calculations for the circular cylinder given in

Chapter 5 are a special case of the one-parameter family of elliptic cylinders. The results of calculations for elliptic cylinders with $H = 1/5$ and $H = 3/2$ are presented in the following figures.

The hydrodynamic pressure fluctuation in phase with the acceleration, p_a , and that in phase with the velocity, p_v (Section 5.3) are shown for typical values of θ measured in the reference plane as a function $\delta = Kx(\pi/2) = Kb$.

For large $\delta \rightarrow \infty$,

$$\frac{p_a}{\delta} = \frac{M(\delta, \theta)A(\delta) - N(\delta, \theta)B(\delta)}{A(\delta)^2 + B(\delta)^2} \sim \cos \theta$$

for all cylinders of this family (Section 5.3). This fact is illustrated by observing the slope of the $p_a(\delta, \theta)$ lines and is particularly evident in Figure 10.

As pointed out in Section 4.4 the free-surface correction $k_4 = m/m_\infty$ is numerically equal to the ratio of the added mass m to the mass of the fluid displaced by a circular cylinder of the same beam in the case of elliptic cylinders. Therefore curves of $k_4(\delta)$ show the frequency-dependence of the inertia-coefficient of Lewis [1929] or the added-mass coefficient of Landweber and Macagno [1957].

Curves of the ratio of waveheight far from the cylinder to the amplitude of vertical oscillation,

$$\bar{A} = h_w/h_o$$

are shown in Figure 14. The damping coefficient may be calculated from the amplitude ratio (Section 5.4).

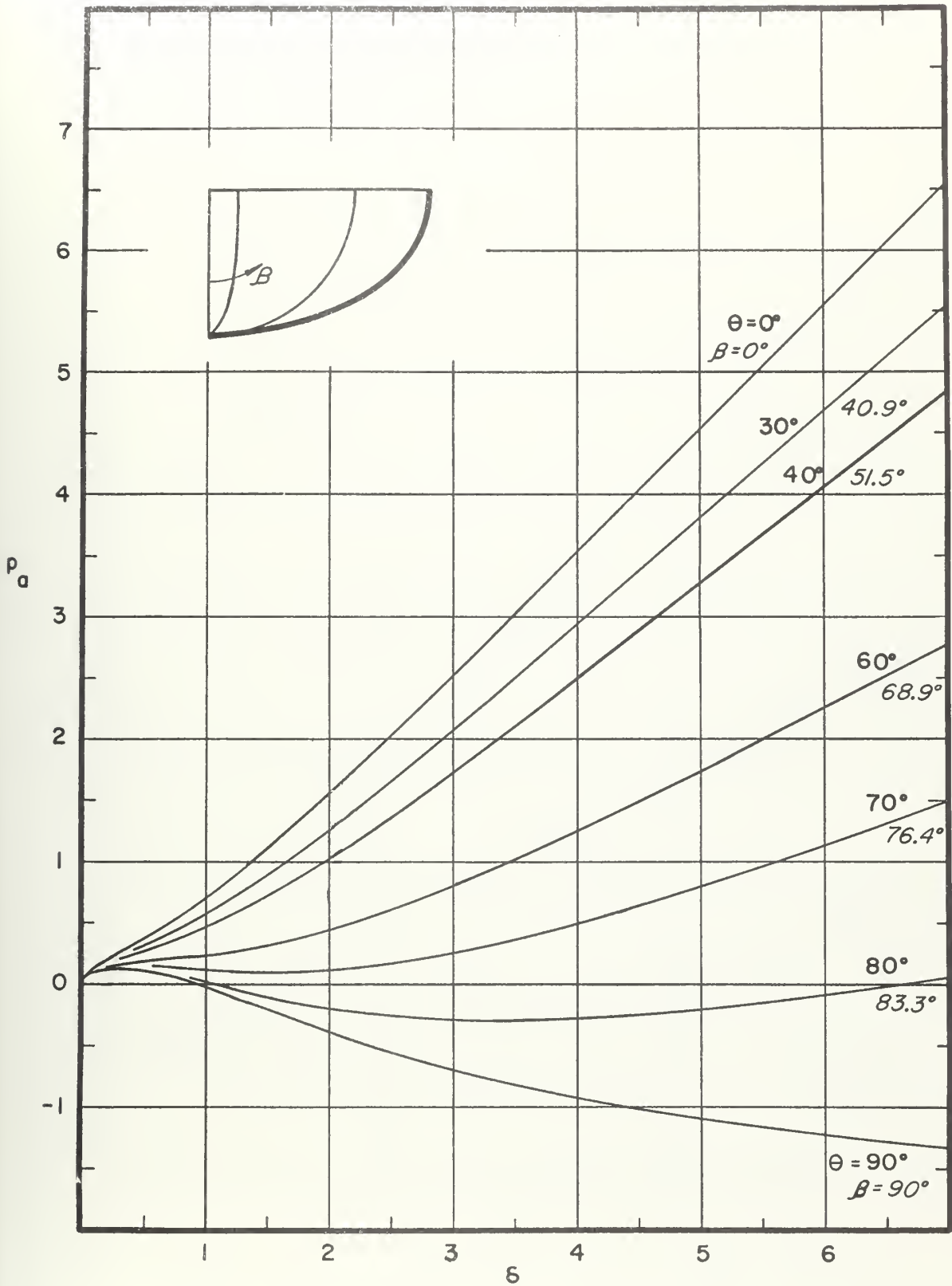


FIGURE 9. $p_a(\delta, \theta)$ FOR THE ELLIPSE $H=3/2$.

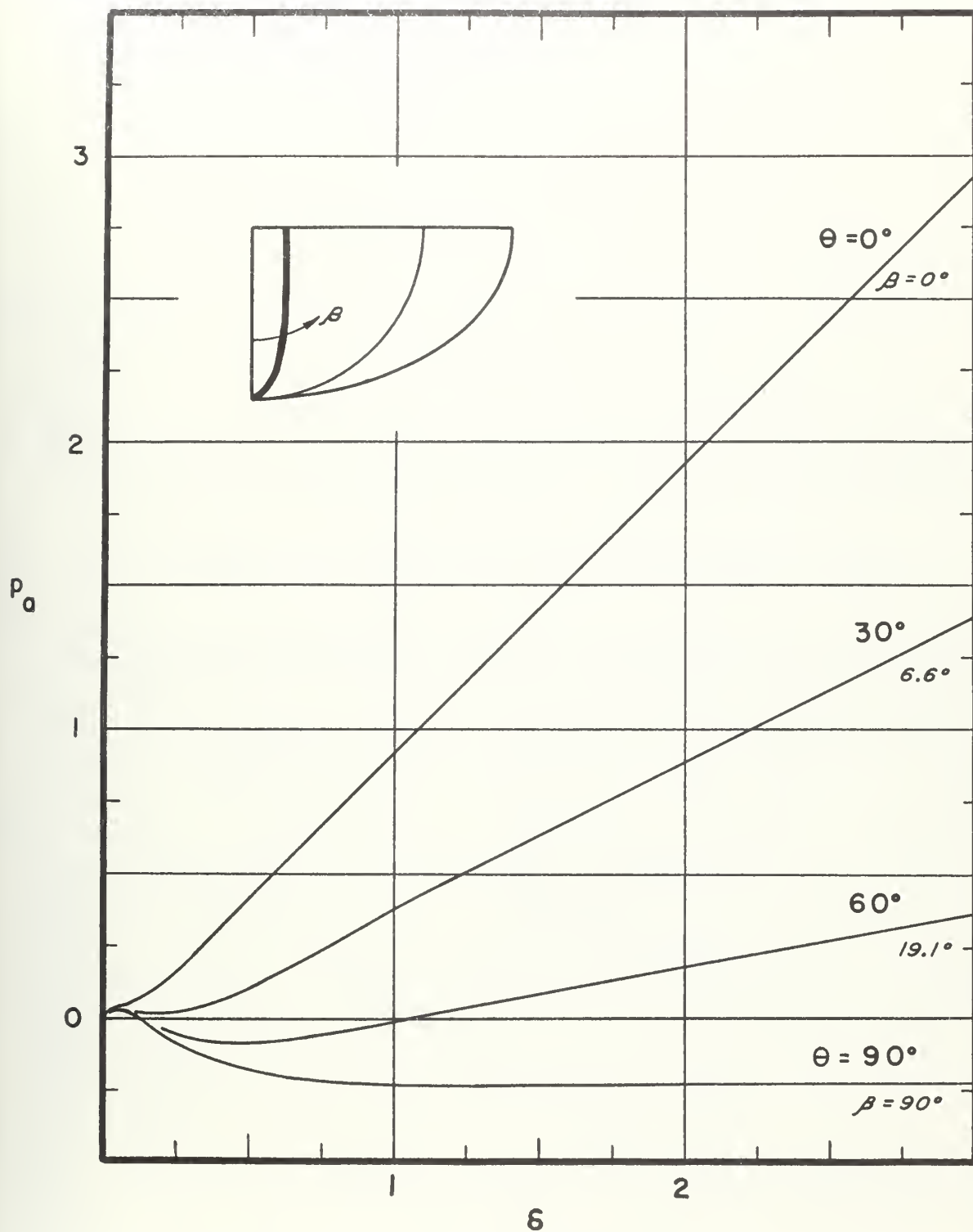


FIGURE 10. $p_a(\delta, \theta)$ FOR THE ELLIPSE $H = 1/5$.

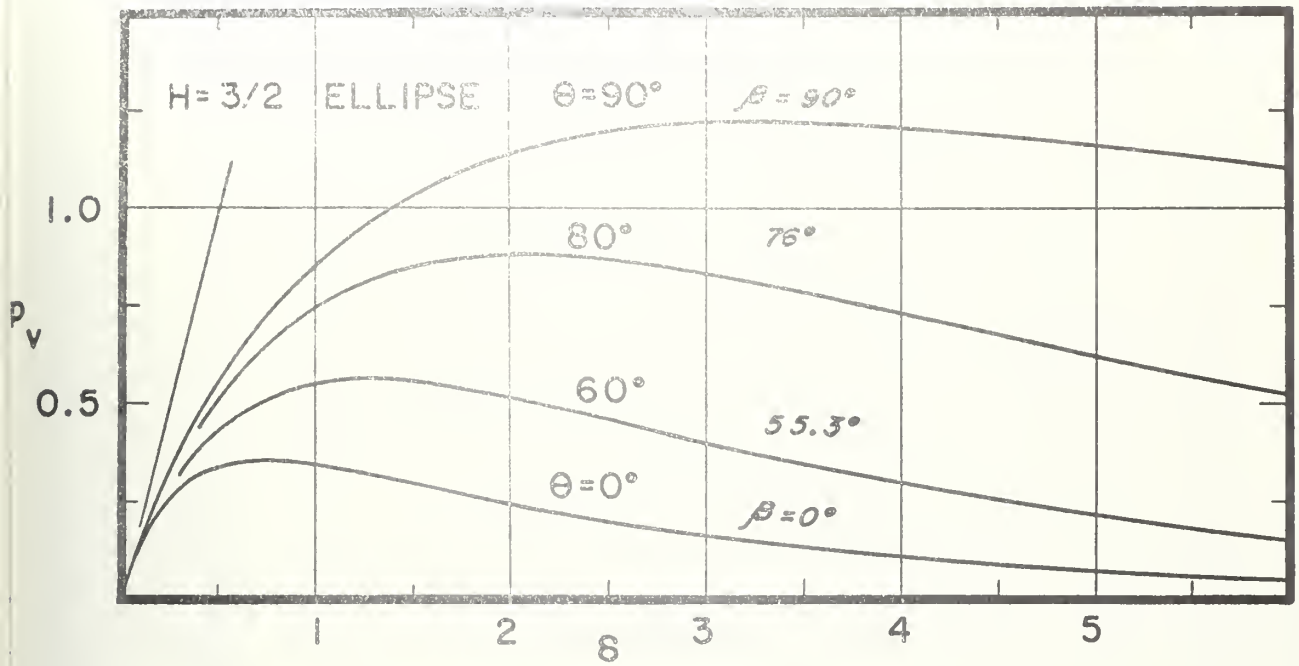


FIGURE 11. $p_v(\delta, \theta)$ FOR THE ELLIPSE $H = 3/2$.

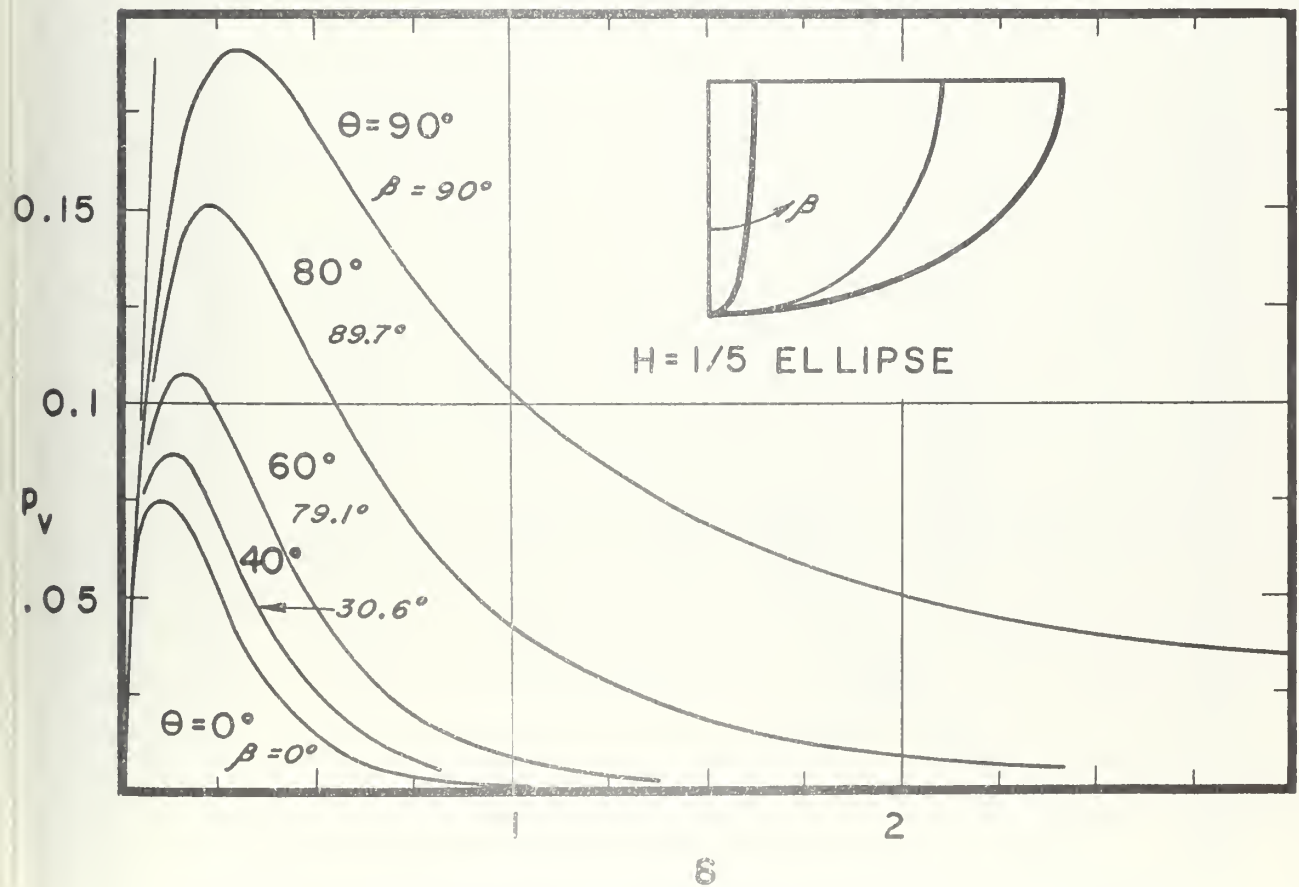


FIGURE 12. $p_v(\delta, \theta)$ FOR THE ELLIPSE $H = 1/5$.

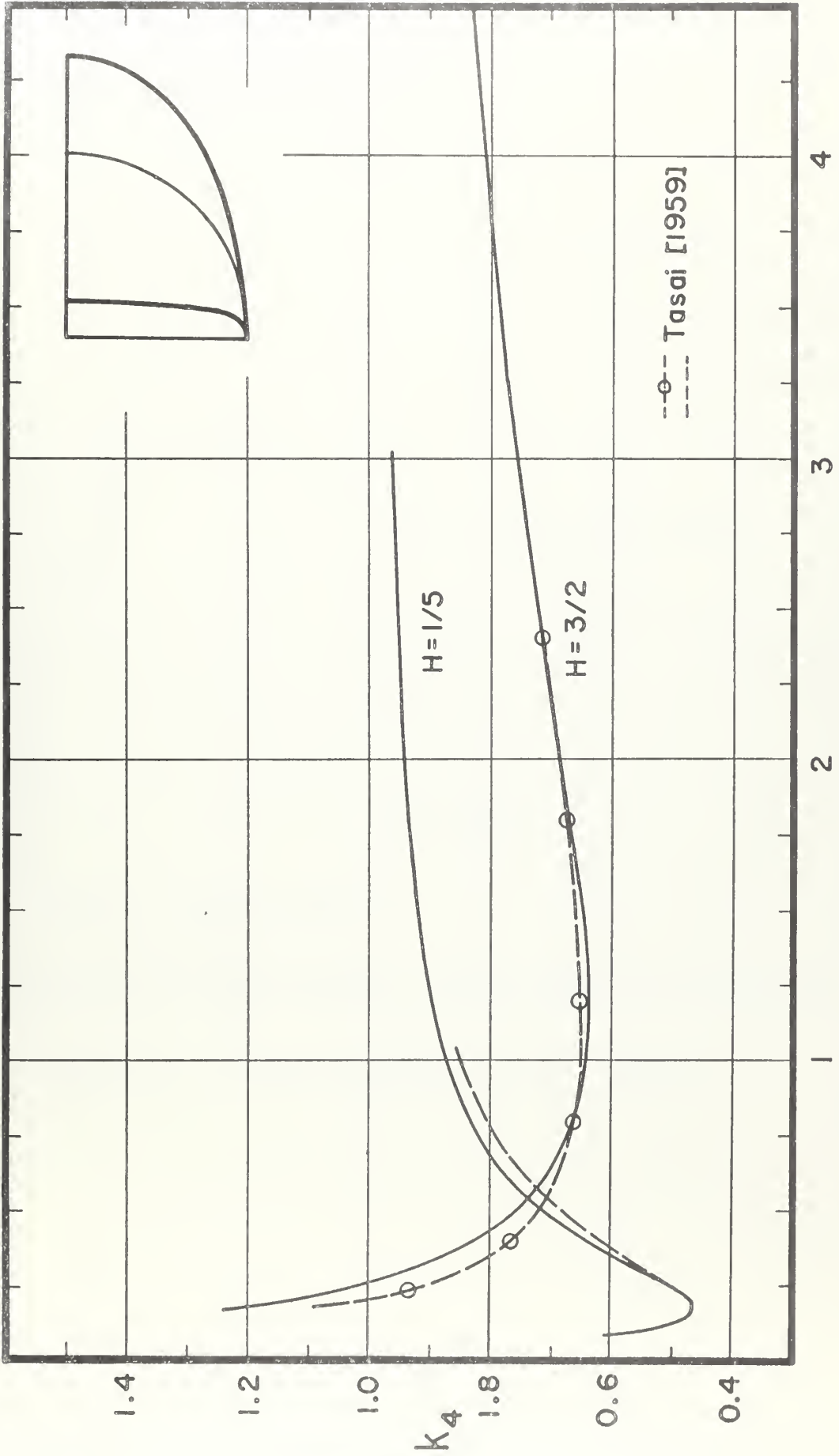


FIGURE 13. K_4 FOR THE ELLIPTIC CYLINDERS $H=1/5, 3/2$.

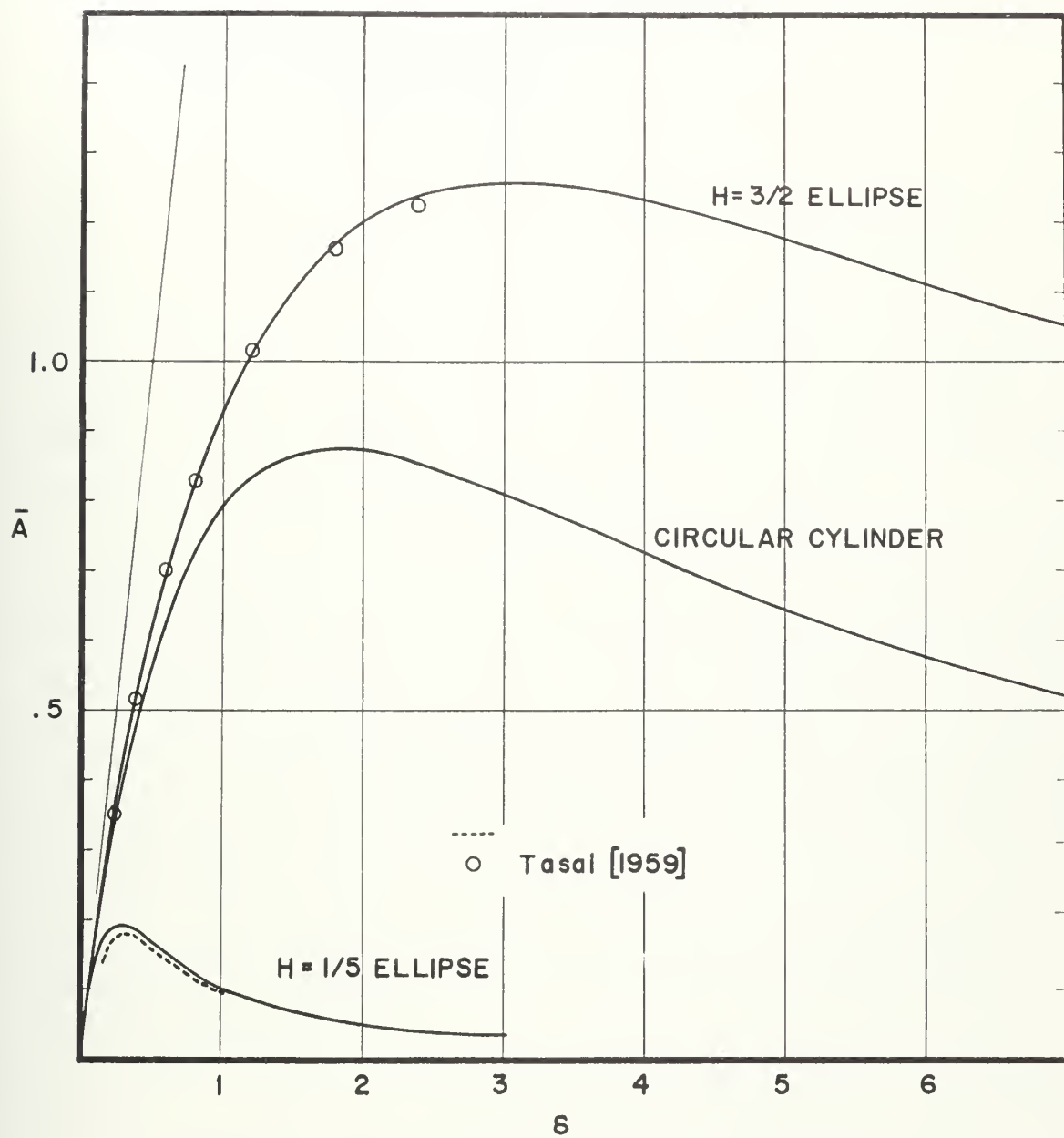


FIGURE 14. \bar{A} FOR THREE ELLIPTIC CYLINDERS.

Tasai [1959] has previously reported calculations for the free-surface correction factor k_4 and the amplitude ratio \bar{A} for the two ellipses reported here over a limited range of the frequency parameter. His method of calculating six expansion coefficients satisfying eight expansion equations in the least-squares sense was reported in Section 5.11. His procedure for evaluating the several integrals was not reported. The trends of all his calculations are confirmed and differences within his range of calculated values (determined graphically from his figures) are almost certainly due to differences in numerical procedures, plus the graphical dispersion.

These curves give insight into the frequency dependence of the various hydrodynamic quantities for forms of various beam-draft ratio and constant area-coefficient. The vertical distribution of area as measured by the fractional depth of the section centroid or the fractional depth of the radius of gyration about the free-surface (x-axis) is also constant.

6.3 Results for Examples From the Two-Parameter (Lewis Form) Family of Cylinders.

The Lewis forms have, for given beam-draft ratio, a range of values of area-coefficient. The vertical distribution of area of the forms of fixed beam-draft ratio also changes (cf. the three-parameter family of the next section). This one added mapping parameter fortuitously provides sections that are more full than the ellipse and generally accepted as ship-like. The upper limit of fullness obtainable is somewhat arbitrary. Lewis [1929] preferred to judge the forms by the practiced eye of a skilled naval architect; Landweber and

Macagno [1957] formalized this decision. The lower limit of fullness is probably also arbitrary since the forms tend to be not aesthetically ship-like and if fine enough, are cusped at $\beta = 0$ for $H \leq 1$ and at $\beta = \pi/2$ for $H \geq 1$.

The sample calculations made to date suggest that the behavior of the various hydrodynamic quantities does not change abruptly as the values of a_1, a_3 encompass the reasonably expected range.

The results of two of the calculations for this family are shown graphically. Both forms have $H = 1$, the same as the circular cylinder. One form is full and ship-like. The other is the section of minimum area and is cusped.

Figures 15 and 16 show curves through calculated points of $p_a(\delta, \theta)$. The asymptotic behavior of p_a/δ for large δ for this family is

$$\frac{p_a}{\delta} \sim \frac{(1+a_1) \cos \theta - a_3 \cos 3\theta}{(1+a_1 + a_3)} \quad \text{as } \delta \rightarrow \infty.$$

This behavior, more complex than simply $\cos \theta$ as in the one-parameter family, is shown by the slopes of the curves in the two figures.

Figure 19 shows curves of the free-surface correction factor, $k_4 = m/m_\infty$. It is recalled that for the more general cylinders the free-surface correction factor k_4 is no longer numerically equal to the added-mass or inertia-coefficient. The calculation of Tasai [1959] for k_4 of the full-form is shown over his range $0.4 < \delta < 2.6$.

The damping coefficients for the full form and the cusped form are shown in Figure 20.

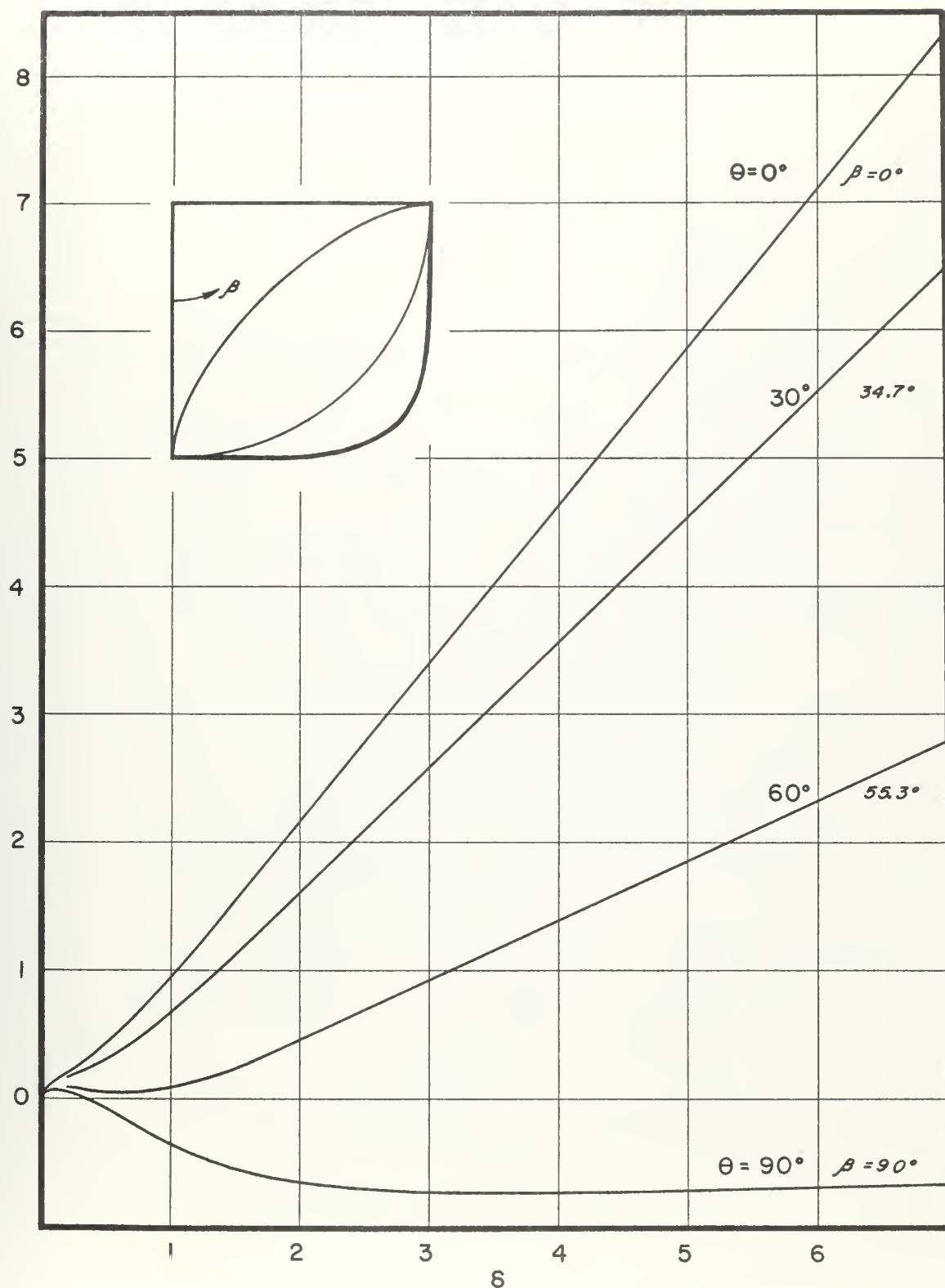


FIGURE 15. $p_0(\delta, \theta)$ FOR THE FULL SECTION, $H = 1$.

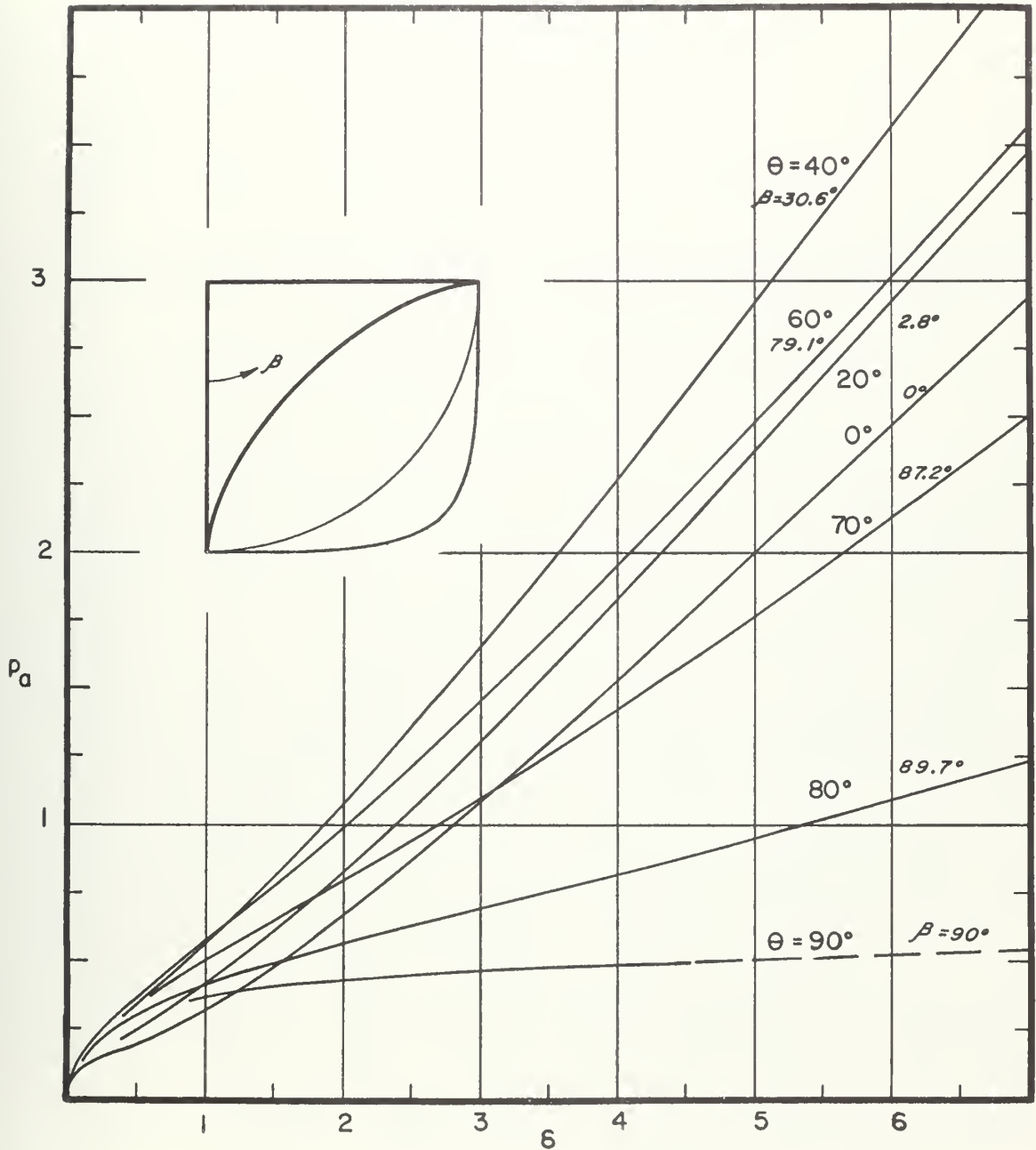


FIGURE 16. $p_a(6, \theta)$ FOR THE CUSPED SECTION, $H=1$.

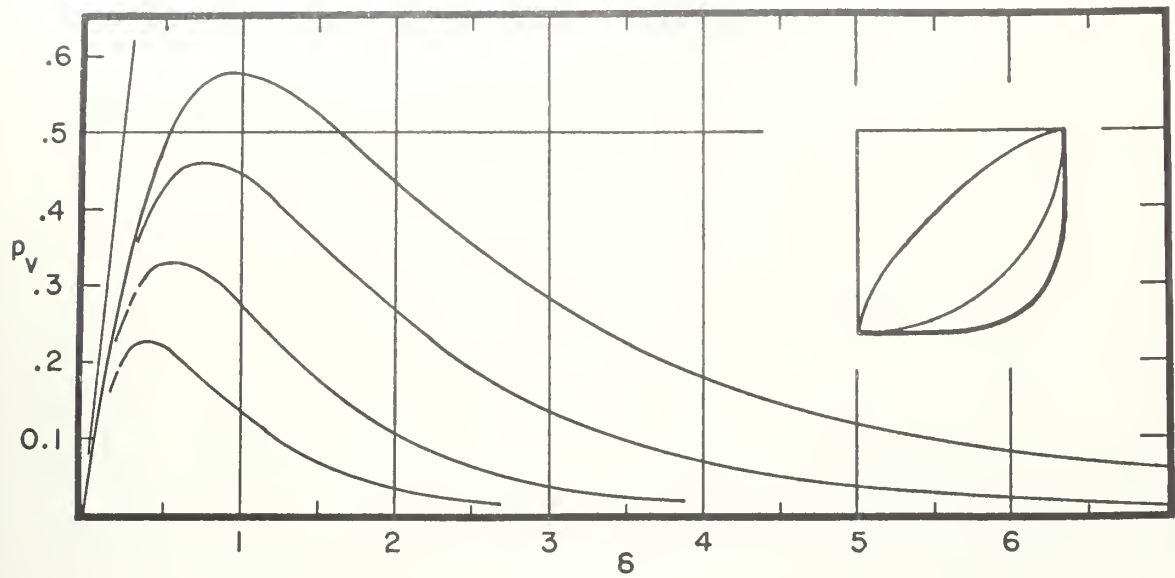


FIGURE 17. $p_v(\delta, \theta)$ FOR THE FULL SECTION, $H=1$.

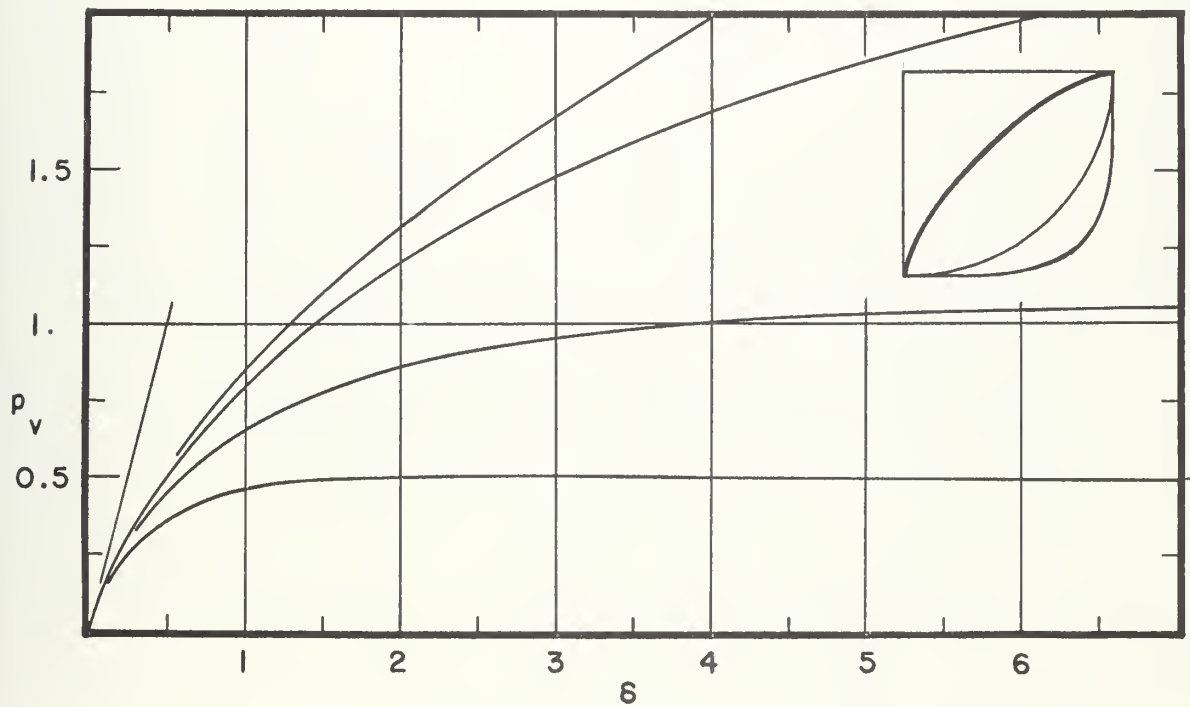


FIGURE 18. $p_v(\delta, \theta)$ FOR THE CUSPED SECTION, $H=1$.

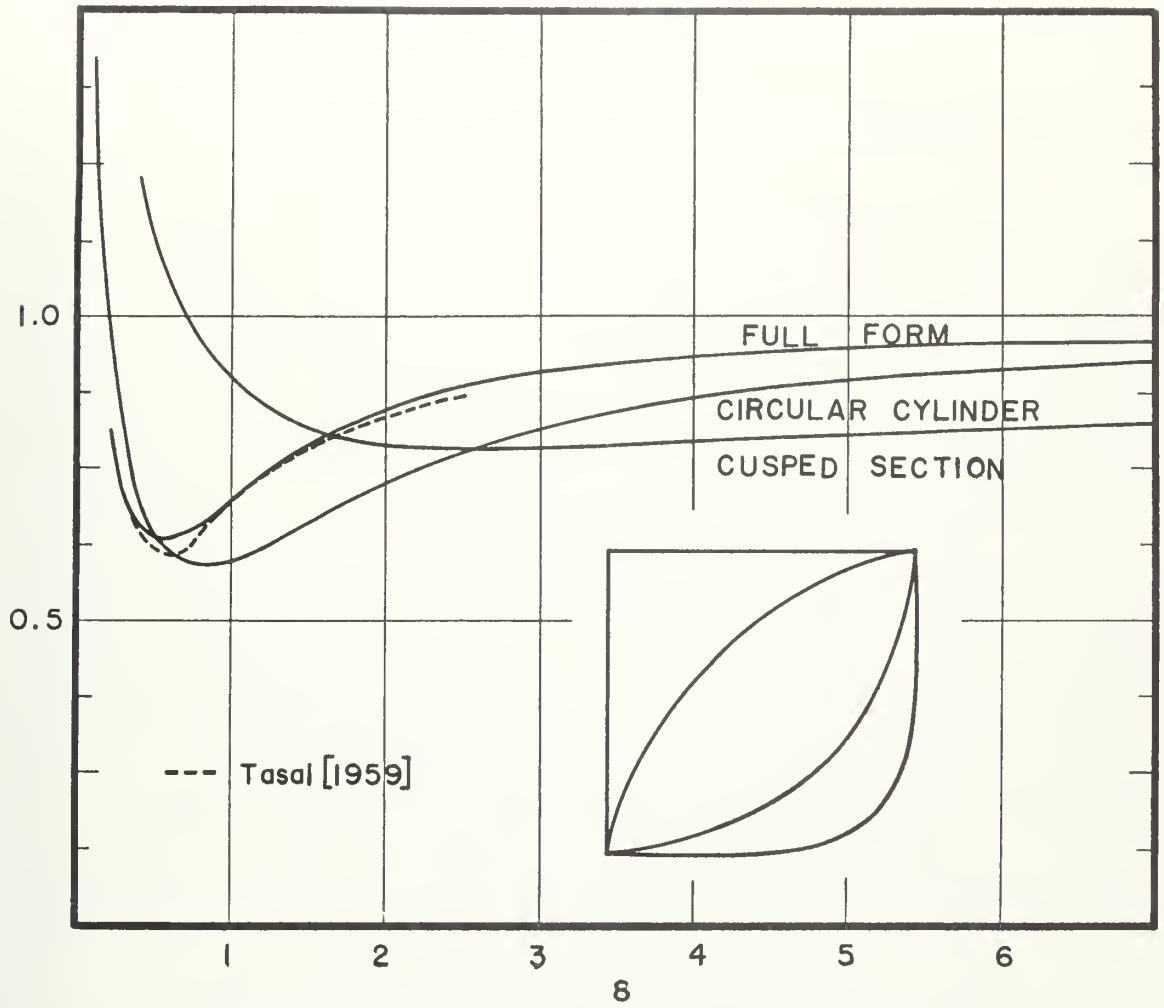


FIGURE 19. k_4 FOR THREE CYLINDERS, $H=1$.

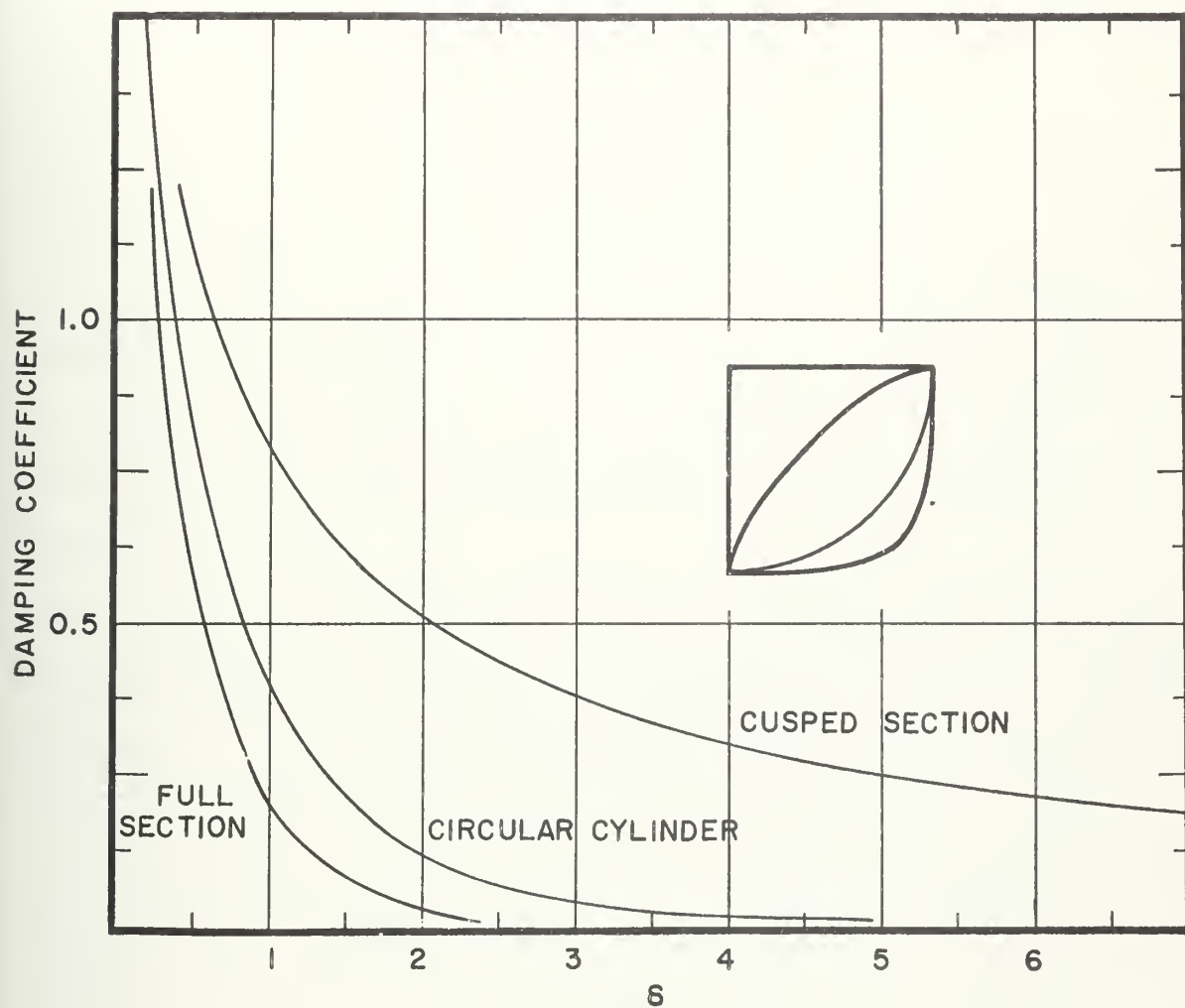


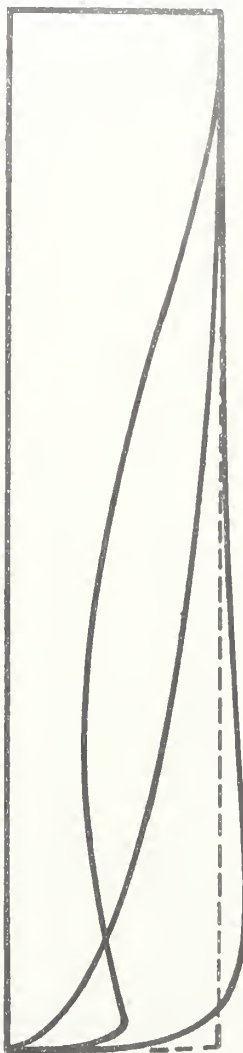
FIGURE 20. THE DAMPING COEFFICIENT $\frac{2\pi}{A^2 + B^2}$
FOR THREE CYLINDERS, $H=1$.

6.4 Results for Examples From a Three-Parameter (Landweber-Macagno) Family of Cylinders.

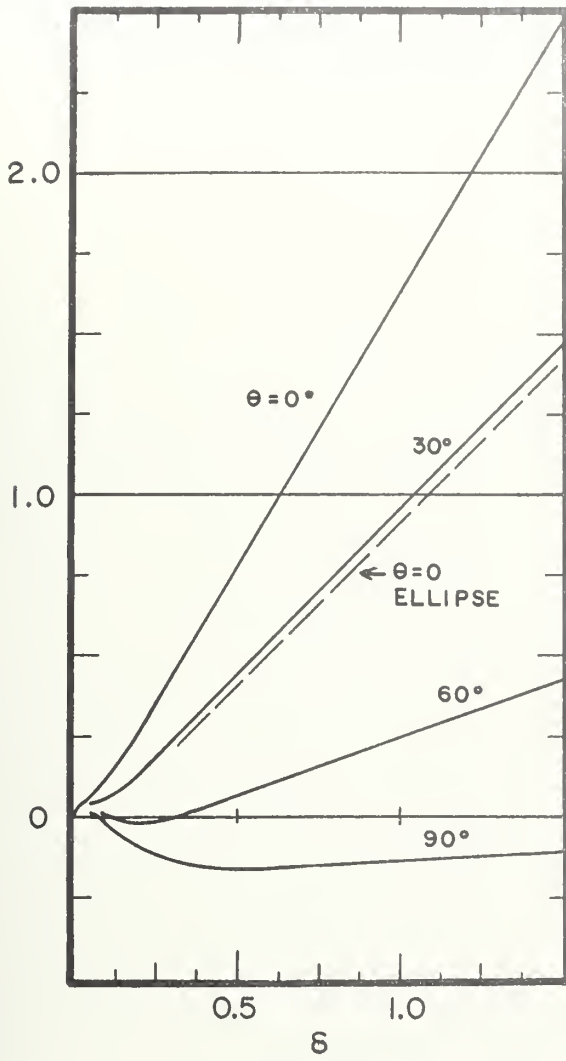
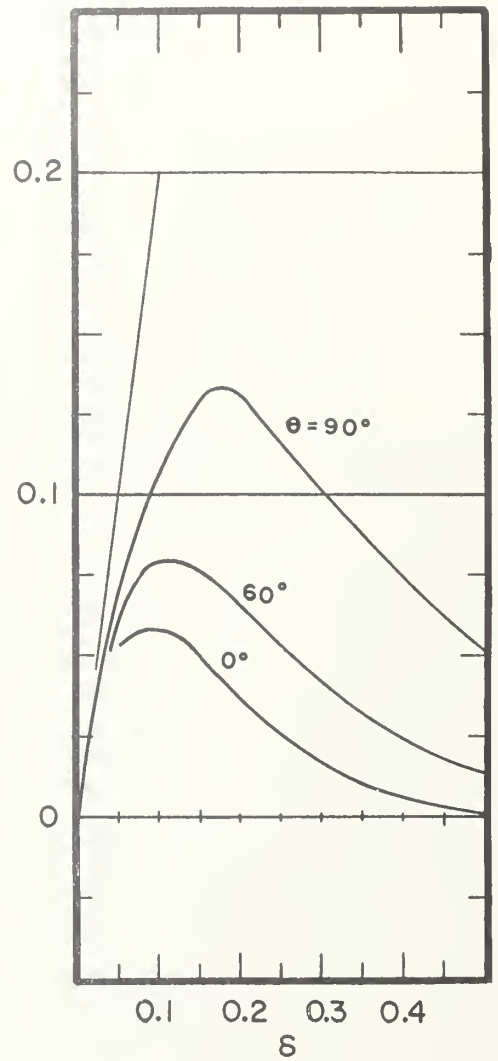
The use of three parameters a_1, a_3, a_5 in the mapping function permits some independent variation of the vertical distribution of area for the ship-like section of given beam-draft ratio and area coefficient. L. Landweber and M. Macagno [1959] chose to measure the vertical distribution of area in terms of the parameter η defined as the moment of inertia of the actual section about x-axis made non-dimensional by the product $x(\pi/2) y(0)^3 = bd^3$. Another useful characteristic of the three-parameter family is that it provides ship-like sections of larger area-coefficient than is possible in the two-parameter family.

Examples are shown which illustrate the behavior of the hydrodynamic quantities for a bulb-like section and a section of maximum fullness. The sections are shown in Figure 21. The full section is an example of sections possible in the three-parameter family that are ship-like and have area coefficients larger than is possible in Lewis forms. The area coefficient for the full section is $S = 1.012$. This section was selected from Figure 4 of the Landweber and Macagno reference cited above. The bulb-like section has an area-coefficient of about 0.6 and it is a member of the special group $a_3 = 0; a_1, a_5$ not zero from which Prohaska [1947] selected examples.

The amplitude of the pressure fluctuation in phase with the acceleration at locations near the vertical centerline of the full section increases much more rapidly with increased $\delta = Kb$ than for the more rounded elliptic or bulbous forms.

FIGURE 21. THREE CYLINDERS, $H = 1/5$.

$\theta = 0^\circ$	BULBOUS $\beta = 0^\circ$	ELLIPTIC 0°	FULL 0°
10	3.5	2.0	5.2
20	5.6	4.2	9.3
30	6.0	6.6	12.0
40	5.6	9.5	13.7
50	6.2	13.4	15.5
60	10.6	19.1	18.7
70	23.6	28.8	25.7
80	51.0	48.6	43.5
90	90.	90.	90.
S	0.59	$\pi/4$	1.012
a_1	- .7430	- $2/3$	-.62332
a_3	0	0	-.10206
a_5	+ .07633	0	.02469

FIGURE 22. $p_q(\delta, \theta)$.FIGURE 23. $p_v(\delta, \theta)$.

$p_q(\delta, \theta)$ AND $p_v(\delta, \theta)$ FOR THE FULL FORM, $H=1/5$.

The asymptotic form of p_a/δ for large δ for the bulbous form is shown in Figure 24.

In Figure 27, showing the free surface correction factor k_4 and the amplitude ratio \bar{A} , data on the elliptic form with the same beam-draft ratio, previously given in Section 6.2, are reproduced for reference. The amplitude ratio for the bulbous shape indicates a relatively high damping coefficient; the full section (larger vertical prismatic coefficient) is relatively less damped in heaving oscillation.

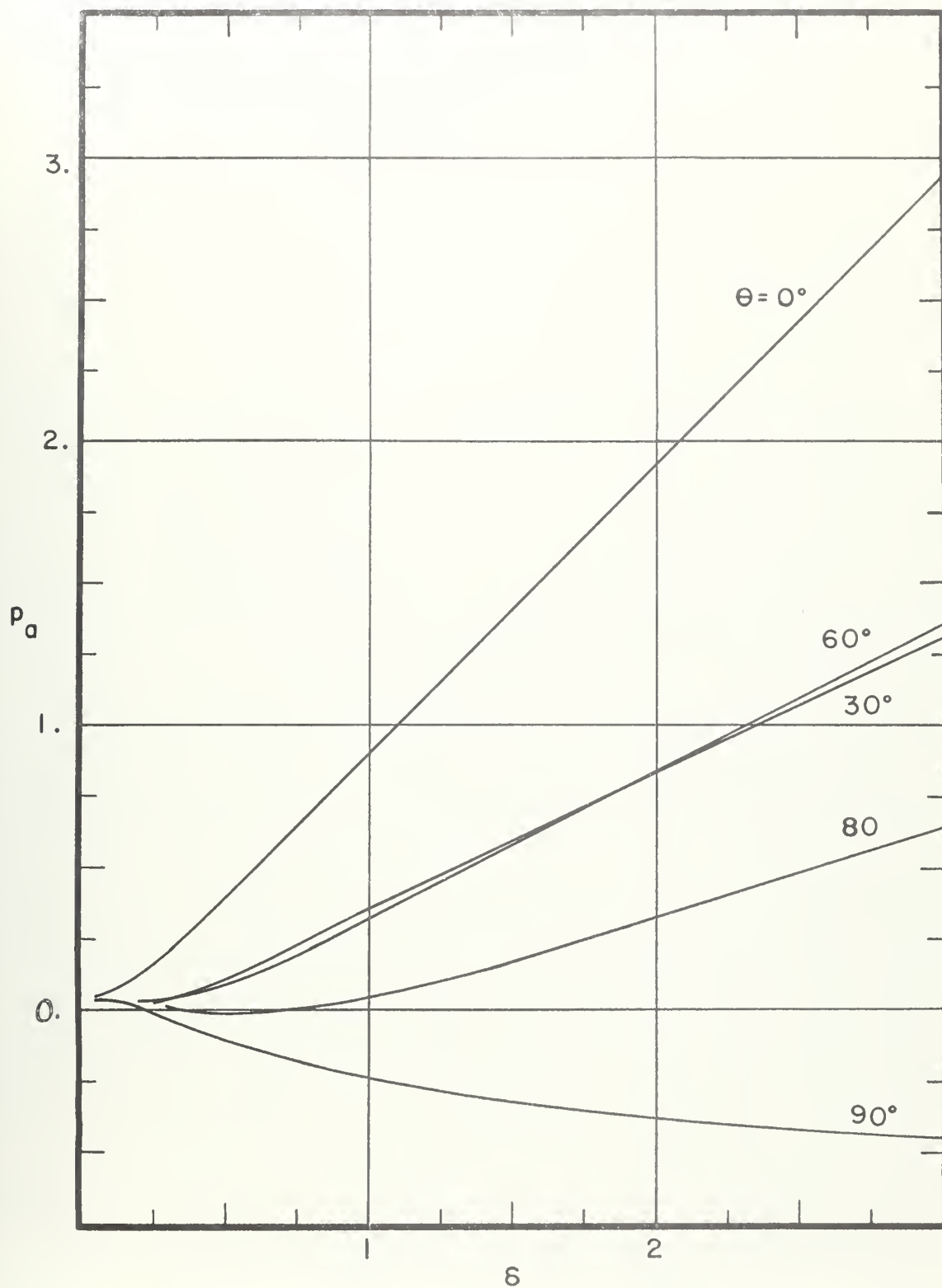


FIGURE 24. $p_a(\delta, \theta)$ FOR THE BULBOUS SECTION, $H=1/5$.

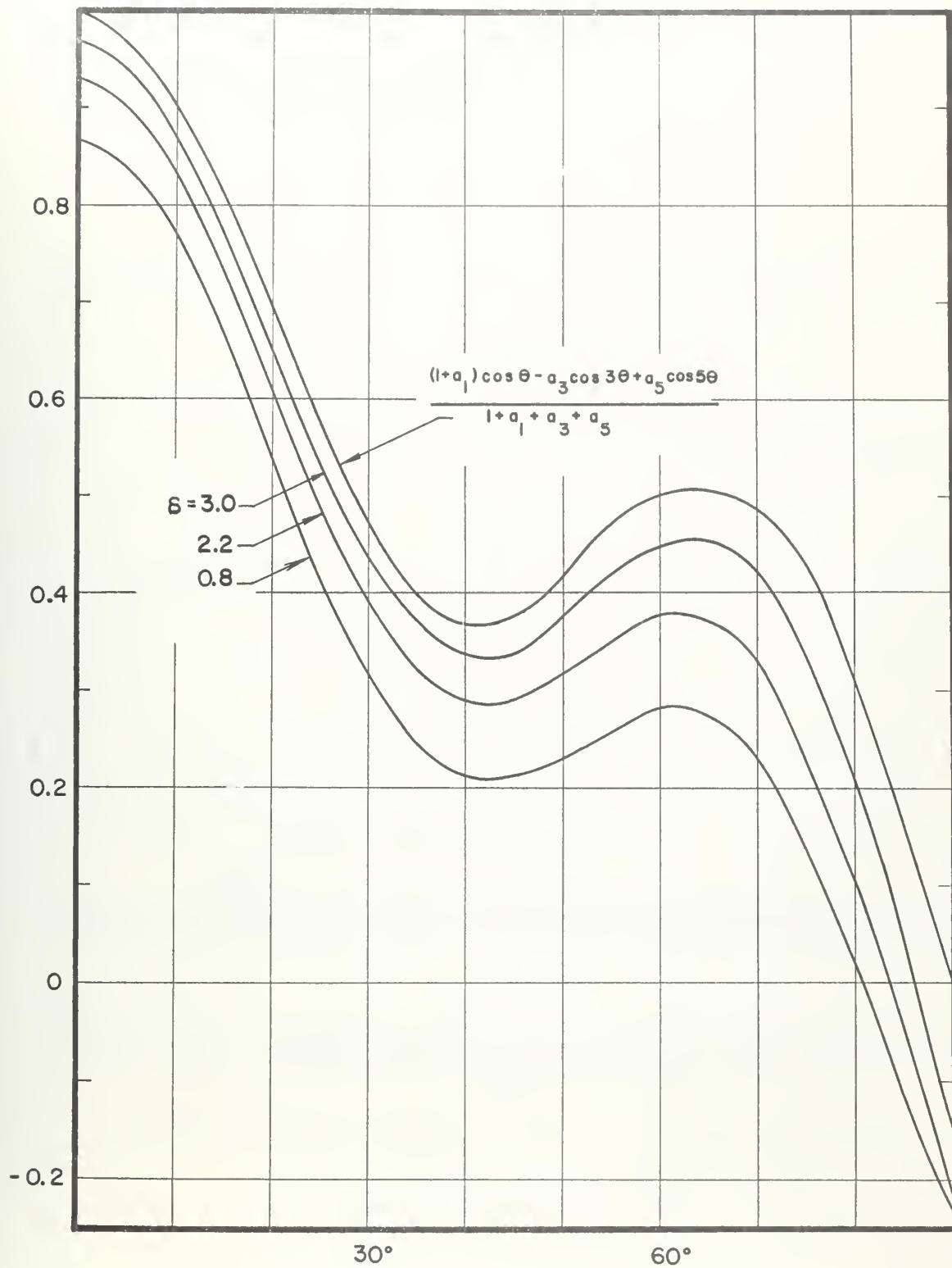


FIGURE 25. THE TREND OF p_a/δ FOR LARGE δ ,
BULBOIS SECTION, $H=1/5$.

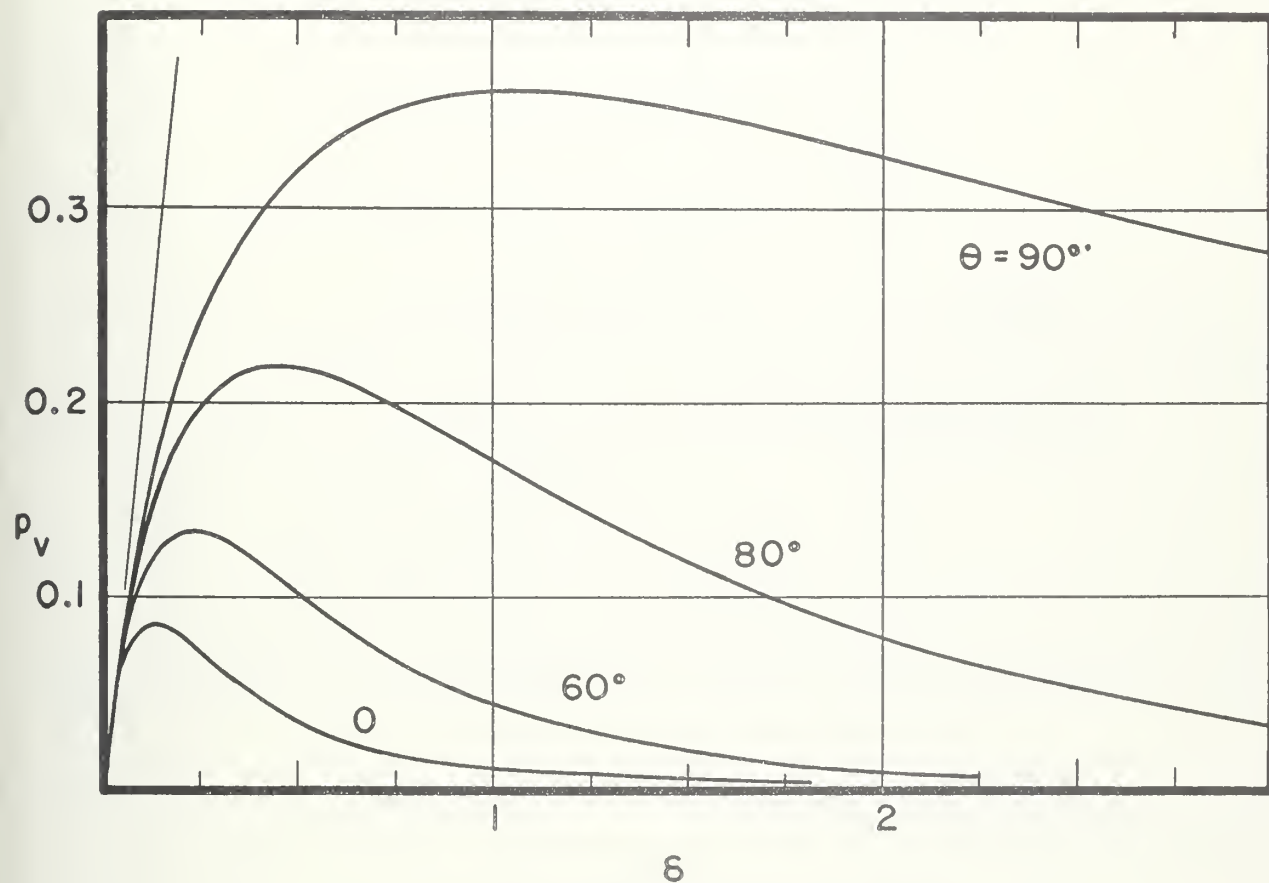


FIGURE 26. $p_v(\delta, \theta)$ FOR THE BULBOUS SECTION, $H=1/5$.

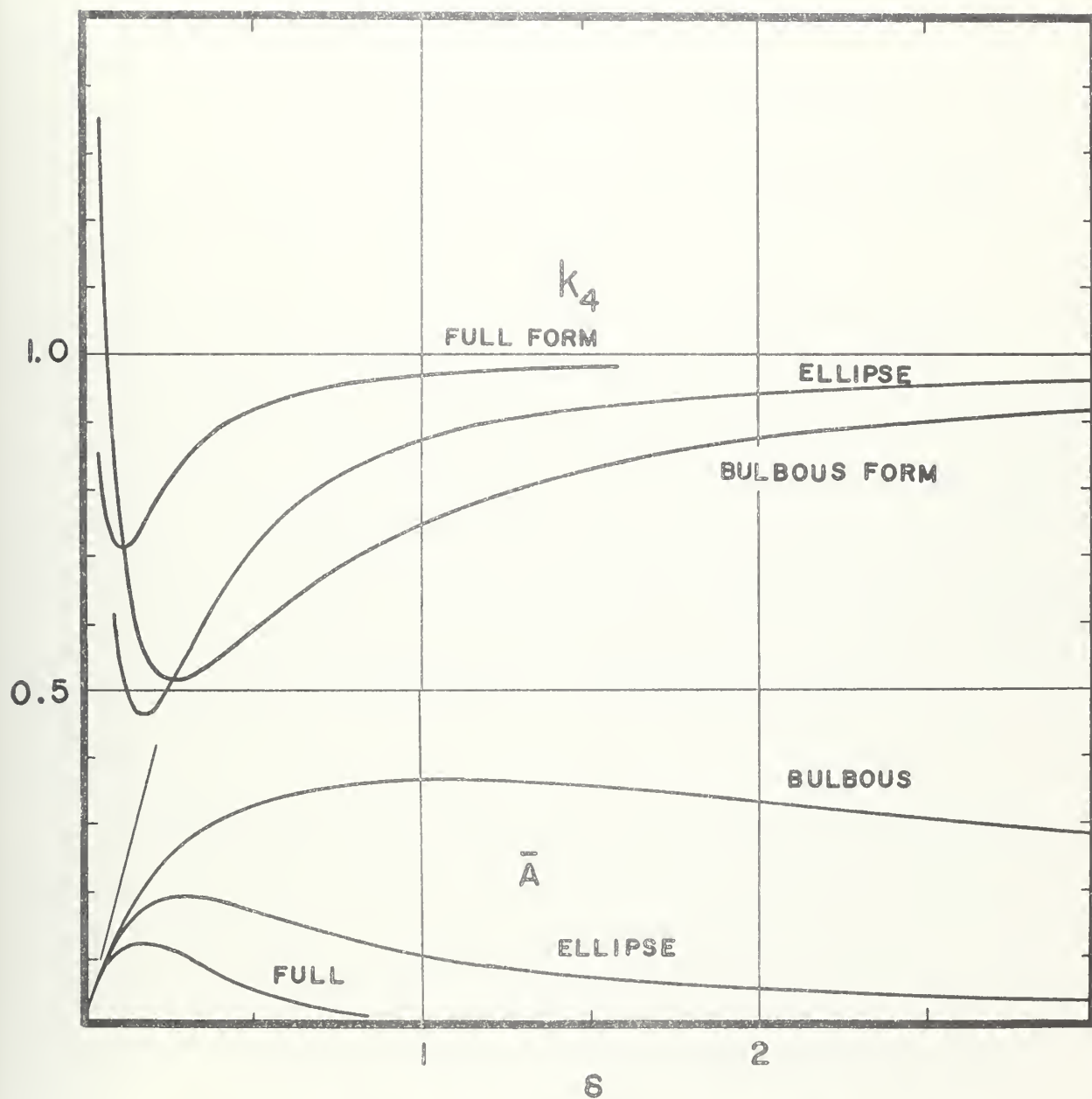


FIGURE 27. k_4 AND \bar{A} FOR THREE CYLINDERS, $H = 1/5$.

VII. Experiment and Results

7.1 Purpose and Direction.

F. Ursell, who obtained the first rigorous solution for the circular cylinder in fluid of infinite depth [1949] also said clearly "experiments are needed" and has reiterated this even in recent times:

"It would be highly desirable to compare these calculations with suitable experiments." [1957].

The response has not been overwhelming. The earlier experiments reported in Chapter I are not strictly comparable, and in later years, three-dimensional experiments (Golovato [1957], Gerritsma [1957]) have received more attention. Apparently, the only modern experiment simulating two-dimensional behavior is that of Yu [1960], who measured waveheight ratio and found satisfactory agreement while the present experimental apparatus was under construction. Yu reported instrumentation difficulty in measuring the vertical force acting on the cylinder.

Pressure fluctuation measurement was selected as the primary objective of the experiment to be discussed. The total pressure fluctuation signalled by a suitable transducer is a distinctive function of the location θ on the cylinder, as well as the frequency δ , according to the preceding theory. It is considered unlikely that reasonable agreement could be expected between experimental results and the distinctive prediction unless the analytic model accurately represents the essentials of physical reality. Vertical force acting on the cylinder was selected as a secondary objective because, first,

this is an integrated result of a predictable primary physical quantity. Second, it appears not feasible to avoid encumbering the measurement of force by ordinary body inertia reaction, which is far from negligible, yet not of concern to this theory.

An additional reason for placing emphasis on the pressure distribution measurement is the expectation that such investigation will help to provide insight into similar problems of naval architectural interest.

The following measurements were obtained with a cylinder of 10-inch radius in forced vertical harmonic motion of small amplitude. Details of the experimental arrangement and simulation of two-dimensional conditions are recorded in later sections. Over a certain range of oscillation frequency, $0.2 < f < 0.6$ cycles per second, the particular arrangement used simulated two-dimensional conditions less successfully and this caused consistent small deviations from theory in this range. The experiments were conducted at the Ship Model Towing Tank, Richmond Field Station, University of California.

7.2 Results of Measurements of the Pressure Fluctuation.

The total pressure fluctuation at a point on the surface of a horizontal circular cylinder given forced vertical oscillations in an ideal fluid of infinite depth is predicted with the aid of the calculations reported in Section 5.3. The total pressure fluctuation, in units of the hydrostatic fluctuation for a forced motion $y = h_0 \sin \omega t$, is

$$\frac{p(\delta, \theta, t)}{\rho g h_0} = [1 - p_e(\delta, \theta)] \sin \omega t + p_v(\delta, \theta) \cos \omega t .$$

Here $p_a(\delta, \theta)$ and $p_v(\delta, \theta)$ are the acceleration- and velocity-phase components of the hydrodynamic pressure given for this case in Section 5.3. The amplitude of the total pressure fluctuation is

$$\bar{p}(\delta, \theta) = \left| \frac{p(\delta, \theta)}{\rho g h_0} \right| = [(1-p_a)^2 + p_v^2]^{1/2}.$$

The predicted results are shown by solid lines through calculated points in Figure 28 for $\theta = 0^\circ$, 40° , and 60° . Experimental points for measurements at the same locations are shown on the same figure. These points are (amplitude of the recorded pressure fluctuation)/(amplitude of the recorded pressure fluctuation for hydrostatic displacement). The distinctive trends, for each θ , of the predicted and measured results are generally confluent. An observed departure from two-dimensional conditions in the experiment is the principal cause for consistent small deviations from predicted results in the range $0.2 < f < 0.6$ cycles/second. The trend toward higher-than-predicted results at $\theta = 60^\circ$ at the higher frequencies observed may be caused by viscous effects in the locations of higher tangential velocity.

7.3 Results of Measurements of the Vertical Force Acting on the Cylinder.

The total vertical force per unit length required to sustain steady-state motion $y = h_0 \sin \omega t$ of the test cylinder is the sum of the hydrodynamic force (Section 3.8),

$$2\rho a^2 \frac{M_0 B + N_0 A}{A^2 + B^2} \ddot{y} + 2\rho a^2 \frac{\pi^2/2}{A^2 + B^2} \dot{\omega y},$$

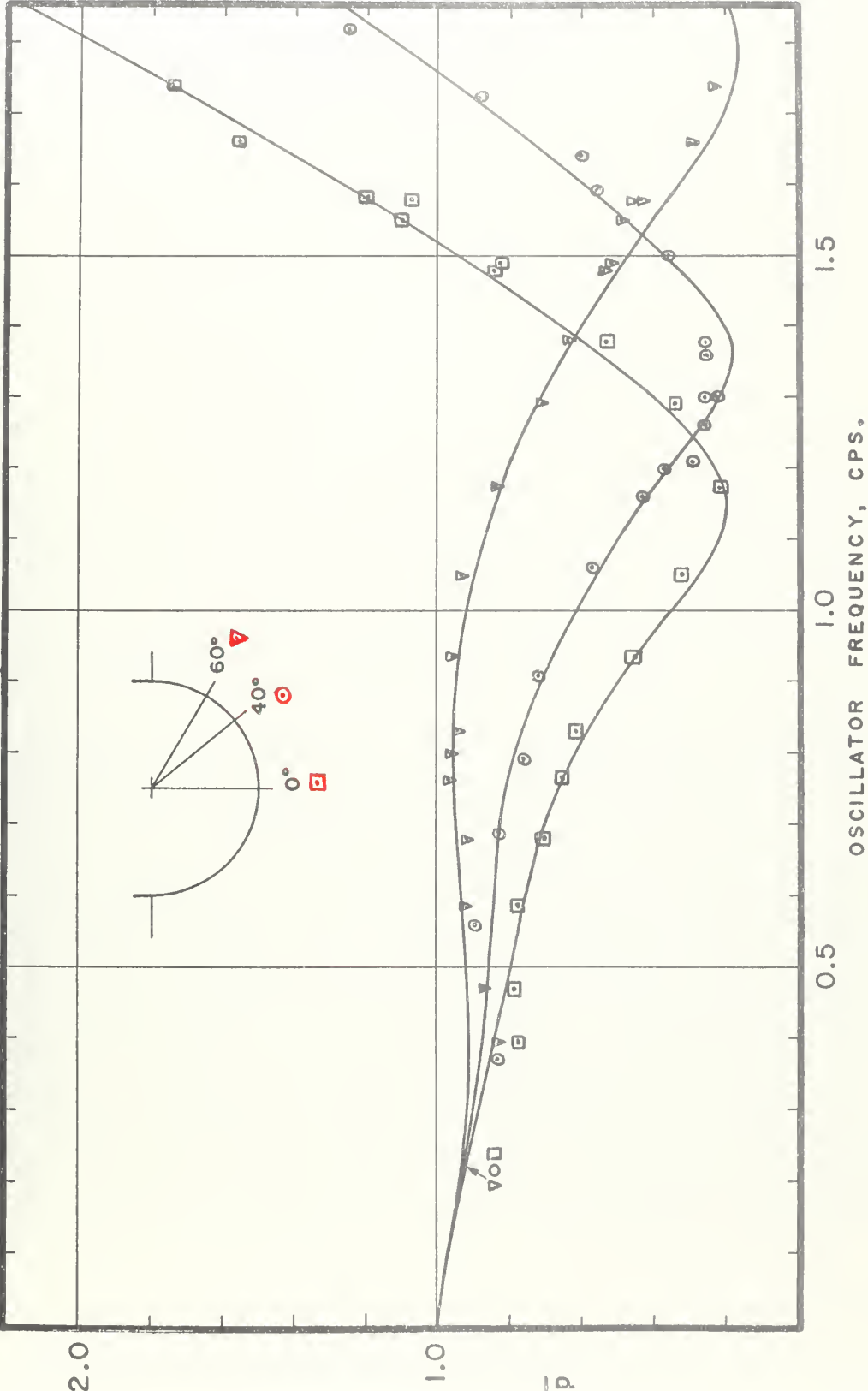


FIGURE 28. THE CALCULATED AND MEASURED AMPLITUDE OF TOTAL PRESSURE FLUCTUATION.

and the hydrostatic force $2\rho g y$ and the inertia reaction of the mass of the cylinder. The mass of the cylinder in this experiment was made equal to that of the displaced fluid for neutral buoyancy at rest. The total force in units of the change in hydrostatic force is

$$\frac{F(t)}{2\rho g a h_o} = [1 - (1+k)\delta\pi/4] \cos \omega t - \frac{2\pi}{A^2 + B^2} (\delta\pi/4) \sin \omega t$$

$$k = \frac{4}{\pi} \frac{M_o B + N_o A}{A^2 + B^2} .$$

The amplitude of the total force fluctuation is the square-root of

$$[1 - (1+k)\delta\pi/4]^2 + \left[\frac{2\pi}{A^2 + B^2} (\delta\pi/4)\right]^2 .$$

The added mass coefficient k and the damping force coefficient $2\pi/(A^2 + B^2)$ for this case are reported in Section 5.4.

The predicted result is shown by the solid line through calculated points in Figure 29. Points for measured values are shown. These points are (amplitude of the recorded total force signal) divided by (amplitude of the recorded signal for hydrostatic displacement). The general agreement is satisfactory. Again, the observed departure from two-dimensional conditions is the principal cause for small differences from predicted results in the range $0.2 < f < 0.6$ cycles/second.

Measured results are generally higher than predicted in the neighborhood of the force minimum around $f \approx 0.9$ cps. In this region

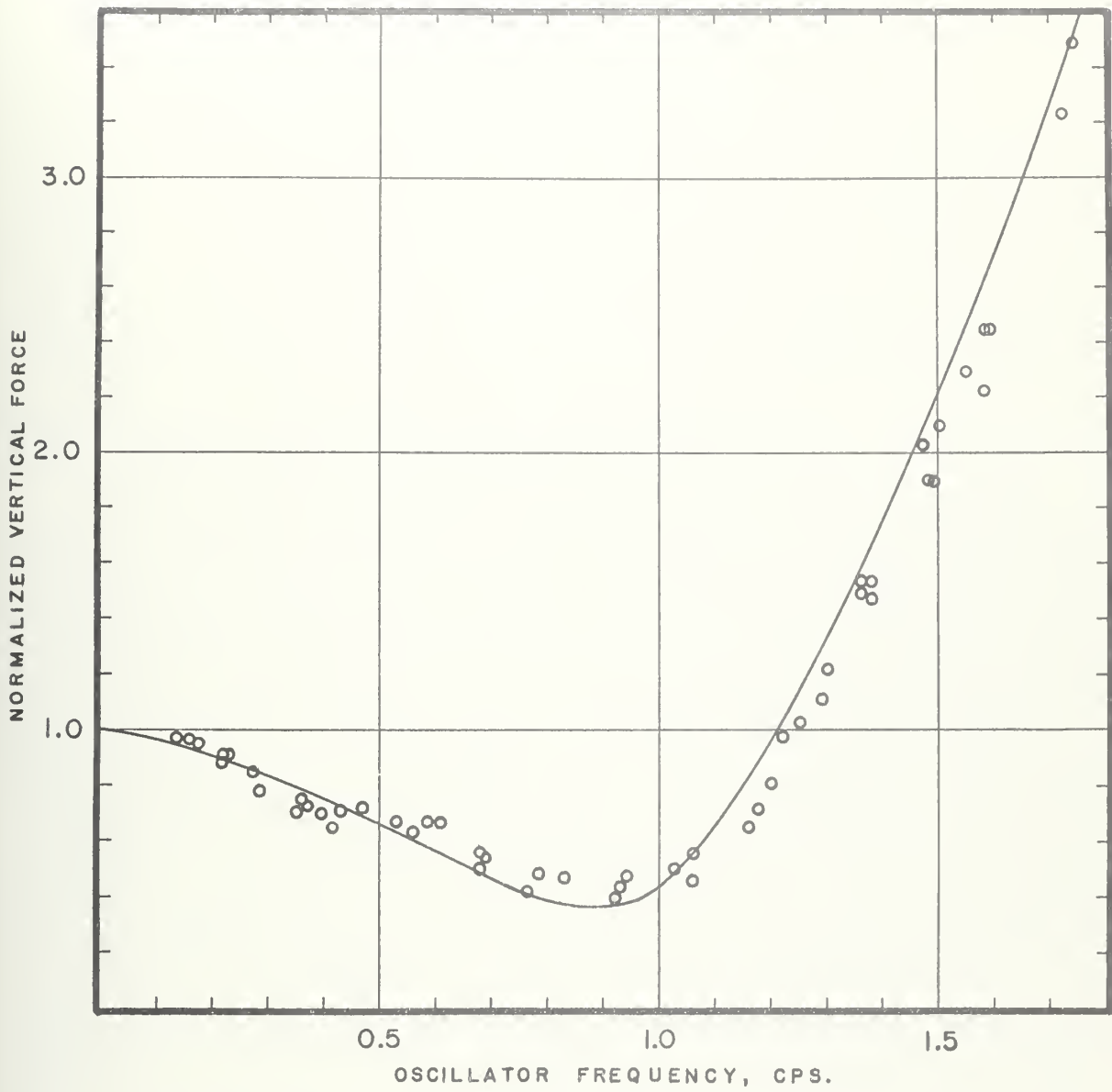


FIGURE 29. CALCULATED AND MEASURED TOTAL VERTICAL FORCE.

$$1 - (1+k)\delta\pi/4 \approx 0$$

and the total force is nearly that in phase with the velocity. Any additional energy dissipation (due to viscous effects, end-effects, etc.) would contribute additional force increments in phase with the velocity and not predicted by the theory. The measured values therefore may well be expected to be higher than predicted and more distinctly so when the much larger component in time-quadrature vanishes.

7.4 The Cylinder and The Experiment Arrangement.

7.41 The Cylinder and The Motion Generator.

The cylinder was fabricated from a one-quarter inch thick plate of aluminum rolled to a circular submerged cross-section with 10-inch outside radius and 12-inch vertical sides above water. The cylinder is 41 inches long. The ends are closed by end-plates of three-quarter inch aluminum plate. Two heavy steel athwartship frames, machined to semi-circular shape, together with the end frames, assure semi-circular shape, contribute rigidity, and anchor parts of two force dynamometers. The model plus the parts of the dynamometer in the model was weighted to neutral buoyancy at the desired water-line. The high vertical walls anchor dynamometer parts, contribute torsional rigidity and may be used in other experiments with deeper submergence. These high weights cause static instability but the overturning moment is small and of little consequence since the model is secured by means of vertical-motion dynamometers to the rigid motion generator.

The vertical-motion force dynamometers consist of an interchangeable set of beam "springs" each 7-1/2 inches long, 2-inches wide and 5/32 or 3/16-inches thick for choice of spring-constant.

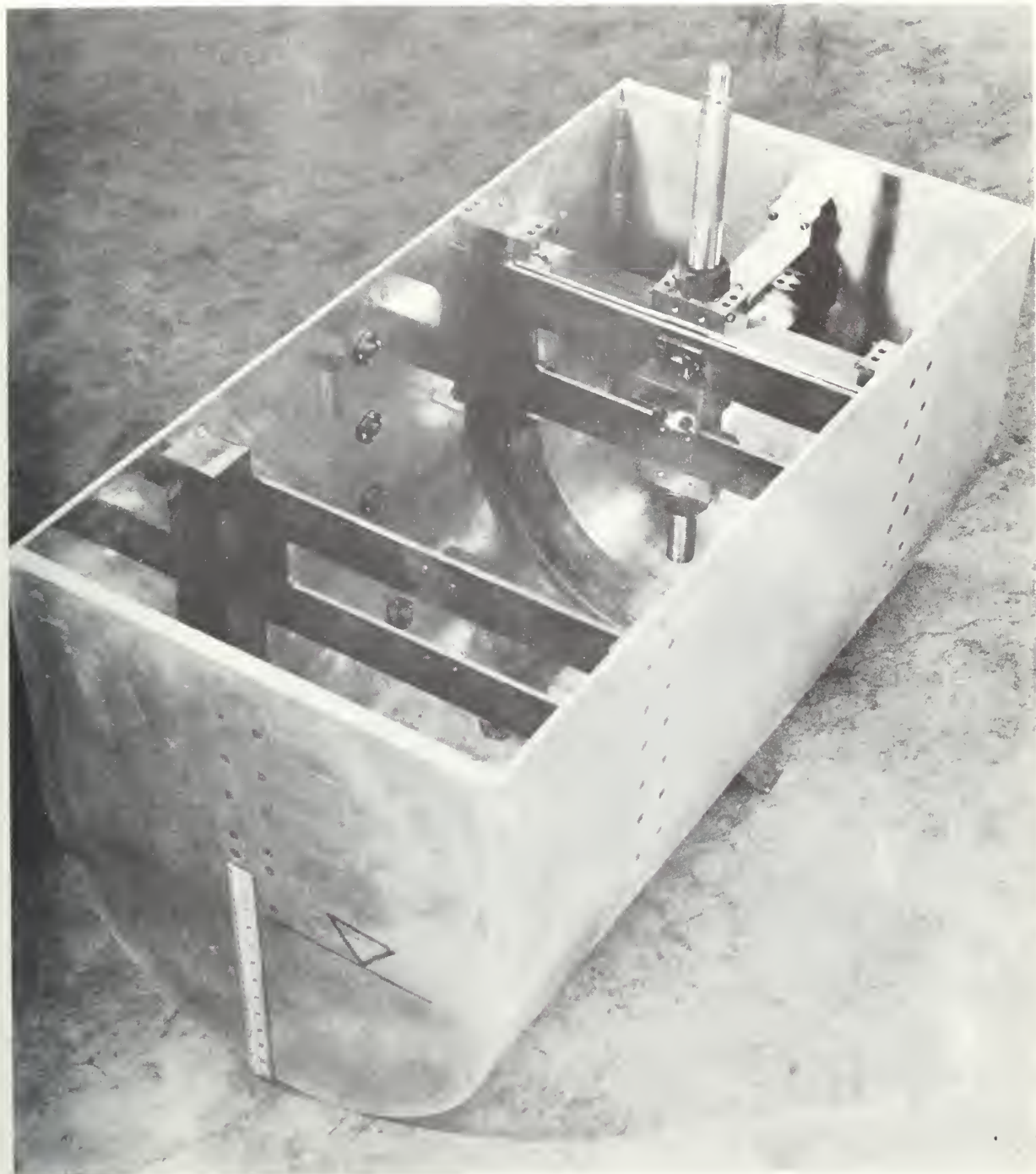


FIGURE 30. THE MODEL

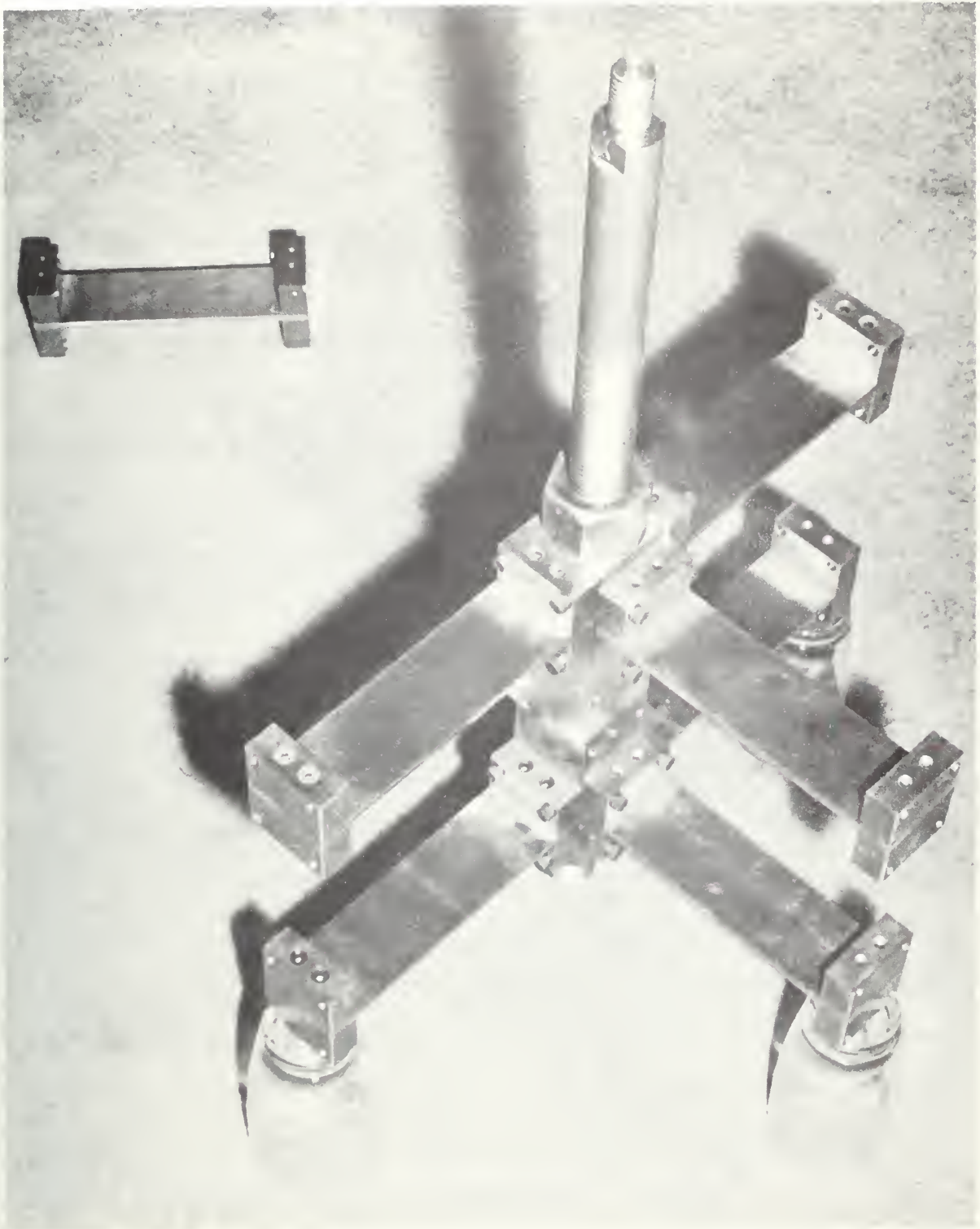


FIGURE 31. THE VERTICAL MOTION DYNAMOMETER

An array of six such springs connects each of two motion-generator reciprocating rods to its steel-frame and end-plate in the cylinder in an array strongly preferential to vertical relative motion. The relative displacement between the model and the reciprocating rod, a measure of the vertical force acting, was sensed by a Statham Instruments Corporation Model G-10-B unbonded strain-gauge displacement transducer. Relative vertical motions of about 0.002 inch were permitted and this is considered a negligible uncertainty in the stroke of the motion generator. The amplitude of the stroke was varied from one-half to one inch and had no observable effect on the recorded measurements. Almost all of the pressure measurements were made with one-half inch stroke.

The motion generator is an elaborate machine designed and build for the Ship Model Towing Tank. A $3/4$ -horsepower constant-speed motor, through a continuously-variable speed reducer, drives a pair of mechanisms patterned after the "scotch-yoke" which translate constant-speed rotation to uniform simple-harmonic reciprocation of two steel rods. The scotch-yoke, at the expense of elaboration, has the advantage of providing almost exact sinusoidal motion. The motion was continuously monitored by mechanically-driven potentiometers on the mechanism providing electrical signals which, because of orientation, were sine and cosine signals.

The pressure gauges were installed in the shell of the cylinder at various angular locations at mid-length. The gauges were unbonded strain-gauge types with sensitive diaphragms about $3/4$ -inch diameter. The diaphragms therefore subtend $(0.75)/10 = 0.075$ radian,

about 4.3 degrees and it is understood results measured "at 40 degrees" admit the diaphragm extended about ± 2 degrees. The Statham Instruments Corporation Type PM-233-TC pressure transducers have calibration factors close to 23 millivolts/psi with strain-gauge bridge excitation of 5 volts. The full-scale range is ± 0.5 psi differential. The differential feature was used to provide rear-side pressurization (by air and static manometer) to balance the hydrostatic pressure preload on the sensitive diaphragm. This contributes to maximum initial sensitivity and linearity; the response of diaphragm-type transducers was studied extensively and is reported in the next chapter. The dynamic response of these gauges is uniform from hydrostatic up through frequencies well above those reported here.

7.42 The Simulation of Two-Dimensional Conditions.

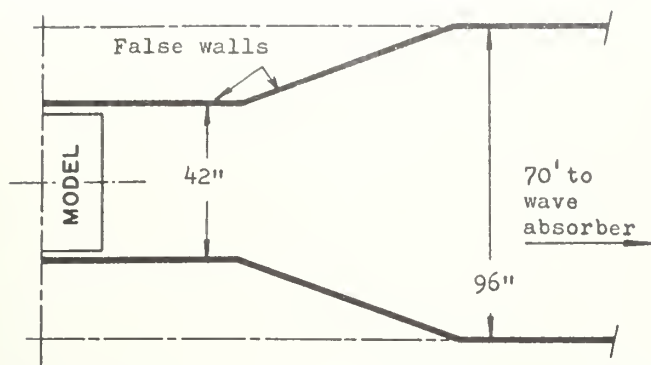
The experiments were conducted in the Ship Model Towing Tank, Richmond Field Station, University of California. The tank is 200 feet long, 8 feet wide and 6 feet deep. The cylinder and motion generator were installed mid-length and transversely between false walls installed in the tank to narrow the width at the model to 42 inches. The model is 41 inches long so there was 1/2 inch clearance at the ends. At the frequencies observed, surface action and disturbances at the ends was not violent but was increasing with frequency. At frequencies above those reported here the surface wave action was not two-dimensional.

The false walls at the model were 8 feet long, extended above the surface, and were solid to the bottom. The walls were 5-pound steel plate rigidly stiffened on the outside by welded flatbar

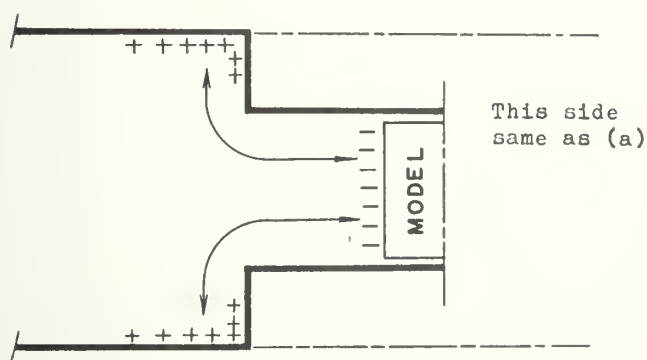
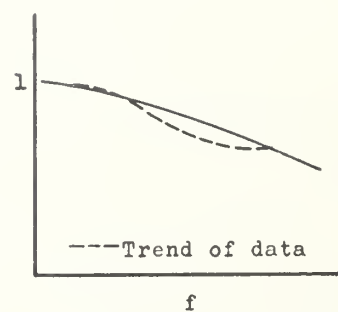
stiffeners. The parallel false walls at the model were joined to the regular tank walls by further sections at each end about 8 feet long. Thus the model was in the 42 inch space between false walls which were parallel for 8 feet and flared out on each side to 96 inch spacing. It is agreed that for the experiment reported here alone, a model 8 feet long without special walls would be preferred, but other work was also in mind. Nevertheless, with the exception discussed below, it appeared that two-dimensional conditions generally prevailed and regular progressive surface waves were generated. Since the motion-generator was over-powered and positively driven, steady-state conditions were approached in the neighborhood of the cylinder very rapidly.

Under certain conditions, described below, a distinct departure from two-dimensional conditions was observed. The influence of this effect as reflected for example in the total force measurement was strongly dependent on the transition conditions at the ends of the parallel walls. Three transition conditions are shown in Figure 32.

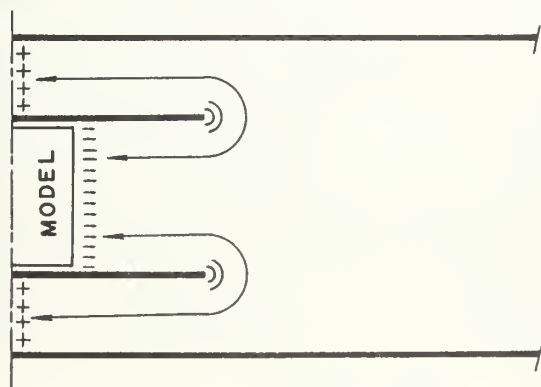
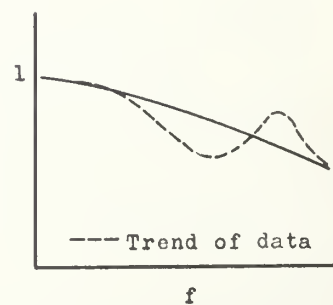
Arrangement (a) is the least abrupt transition from 42 inch spacing at the model to the 96 inch tank width. This is the arrangement used for the data recorded in the preceding sections. The consistent lower-than-theoretical experimental values in the range about $0.2 < f < 0.6$ cycles/second are believed to be caused principally by this transition. The effect is much more intense with more abrupt transitions. Two other arrangements were tried and are illustrated in the figure together with sketches showing the trend of total force measurements in the critical frequency range. The consistent pattern leads to the belief that parallel walls with a fitted model would



ARRANGEMENT (a)



ARRANGEMENT (b)



ARRANGEMENT (c)

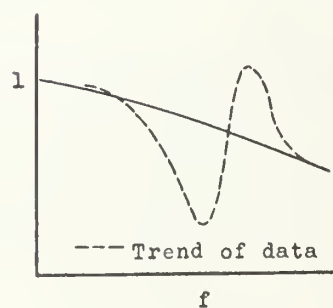


FIGURE 32. TOP VIEW OF ARRANGEMENTS. (b) and (c) accentuate departure from two dimensional conditions.

eliminate this cause of deviation of measured from predicted values. In all arrangements the surface wave-action, even in this critical range, appeared to be normal and two-dimensional in the near neighborhood of the model except for minor disturbances in the corners at the ends.

7.43 Electrical Instrumentation.

The unbonded strain-gauge displacement transducers in the force dynamometer and pressure transducers in the shell of the model (Section 7.41) were connected to Brush Instruments Division, Clevite Corporation, Model RD-5612-00 carrier and recording amplifiers. The carrier frequency is nominally 2 kcps, the bridge excitation voltage normally available is less than maximum usable by the transducers but signal strength was sufficient and reliable.

The electrical signals monitoring the motion (Section 7.41) were connected to the direct-current recording amplifier sections of other Brush RD-5612-00 units.

All electrical signals were recorded on an 8-channel Brush Instruments Model RD-2684-50 linear chart recorder. Data were reduced from the records manually; recorded amplitudes measured in the range 0.6 to 4 centimeters.

The frequency of oscillation was computed from the recorded motion sinusoids and known chart-speeds and also compared with revolutions counted by a Berkeley Instruments Corporation "events-per-unit-time" counter. This instrument was given electrical pulses from cam-operated microswitches and the number of counts in a known time interval confirmed the oscillation frequency.

VIII. General Study of Instrumentation for Measurement of Pressure Fluctuations.

8.1 General Characteristics of the Pressure Measurement.

This chapter presents an analysis of pressure transducers and their use in measuring the hydrostatic and hydrodynamic pressure distribution on a body oscillating in a free surface. The material is part of a general study of instrumentation pertinent to the experimental investigation reported in the preceding chapter and is of interest in similar investigations.

The predicted values for the experimental case may be used to fix ideas on the pressure fluctuation magnitudes and frequency range. The fluctuation is periodic at the model-motion frequency. Its amplitude is

$$\bar{p}(\delta, \theta) = \left| \frac{p(\delta, \theta)}{\rho g h_0} \right| = [(1-p_a)^2 + p_v^2]^{1/2},$$

where $p_a(\delta, \theta)$, $p_v(\delta, \theta)$ are the acceleration- and velocity-phase components calculated for the example in Section 5.3. Curves showing this result are given for various θ in Figure 28.

At low frequencies, $\delta < 0.2$, $\bar{p}(\delta, \theta) \approx 1$ independent of location θ . That is, the pressure fluctuation is approximately the hydrostatic change due to slow heaving. The surface is barely distorted, and the pressure change is nearly independent of location. This is rigorously correct as $\delta \rightarrow 0$. Since the displacement is assumed to be small with respect to body dimensions, this reference pressure change is small.

The amplitude of the pressure fluctuation goes through a minimum at a characteristic frequency depending on the location θ . For example, the minimum is about 20% of the hydrostatic change at locations in the bottom sixty-degree sector and occurs at $1.5 < \delta < 3$. Twenty percent of the expected hydrostatic pressure fluctuation is a useful index for the minimum expected pressure fluctuation. For the 20-inch-diameter cylinder used in the experimental part of this work, 20 percent of the one-half inch motion in water corresponds to about 0.004 psi.

At higher frequencies, the magnitude of the pressure fluctuation increases. Ultimately, cavitation at the bottom center-line or viscous effects or short surface wavelength violate the assumptions preceding these predictions.

The frequency range of interest in the experiments with a cylinder of 20 inch diameter was 0-2 cycles per second, that is, about $0 < \delta < 3$.

The low frequencies and preference to record hydrostatic pressure suggest a diaphragm-type transducer. Piezoelectric-type hydrophones are contra-indicated by this requirement because of their limited low frequency response.

The low pressures and pressure fluctuations dictate high sensitivity. For ship-like cylinders of about 1-foot beam the minimum detectable pressure change should be about 0.001 psig (about $1/40$ inch water or +110 DB ref $0.0002 \text{ dynes/cm}^2$). This requirement is easily met by a piezoelectric transducer but the high sensitivity conflicts with the requirement for small diameter in the case of diaphragm types.

For experimental convenience, cylinder dimensions must be manageable and for maximum utility the transducers should be compatible with the ship models ordinarily used.

8.2 Piezoelectric Transducers.

8.21 Open Circuit Operation; the Piezoelectric Wafer.

The piezoelectric transducer gives promise for this application because of its sensitivity. Its disadvantages are limited low-frequency response and sensitivity to local vibrations of its mount.

To illustrate the operation of a piezoelectric transducer and its major disadvantage, consider the response of a disc to normally incident pressure signals. The disc area is A , its thickness t . Assuming a material similar to barium titanate, the disc is polarized across the thickness direction, \vec{z} . The rear face is blocked by a relatively large mass.

This wafer of piezoelectric crystal, compressed in the direction of its thickness t with a pressure p to a stress level $p = F/A$, generates a proportional electric field in the direction of polarization:

$$\vec{E} = kp\vec{z},$$

$$\vec{E} = V/t = kp.$$

The potential difference across the wafer is

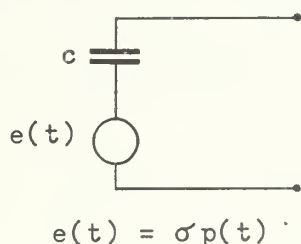
$$V = (kt)p = \sigma p$$

σ = pressure sensitivity, volts/microbar.

The constant k in units of volts/cm thickness/microbar pressure is typically 1.41×10^{-5} for ceramic "B" Barium Titanate and 2.41×10^{-5} for common piezoelectric materials called PZT-4 and PZT-5. (1 microbar = 1 dyne/cm²).

The open circuit sensitivity of a piezoelectric transducer is therefore independent of diameter and is easily of the order of -110 db referred to 1 volt per microbar. Thus piezoelectric transducers easily meet the required characteristics of high-sensitivity and small diameter.

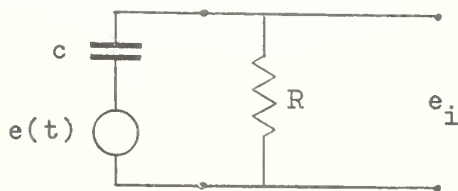
The required low frequency response requires closer examination due to the loading effect on the crystal of the external circuitry. To examine this, one uses the equivalent circuit of the crystal element. This consists of a voltage generator of zero internal impedance in series with an impedance equal to the internal impedance of the crystal. The voltage output of the conceptual generator is equivalent to the crystal pressure sensitivity. The internal impedance of the crystal is considered constant and equal to that of the capacitor formed by the crystal of dielectric material between equal-potential conducting surfaces.



8.22 Low Frequency Response of a Piezoelectric Transducer and Amplifier.

The input impedance of an amplifier connected to a piezoelectric transducer degrades the low-frequency response relative

to the open-circuit performance. This is seen by considering the amplifier input signal e_i :



In the usual circuit-analysis technique we use

$$s = j\omega$$

$$E_i(s) = \text{transform of } e_i(t)$$

$$E(s) = \text{transform of } e(t)$$

$$= \sigma P(s)$$

$$E_i(s) = E(s) \frac{s}{s + 1/\tau} = \sigma P(s) \frac{s}{s + 1/\tau}$$

$$\tau = Rc .$$

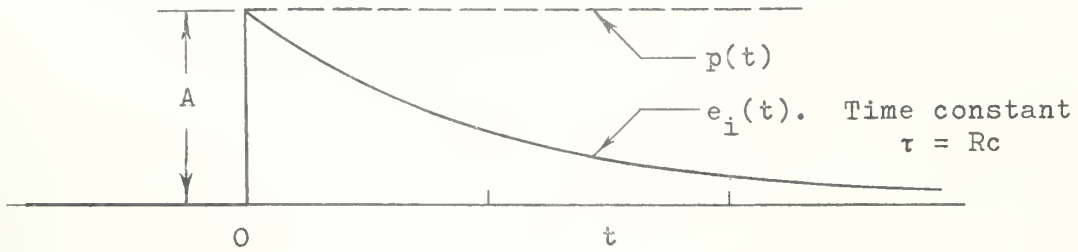
Consider a step-change in pressure:

$$p(t) = \begin{cases} 0 & t < 0 \\ A & t \geq 0 . \end{cases}$$

The amplifier input signal is

$$e_i(t) = \sigma A e^{-t/\tau} \quad (t \geq 0) .$$

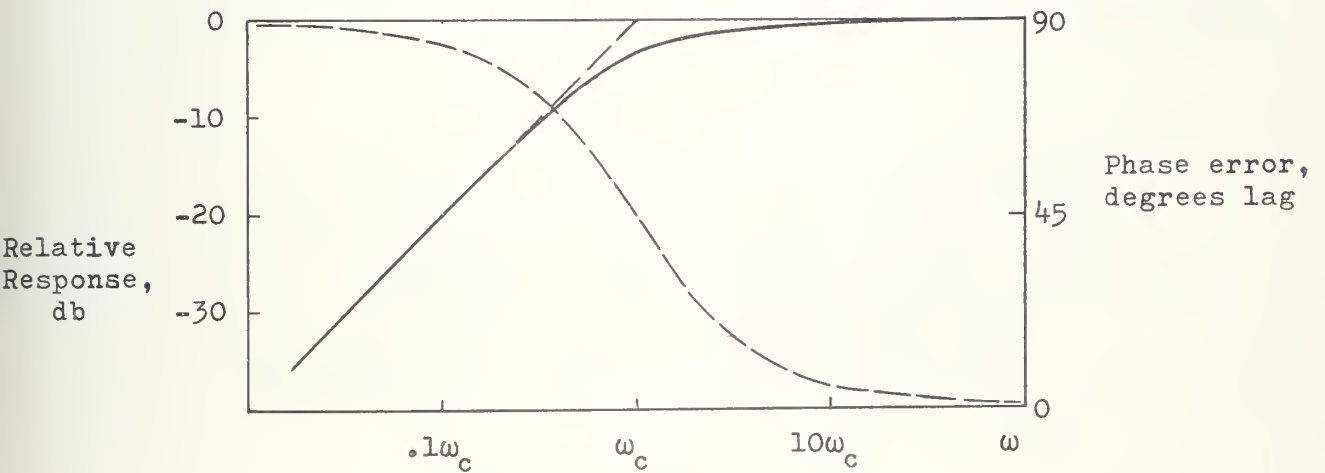
The open-circuit (unloaded) response of the crystal transducer would have been σA . The penalty imposed by the external amplifier (load) is the exponential decay of the hydrostatic response with a time constant τ .



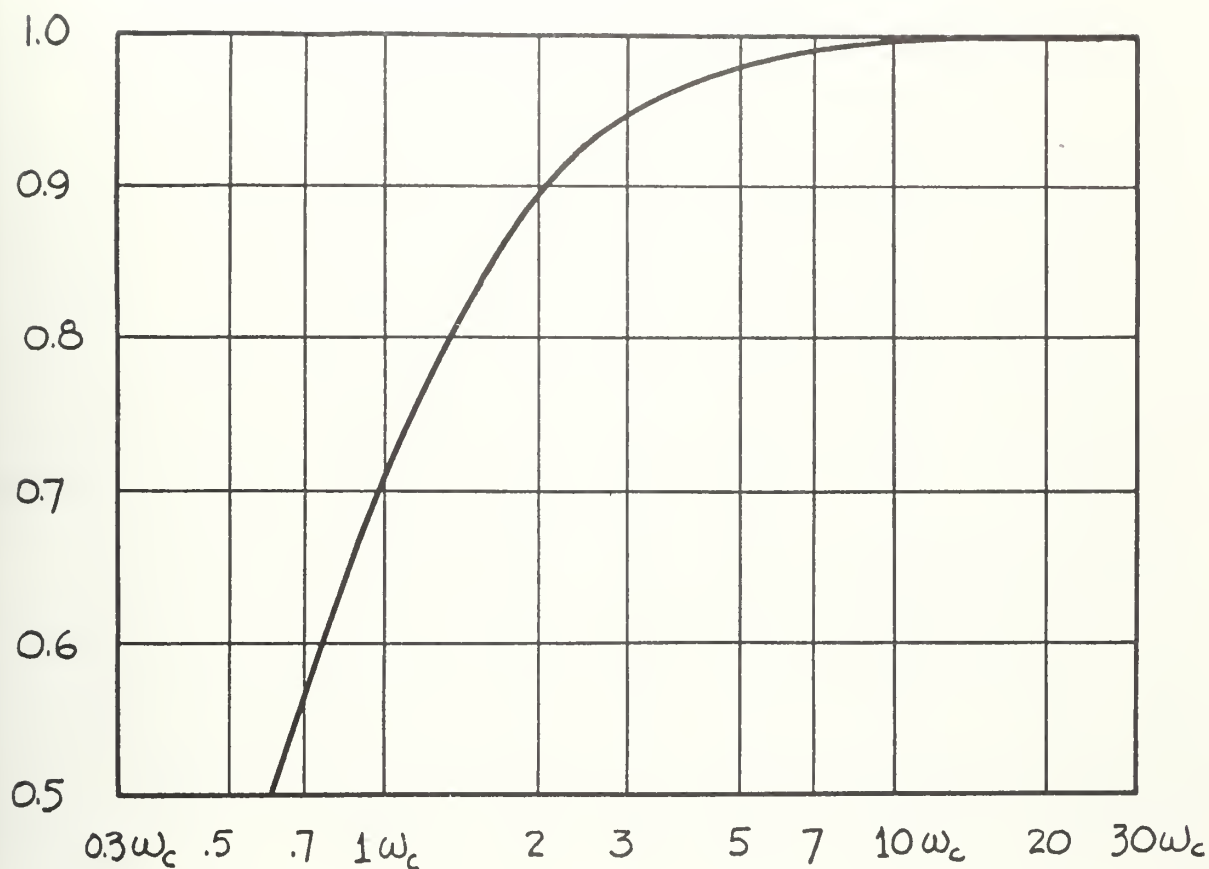
Response to a hydrostatic change in pressure.

The steady-state response to a sinusoidal time-varying pressure decreases in amplitude and is increasing in phase error below the cutoff frequency. The cutoff frequency is

$$\omega_c = 1/\tau = 1/Rc .$$



Amplitude Response and Phase Error relative to Open-Circuit Response of a Piezoelectric Crystal for Sinusoidal Pressure Fluctuation of Frequency ω .



FRACTIONAL AMPLITUDE RESPONSE
OF A PIEZOELECTRIC TRANSDUCER AND
D.C. AMPLIFIER AS A FUNCTION OF
FREQUENCY NEAR CUTOFF $\omega_c = \frac{1}{C}$

FIGURE 33.

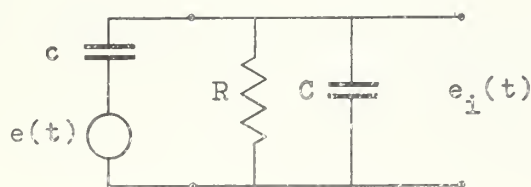
These results show that the low frequency response of the piezoelectric transducer plus amplifier is limited by the amplifier input impedance R and the crystal equivalent capacitance c . The amplifier input impedance is bounded by practical considerations of the associated thermal noise and by susceptibility to extraneous response due to the high impedance level. The crystal equivalent capacitance c can be increased by increasing the wafer diameter, which conflicts with small size; or by decreasing wafer thickness, which decreases sensitivity; or by stacking thin wafers, which increases complexity of the transducer.

Therefore it can be expected the use of piezoelectric transducers will be met with increasing difficulty as the desired low frequency response is extended.

Some techniques are suggested to partly alleviate this limitation.

8.23 Extending Low Frequency Response by Capacitive Loading.

The low frequency response of piezoelectric transducer plus amplifier may be extended at the expense of sensitivity. The amplifier input resistance R is shunted with a capacitance C .



$$E_i(s) = E(s) \frac{c}{C + c} \frac{s}{s + 1/\tau}, = \sigma \frac{c}{C + c} P(s) \frac{s}{s + 1/\tau},$$

$$\tau = R(C + c) \quad .$$

Comparing this result with that of the amplifier alone,

(i) The apparent sensitivity is reduced by a factor
 $c/(C+c) \leq 1.0$

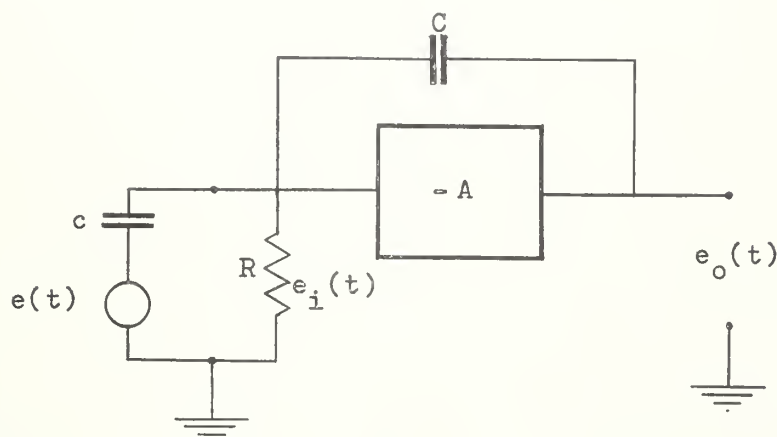
(ii) The hydrostatic time-decay factor is increased by
 a factor $(C+c)/c$. This is equivalent to reducing
 the low-frequency cutoff frequency by the factor
 $c/(C+c) \leq 1.0$

With this technique the relative response is kept uniform to a new lower cutoff-frequency at the expense of being at a lower absolute level. The degree to which this can be pursued thus depends on the original crystal sensitivity and the magnitude of pressure fluctuations which are to produce measureable signals within the absolute level capability of the available amplifier. That is, the signal to noise ratio at the reduced apparent sensitivity will limit an attempt to indefinitely extend the low-frequency response by this technique.

8.24 Extending Low-Frequency Response by Feedback Amplifier Technique.

Manipulations of the low-frequency cutoff and of the apparent sensitivity, interdependent in the preceding technique, can be largely separated at the expense of increased electronic complexity. An operational amplifier of standard design is introduced with capacitive feedback. The amplifier will have a large gain, $-A$, with negative sense meaning phase reversal. The amplifier is realistically assumed to have constant gain over frequencies of interest

and to have negligible output impedance. The input impedance cannot be neglected and as before is R . This amplifier is to be considered as a preamplifier or buffer for operational purposes between the piezoelectric transducer and the usual recording system.



By the usual circuit-analysis methods and without further assumptions,

$$E_o(s) = - E(s) \frac{1}{\frac{1}{A} + \frac{C}{c} (1 + \frac{1}{A})} \frac{s}{s + \frac{1}{\tau''}}$$

$$= - \sigma \frac{1}{\frac{1}{A} + \frac{C}{c} (1 + \frac{1}{A})} \frac{s}{s + \frac{1}{\tau''}} P(s)$$

$$\tau'' = R[c + C (1+A)] .$$

Comparing this result with those preceding it is seen the sensitivity and time constant are changed by functions of C and A . If the feedback element C is reduced to zero the relations are simply those for an amplifier following an amplifier-loaded piezoelectric transducer. If C is not zero and the realistic assumption is

made that

$$|A| \gg 1$$

then the relations are simplified. Compared with the amplifier-loaded case,

- (i) the sensitivity is modified by the factor c/C
- (ii) the time constant is increased by the factor $C(1+A)/c \approx CA/c$.

This is equivalent to reducing the low-frequency cutoff by a factor c/CA .

It is striking to observe then that if C is made approximately equal to c , then

- (i) the sensitivity is equal to the open circuit sensitivity.
- (ii) the low-frequency cutoff is reduced by the factor $1/A$, where A is a large number.

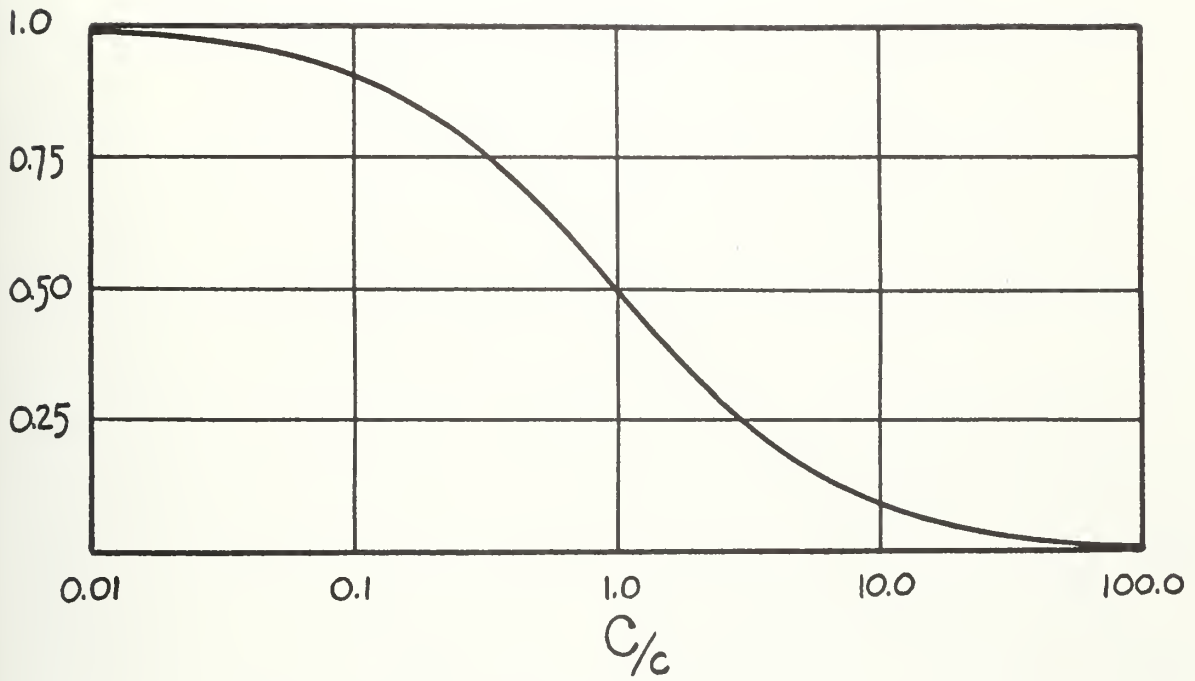
It appears this should be a useful technique for extending low-frequency response with nearly independent control of the apparent sensitivity and the extent of cutoff reduction. Practical limitation on the extent of this manipulation is not clear.

8.3 The Pressure Sensitivity of Diaphragm-Type Transducers.

8.31 Definition of Sensitivity.

The transducers considered consist of two elements.

- (i) the mechanical pressure receiver. Primarily this will be a diaphragm but may be a tube, bellows or



FRACTIONAL RESPONSE AS A FUNCTION
OF (ADDED / INTERNAL) CAPACITANCE

FIGURE 34.

capsule which deflects under pressure and seals the device against fluid ingress.

- (ii) the deflection detection schema. This converts the pressure-receiver (diaphragm) deflection to a signal in useful form. In order to take advantage of electronic (linear) amplification, electrical schemes are of most interest in devices of high sensitivity and resolution. Examples may be found using various physical principles: variable resistance, capacitance, reluctance, light flux, etc.

Pressure variations on the pressure receivers of several different types of transducers change the internal energy in the detection device a negligible amount compared with the change in elastic strain energy in the pressure receiver. Limiting consideration to such stiffness-controlled transducers, it is possible to analyze the two elements of the transducer separately, and the transducer pressure sensitivity is the product of the sensitivities of each element:

$\delta = \delta(p)$, the diaphragm deflection at the center;

$e_o = e_o(\delta)$, the transducer signal output;

$$\frac{de_o}{dp} = \frac{d\delta}{dp} \frac{de_o}{d\delta}.$$

The effectiveness of the pressure measurement system cannot be judged on transducer sensitivity de_o/dp alone because this signal will be contaminated by a noise signal. Also, a response index will be required characterizing the least readable amplitude fluctuation of the indicating needle or chart line. Before attacking these

problems it is fundamental to study the deflection-pressure relation $\delta = \delta(p)$. This section will consider this relation and the pressure sensitivity,

$$\sigma = \frac{d\delta}{dp} .$$

8.32 Small Deflections of Clamped-Edge Flat Circular Plates; Kirchhoff Theory.

The theoretical maximum pressure sensitivity of a diaphragm is generally considered to be the initial sensitivity of a flat circular plate under uniform pressure load on one side producing infinitesimal inextensional strain.

By inextensional strain is meant that the plate neutral plane is not extended. The internal strain energy is greater and the plate is stiffer if extensional strains exist. Inextensional conditions are consistent with Kirchhoff plate theory.

The common and useful practice of diaphragm corrugations invariably introduces locations of extensional strain. Corrugated diaphragms realize less sensitivity than the theoretical initial sensitivity of the equal flat disc in Kirchhoff plate theory.

The Kirchhoff theory, neglecting stretch and shear of the plate neutral plane, yields the following result for the deflection δ at the center of a clamped-edge flat disc of diameter D uniformly loaded by a pressure p on one side:

$$\delta = \frac{3}{256} \frac{p D^4}{E t^3} ,$$

where

F = a plate modulus $E/(1-\mu^2)$, not $Et^3/12(1-\mu^2)$,
 t = thickness.

The deflection is linear in pressure; the pressure sensitivity is independent of the deflection.

Non-dimensional expressions for deflection and for pressure are:

$$\frac{\delta}{t} = \frac{3}{256} \left(\frac{p}{F}\right) \left(\frac{D}{t}\right)^4$$

$$\left(\frac{\sigma F}{D}\right) \left(\frac{t}{D}\right)^3 = \frac{3}{256} .$$

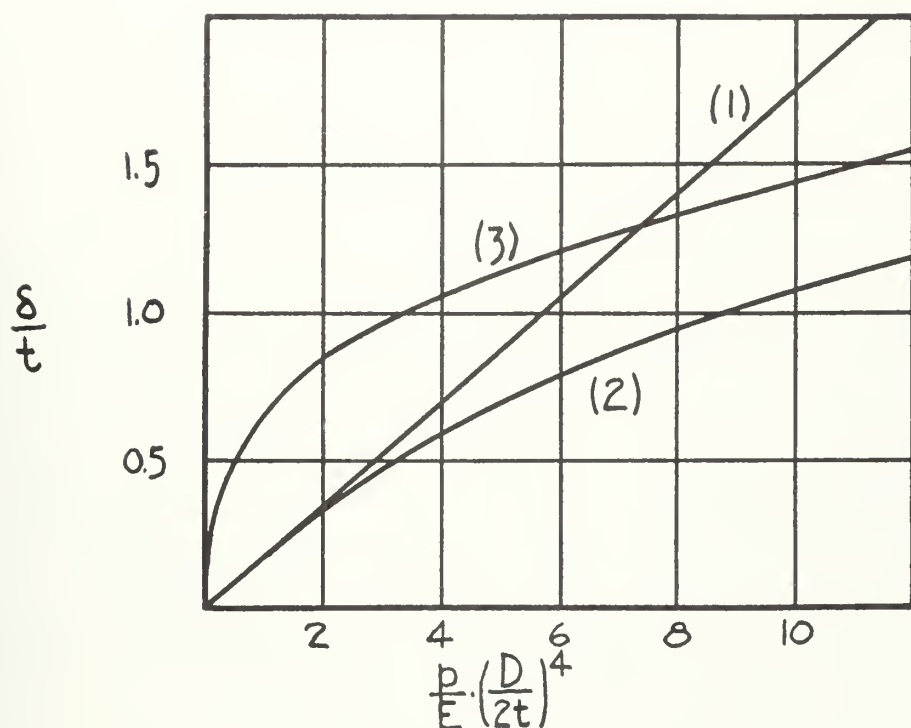
These relations are illustrated graphically in Figure 35 and 36. These representations are subject to the assumptions of their theory. Thus it is clearly not correct that δ/t increases linearly indefinitely and it is not possible to indefinitely increase sensitivity $\sigma F/D$ by decreasing t/D .

We will consider several cases illustrating that the pressure sensitivity actually achieved by a thin diaphragm will probably be less than this theoretical maximum.

8.33 Pressure Sensitivity of Flat Circular Plates with Deflection not Infinitesimal.

For practical purposes it is not always possible to limit diaphragm deflections to deflections small in comparison with diaphragm thickness. Such factors as hydrostatic preload or practical deflection detection schemes lead to larger deflections and, as we will see, possibly decreased sensitivity.

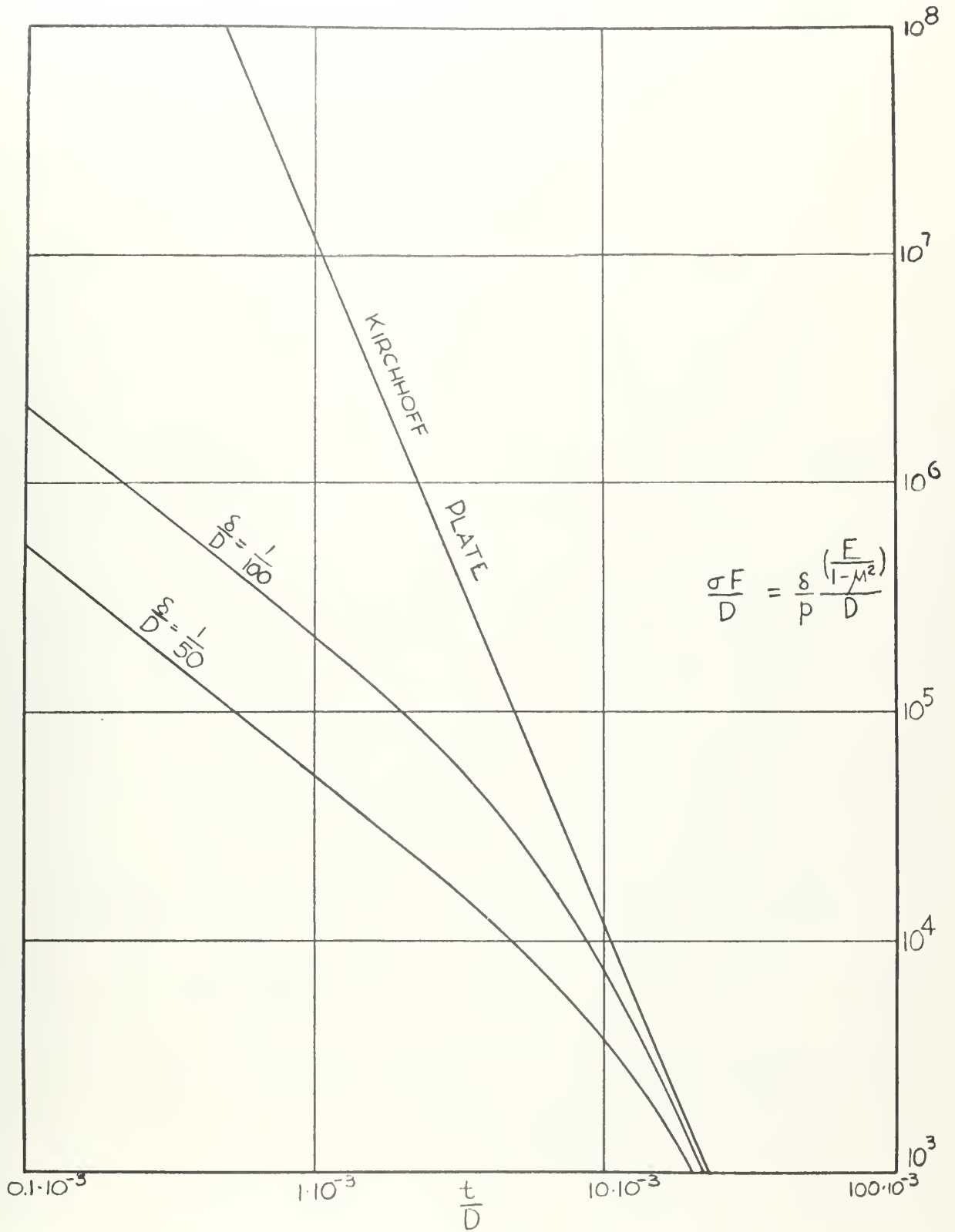
The exact solution of the equations of equilibrium of a flat



NONDIMENSIONAL DEFLECTION OF
OF FLAT CIRCULAR DIAPHRAGMS
WITH CLAMPED EDGES AND NO
INITIAL TENSION

- (1) KIRCHHOFF
- (2) WAY
- (3) HENCKY

FIGURE 35.



NON-DIMENSIONAL PRESSURE SENSITIVITY
OF A FLAT CIRCULAR PLATE

FIGURE 36

circular disc uniformly loaded on one side and with clamped edges and no initial tension is due to S. Way [1934]. This solution is available in tabular or graphic form but not in algebraic or series form. This solution is also illustrated in Figure 35.

Approximate solutions are due to A. Nadai [1925], S. Timoshenko [1940], and A. Griffith [1927]. Another approximate solution is reported by E. Waters in the discussion accompanying the solution by Way [1934]. These approximate solutions are expressed in algebraic form. The deflection-pressure function is nonlinear and additional definitions of sensitivity are useful.

Pressure sensitivity is $d\delta/dp$ as before and may be called the instantaneous pressure sensitivity. Initial sensitivity is defined as the limit of the pressure sensitivity for infinitesimal deflections:

$$\sigma_i = \lim_{p \rightarrow 0} \frac{d\delta}{dp} .$$

Average sensitivity at a given deflection and pressure is

$$\bar{\sigma} = \frac{\delta(P_o)}{p_o} .$$

The ideal flat-disc case has constant pressure sensitivity $d\delta/dp$ equal to the initial sensitivity $d\delta/dp]_{p=0}$ and average sensitivity $\delta(p_o)/p_o$.

The graphical presentation of the large deflection case suggests that the initial sensitivity is equal to that in the ideal case. The pressure sensitivity decreases for increasing deflection. The

average sensitivity at a given pressure, from algebraic expressions similar to those of the approximate solutions of Timoshenko, Nadai, Griffith or Waters is

$$\frac{\bar{\sigma}_F}{D} = \frac{\delta(p_o)F}{p_o} = \frac{3}{256} \frac{1}{\left(\frac{t}{D}\right)^3 + 0.545 \left(\frac{\delta(p_o)^2}{D}\right) \left(\frac{t}{D}\right)}$$

[the constant 0.545 may vary about ± 10 percent depending on Poisson's ratio and the approximation. Timoshenko reports 0.583 for $\mu = 0.25$ and 0.488 in another approximation. Our constant happens to be an average and agrees with Griffith for $\mu = 0.29$]. This is illustrated in Figure 36 for two assumed values of

$$\frac{\delta(p_o)}{D} = \frac{1}{50} ; \frac{1}{100} .$$

It is seen the average sensitivity may well be markedly lower than the theoretical maximum. The instantaneous pressure sensitivity is always less than the average sensitivity at finite deflections.

Corrugated diaphragms such as those of the National Bureau of Standards series realize average sensitivities somewhere between the ideal maximum and the value of the average sensitivity for $\delta(p_o)D = 1/100$.

This limitation of sensitivity to values less than maximum theoretical applies when deflections are approaching $0.4t$ or more. High sensitivity requires small t/D ratio for a given material. Measurable deflections which are a small part of t force larger D . Fortunately, sensitivity is proportional to the fourth power of diameter. Conversely, attempts to reduce diameter are penalized by this

power. An attempt to achieve high sensitivity at given limited diaphragm diameter by reducing diaphragm thickness t (i.e., small t/D) will ultimately face this limitation when the detectable deflection is of the order of t . Another problem, described in the next section, is a loss in sensitivity characteristic of thin diaphragms.

8.34 The Large Deflection of a Thin Diaphragm with Zero Initial Tension; the Solution of Hencky.

The following comparisons of thin diaphragms, or membranes, with circular plates having bending stiffness will use the center deflection as a basic measure. It is well to observe that this may be an incomplete criterion, depending on the means employed to detect diaphragm distortion. Center deflection is sufficient if the detection system depends only on this, or if the deflection form of the cases compared is similar. The deflection form of stiff plates and membranes are not geometrically similar. Therefore the volume sensitivity, the volume swept by the deflecting diaphragm per unit pressure, is different in each case. A practical case in which this would be significant is when the change in capacitance is used to detect deflection. A membrane, sweeping out a larger volume than a stiff plate at the same center deflection, produces significantly greater unit change in parallel-plate capacity (see for example Lilly, Legallis, and Cherry [1947]). Since the primary index is center deflection, attention will be given only this item.

One may suspect that a sufficiently thin diaphragm would have no effective bending stiffness, so that deflections would develop

only membrane tension stresses. Kirchhoff theory and the solution of Way do not apply. H. Hencky [1915] has achieved an exact solution by power series methods for the equations of equilibrium of a flat disc uniformly loaded on one side, subject to the assumptions $t^3 \ll t$ and no initial tension.

A commonly used plate modulus defined as

$$\frac{t^3}{12} F = \frac{Et^3}{12(1-\mu^2)}$$

is in effect reduced to negligible value by Hencky's assumption.

Hencky's result for deflection at the center of this disc is

$$\frac{\delta}{t} = 0.662 \sqrt[3]{\frac{pD^4}{Et^4 16}}.$$

[The constant 0.662 is given by Hencky for Poisson ratio $\mu = 0.3$; other authors have values ± 5 percent or less].

This result is essentially predicted by the approximate solutions for the large-deflection case discussed above with the added assumption

$$\left(\frac{t}{D}\right)^3 \ll 0.545 \left(\frac{\delta(p_o)}{D}\right)^2 \left(\frac{t}{D}\right),$$

so that from those approximate solutions

$$\frac{\bar{\sigma}_F}{D} = \frac{\delta(p_o)}{p_o} = \frac{3}{256} \frac{1}{0.545 \left(\frac{\delta(p_o)}{D}\right)^2 \left(\frac{t}{D}\right)}$$

or in equivalent form

$$\frac{\delta}{t} = 0.68 \sqrt[3]{\frac{p D^4}{E t^4 16}}.$$

Hencky's solution has the elegance of exactness; this coincidence is given as a suggestion of reasonable continuity between solutions recorded here.

Hencky's solution is also shown graphically with the preceding solutions in Figure 35.

The instantaneous sensitivity is conveniently found from the Hencky solution by logarithmic differentiation,

$$\frac{d\delta}{\delta} = \frac{1}{3} \frac{dp}{p},$$

so that

$$\sigma = \frac{d\delta}{dp} = \frac{1}{3} \frac{\delta}{p} = \frac{1}{3} \frac{0.662 \sqrt[3]{\frac{p D^4}{E t^4 16}}}{p}.$$

The initial sensitivity is indicated to be indefinitely large, which is apparent from the slope of the deflection curve. Unfortunately the very high initial sensitivities appear to be not realizable. A physical interpretation of the infinite initial slope of the deflection curve may be that the no-load rest position of a thin diaphragm without initial tension is unstable. This is possibly a part of the phenomena called "oil-canning." Further, if one draws on the analogous result from the approximate solution, the necessary condition

$$\left(\frac{t}{D}\right)^3 \ll 0.545 \left(\frac{\delta(p_0)}{D}\right)^2 \left(\frac{t}{D}\right)$$

is not fulfilled for practical (t/D) at sufficiently low $\delta(p_0)$.

The assumption for this case implies large (D/t) , small

t/D , so that very small pressures are equivalent to values of pD^4/Et^4 producing operating points of δ, p away from the initial region. A small hydrostatic preload does this for instance. For finite deflections the instantaneous sensitivity decreases rapidly to values less than the constant value of the ideal disc or the corresponding values of the large deflection (Way) solution. The theoretical average sensitivity of the Hencky-type diaphragms would appear to exceed that of the Way-type diaphragm. This is considered illusory because the instability of the no-load initial position of Hencky diaphragms would in practice mean an average sensitivity measured from some initial non-zero deflection.

This section has employed the Hencky solution to show that exploiting thin diaphragms without initial tension and in the limit having entirely negligible bending stiffness is not likely to lead to practical sensitivities equal to the theoretical sensitivity of the Kirchhoff diaphragm. A characteristic of this limitation of sensitivity is the assumption of no initial tension. We consider now whether there is benefit in adding initial tension.

8.35 The Small Deflection of a Thin Membrane with Initial Tension.

An exact solution to the equilibrium equations for small deflections of a thin circular disc uniformly loaded on one side and subject to a large initial tension T is known. The formulation of this problem assumes that the bending stiffness of the plate $[\bar{F} = Et^3/12(1-\mu^2)]$ is negligible. It is also assumed that the initial radial stress (initial tension) is sufficiently large so that

the pressure load is brought to equilibrium by opposing tension components due to the curvature of the membrane and not by additional stress. This solution is that of the membrane equation

$$\nabla^2 \delta(r) = -\frac{p}{T}$$

which yields for deflection at the center

$$\delta = \frac{pD^2}{16T} .$$

The deflection is linear in pressure; the pressure sensitivity is constant.

In order to compare this with previous results, we make substitutions, with ϵ_0 equal to the initial unit strain,

$$T = \epsilon_0 \frac{E}{1-\mu} t = \epsilon_0 (1+\mu) Ft,$$

so that

$$\frac{\delta}{t} = \frac{3}{256} \left(\frac{p}{F}\right) \left(\frac{D}{t}\right)^4 \left[\frac{16}{3(1+\mu)\epsilon_0} \left(\frac{t}{D}\right)^2 \right] .$$

This is the same form as that for the ideal disc times the bracketed factor. That factor, for practical values of (t/D) , reduces to unity for initial strains ϵ_0 of the order 10^{-4} or less.

The pressure sensitivity of the membrane is constant

$$\sigma = \frac{\delta}{p} = \frac{D^2}{16T} .$$

In non-dimensional form,

$$\frac{\sigma F}{D} = \frac{3}{256} \frac{1}{\left(\frac{t}{D}\right) \left[\frac{3(1+\mu)}{16} \epsilon_0 \right]} .$$

If one compares this form with the result from Hencky's solution, the factor $3(1 + \mu)\epsilon_0/16$ and $0.545 (\delta/D)^2$ are seen to have equivalent roles in reducing the non-dimensional pressure sensitivity $\sigma F/D$. The apparent high sensitivities of the Hencky solution at small δ are not realizable nor are those of the membrane solution for small initial strain since in either case the assumption inherent in the appropriate exact solution is not satisfied.

We will now consider that the Hencky solution may represent one extreme condition of a diaphragm with no bending stiffness and the membrane solution another. The Hencky solution is for zero initial strain. The membrane solution is for such large initial strain that radial stress may be considered constant. The region between should be considered since both Hencky and Membrane Solutions give the illusion of initial sensitivities greater than that of an ideal Kirchhoff diaphragm.

8.36 The Large Deflection of a Thin Diaphragm with Initial Tension.

The membrane solution is not valid for small initial tension and Hencky's solution includes no initial tension as a boundary condition. An exact solution of the equations of equilibrium for a flat circular disc, assumed sufficiently thin so that $t^3 \ll t$, or in effect so that the bending stiffness is negligible, and subject to initial tension or initial strain, is reported in Appendix B. This solution bridges the gap between that of Hencky and the membrane solution.

As a result of this solution

$$\frac{\delta}{t} = K \sqrt[3]{\frac{p D^4}{E t^4 16}}.$$

Here K for a given plate is a function of initial strain and the pressure (that is, the finite deflection) and is shown graphically in Figure 37. For zero initial strain

$$K(0) = 0.662;$$

that is, Hencky's solution is reconstituted. $K(\epsilon_0)$ decreases in value for increasing ϵ_0 . For large initial strain one has the asymptotic solution

$$K(\epsilon_0) \sim \frac{1}{4} \frac{(1-\mu)}{\epsilon_0 E} \sqrt{\frac{E p^2 D^2}{t^2 4}} \quad \text{as } \epsilon_0 \rightarrow \infty$$

so that

$$\delta \sim \frac{p D^2}{16 t \frac{E \epsilon_0}{1-\mu}} = \frac{p D^2}{16 T} \quad \text{as } \epsilon_0 \rightarrow \infty.$$

The membrane solution is asymptotically recovered as it should be for large values of initial tension.

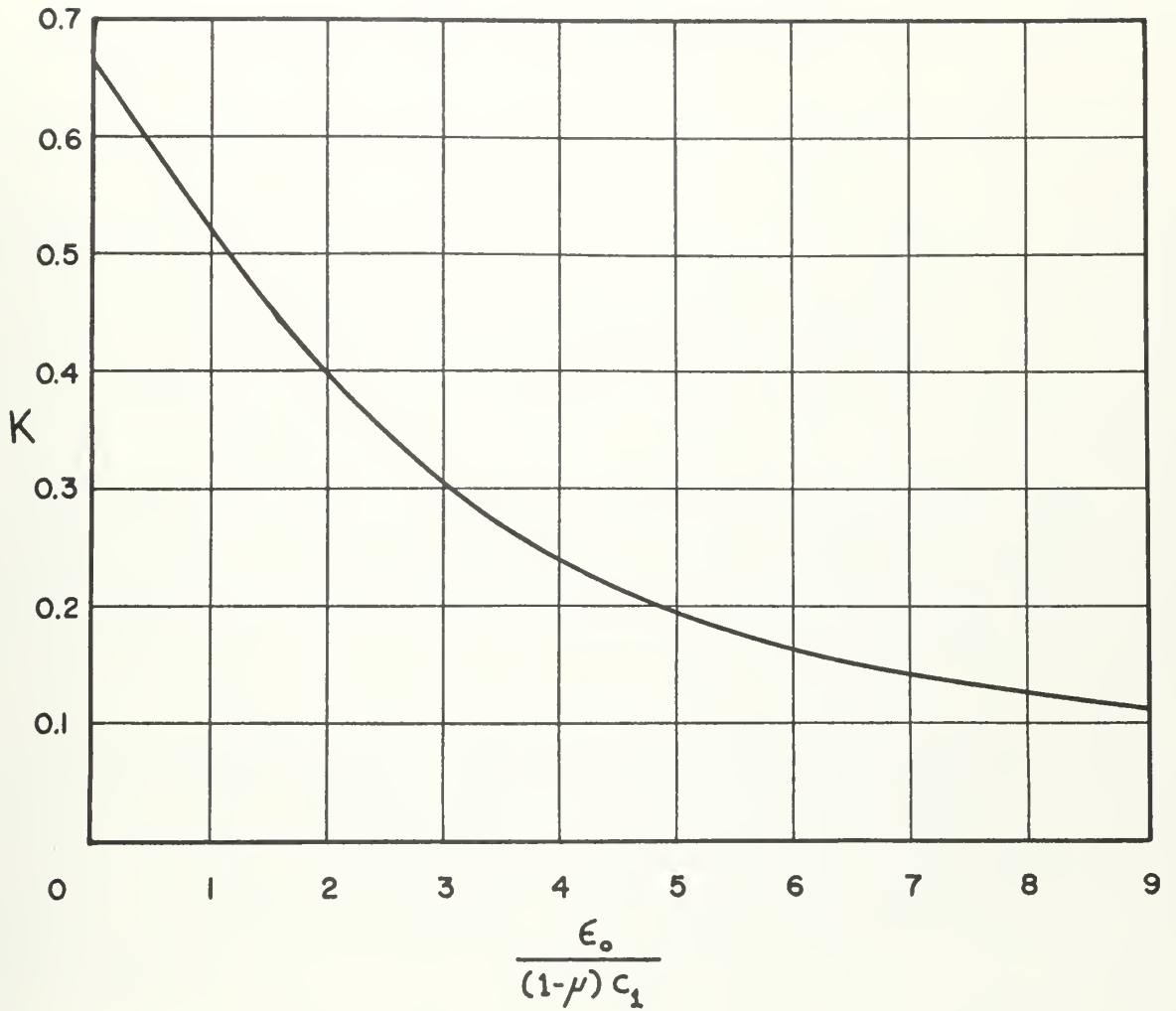
The average sensitivity is

$$\bar{\sigma}^3 = \left(\frac{K^3}{p^2} \right) \frac{D^4}{E t 16}.$$

For initial tension zero the term K^3/p^2 tends asymptotically to

$$\left. \frac{K^3}{p^2} \right|_{T=0} \sim \frac{0.662^3}{p^2} \quad \text{as } p \rightarrow 0$$

but this is not useful on the basis of previous remarks because of



DEFLECTION COEFFICIENT K AS A FUNCTION OF
INITIAL STRAIN ϵ_0 (per unit) AND LOAD, $c_1 = \frac{1}{4} \sqrt[3]{\frac{pa^2}{Et}}$

FIGURE 37.

small residual bending stiffness or because of initial tension essential for stability of very thin plates. In case of initial tension T not zero, the constant tends asymptotically to

$$\left. \frac{K^3}{p^2} \right|_{T \neq 0} \sim \frac{t}{T^3} \frac{ED^2}{256} \quad \text{as } p \rightarrow 0,$$

recovering the membrane action.

8.37 Composite Approximate Solution for the Finite Deflection of a Clamped Edge Diaphragm under Uniform Load.

It remains to state a composite approximate solution for the finite deflection of a diaphragm taking into account bending stiffness, the influence of finite deflections and admitting initial tension.

Griffith [1927] reports carrying out an iterative procedure starting from the Kirchhoff (exact) solution for infinitesimal deflections in the general equilibrium equations. His result in our algebraic form is

$$\frac{\bar{\sigma} F}{D} = \frac{3}{256} \frac{1}{\left(\frac{t}{D}\right)^3 + \left(\frac{t}{D}\right) \frac{(1+\mu)(173-73\mu)}{360} \left(\frac{\delta}{D}\right)^2 + \left(\frac{t}{D}\right) \frac{5(1+\mu)}{24} \epsilon_0}.$$

An argument will be made that this form, adjusted, is a correct one for an empirical correlation of the sensitivity of general diaphragms.

The form reduces to the exact (Kirchhoff) solution in the initial case with the deflection δ and initial strain ϵ_0 made zero.

For initial strain ϵ_0 made zero and neglecting the cube of

t/D this form is comparable with the exact solution of Hencky and can be made coincident by small adjustment of the constant

$$(1 + \mu) (173 - 73\mu)/360.$$

With only the initial strain term neglected this form is consistent with approximate solutions of the large deflection case which in turn are useful algebraic forms representing the exact solution of Way. The constant $(1 + \mu) (173 - 73\mu)/360$ may require adjustment but not to an extent practically conflicting with the preceding adjustment.

For large values of initial strain and neglecting the displacement and $(t/D)^3$ terms this form does not reduce to the exact membrane solution without a ten percent change in the constant $5(1 + \mu)/24$ to $45(1 + \mu)/240 = 3(1 + \mu)/16$ and becomes exact with this change.

Neglecting only the term $(t/D)^3$ representing bending stiffness, the sensitivity is controlled by finite displacement (Hencky) or initial tension (membrane action).

The particular advantage of this empirical form is that it makes clear that the pressure sensitivity of a flat disc diaphragm will not be greater than the theoretical maximum of the Kirchhoff theory and displays that, for very thin diaphragms, the loss of sensitivity due to practically unavoidable values of δ/D or ϵ_0 will be considerable.

8.4 Dynamic Response of Flat Circular Diaphragms.

8.41 Error Due to Dynamic Response Characteristics of the Diaphragm.

The preceding investigation of the pressure sensitivity of

circular diaphragms was limited to static pressure loads and did not consider dynamic effects. The dynamic response of the transducer should be considered if the pressure fluctuations include components at frequencies comparable with some fraction of the lowest significant frequency in the response of the diaphragm.

A convenient model for estimating dynamic error is to consider the pressure receiver to be a one-degree-of-freedom linear mechanical system with a natural frequency equal to the lowest natural mode frequency of the diaphragm in free vibration. With this model the magnitude of dynamic error at pressure fluctuation frequencies ω_p small in comparison with the diaphragm lowest-mode frequency ω_n is proportional to $(\omega_p/\omega_n)^2$ and is minimum for a damping constant about 70 percent of critical damping.

For frequencies encountered in the experimental part of this work it is not difficult to obtain ratios ω_p/ω_n that are small. For other model sizes or more violent oscillations this may be more difficult.

The high natural frequency of clamped stiff plates or stretched diaphragms is helpful in reducing this error.

8.42 The Lowest Natural Mode Frequency of Circular Diaphragms.

The dynamic response in vacuum of a circular flat diaphragm with clamped edges is studied in W. Mason [1942]. The solution is applicable to diaphragms with given values of initial tension. The result is not conveniently expressed algebraically. A convenient graphical solution for the lowest mode frequency is given by

J. Patterson [1952] in the form $\omega_n 2r^2 \sqrt{3 \rho(1-\mu^2)} / t \sqrt{Eg}$ as function of $12\varepsilon_0 r^2(1-\mu^2)/t^2$. This function is shown graphically in Figure 38.

The least value of the lowest mode frequency for a given diaphragm occurs for zero initial strain. For this condition the above form gives

$$\omega_n 2r^2 \sqrt{3 \rho(1-\mu^2)} / t \sqrt{Eg} = 10.22 .$$

This corresponds to the clamped edge stiff plate equation for the lowest mode frequency found in handbooks as

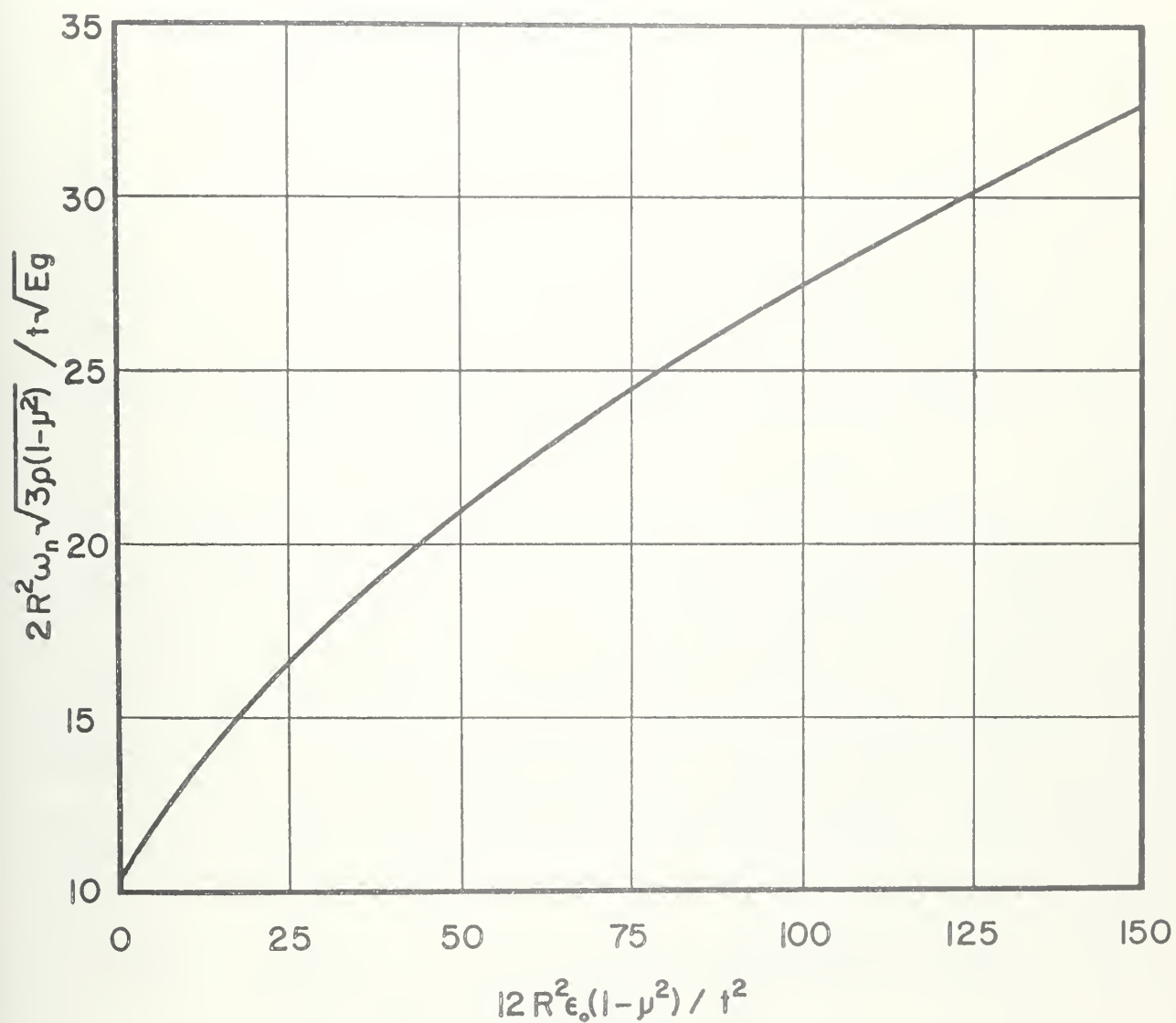
$$\omega_n r/V = 3.0 t/r ,$$

where V is the speed of sound in the diaphragm material. [The constants by various authors may vary less than five percent]. This form will probably be more convenient than the preceding because of the practical difficulty of knowing E and, particularly, ε_0 .

A simplified form is also available for the case of large initial tension, corresponding to the membrane solution,

$$\omega_n r/V = 2.4 \sqrt{T/Et} .$$

The assumptions essential to the latter, or the complete solution first given, show that this value of ω_n must exceed that of the zero initial tension case. Sample calculations of the clamped-edge stiff-plate case show the conveniently high values of ω_n for small gauges if one takes the velocity of sound in thin



GRAPHICAL SOLUTION FOR THE FUNDAMENTAL NATURAL FREQUENCY OF A CLAMPED, CIRCULAR, FLAT DIAPHRAGM (FOLLOWING PATTERSON [1932]).

FIGURE 38.

plates $(Eg/\rho(1-\mu^2))^{1/2}$ to be for example about 17,000 feet per second in steel.

8.5 Pressure Gauges Mounted Internally.

8.51 Advantage and Disadvantage.

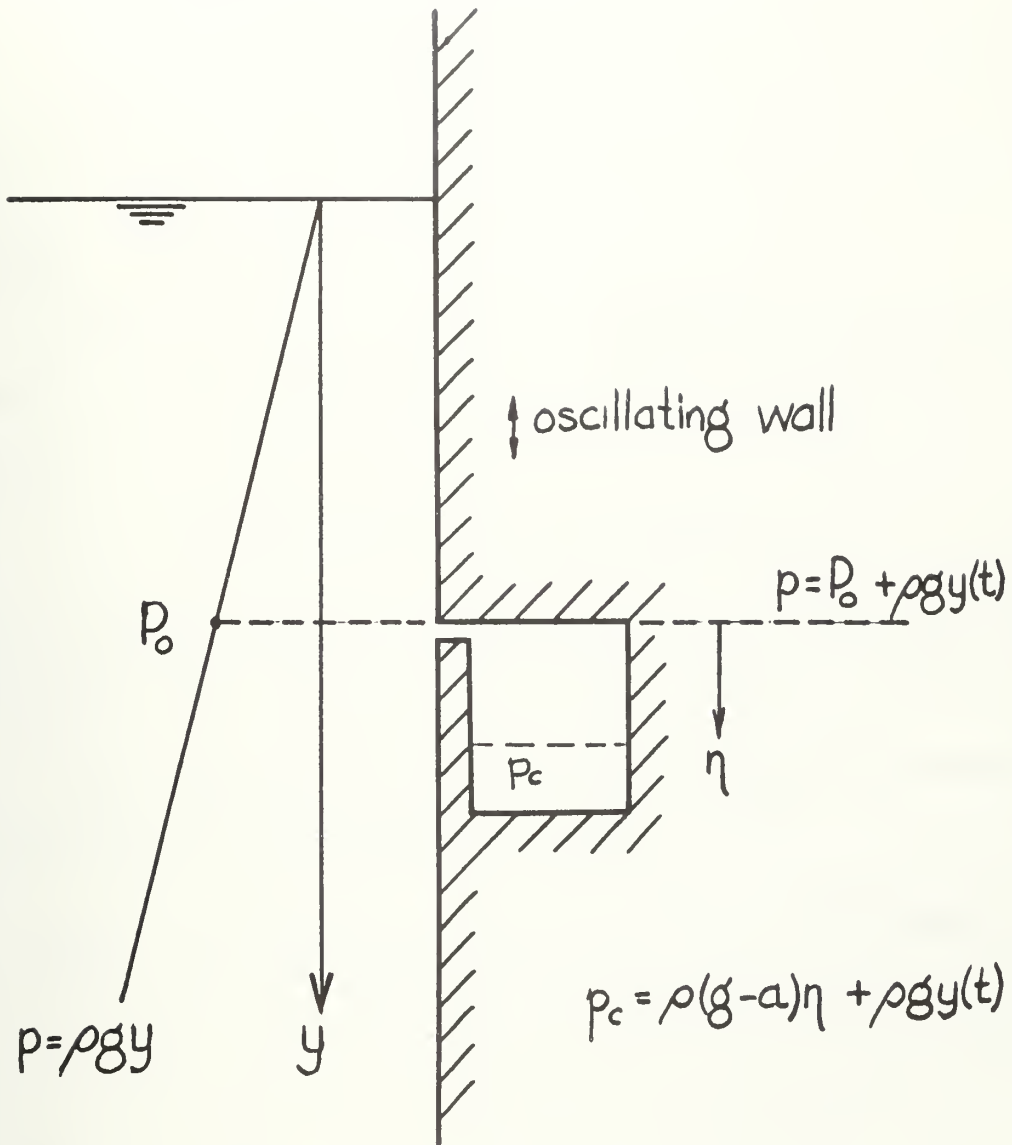
The pressure sensitivity of a diaphragm-type pressure receiver is a strong function of the diameter. The required pressure sensitivity is determined by the pressure fluctuation amplitude that is expected and the minimum deflection that is detectable. Further, the required diameter may exceed the maximum physical dimension allowable on the surface of the oscillating model.

The apparent physical diameter on the body surface can be reduced by mounting the pressure gauge diaphragm internally. There is necessarily then an internal instrument cavity and connecting passage or tube. These introduce two effects which could require compensation in the measurement; they are (i) the effect of acceleration of the enclosed fluid on the indicated pressure; (ii) attenuation of pressure fluctuations in the tube and cavity.

8.52 The Effect of Acceleration of the Enclosed Fluid on the Indicated Pressure.

The fluid enclosed in the instrument cavity and tube is forced to accelerate with the body. Therefore there is a pressure gradient in the enclosed fluid due to body acceleration. The top surface of a cavity is a suitable location for a horizontal diaphragm.

As an example, consider an instrument cavity in the vertical flat side of a vertically oscillating wall. The fluid is assumed



AN INSTRUMENT CAVITY IN AN
OSCILLATING WALL.

FIGURE 39.

inviscid, incompressible, and at rest. Because the wall and motion are vertical the fluid external of the instrument cavity remains undisturbed. The external hydrostatic pressure is instantly communicated to the top of the instrument cavity by an infinitesimal port. The external hydrostatic gauge pressure at this port is $p_0 + \rho g[\delta y(t)]$, where $\delta y(t)$ is the oscillatory motion and p_0 is the hydrostatic pressure at the initial position.

There is a pressure gradient in the fluid in the instrument cavity due to body acceleration $a = d^2y/dt^2$. The pressure in the cavity is

$$p_c(\eta) = \rho(g - a)\eta + p_0 + \rho g[\delta y(t)],$$

where η is the vertical distance down from the cavity top to the horizontal plane at which the pressure is $p_c(\eta)$.

For a top port the indicated pressure on the top surface is a direct measure of the external pressure.

8.53 The Dynamic Response of the Internally-Mounted Gauge.

The question arises: what is the dynamic pressure sensitivity of the pressure receiver to pressure fluctuations at the entrance of the connecting tube? It is clear that the hydrostatic pressure sensitivity is not affected, but it is also well-known that dynamic effects may appear.

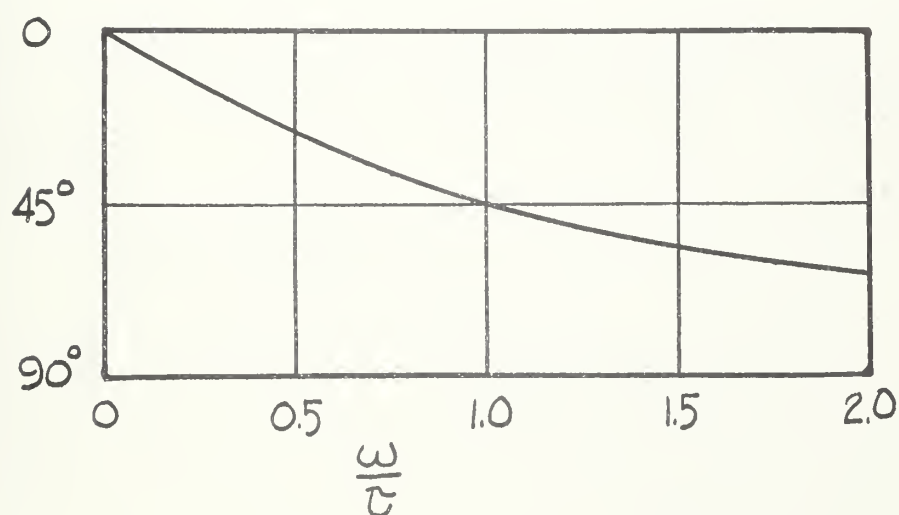
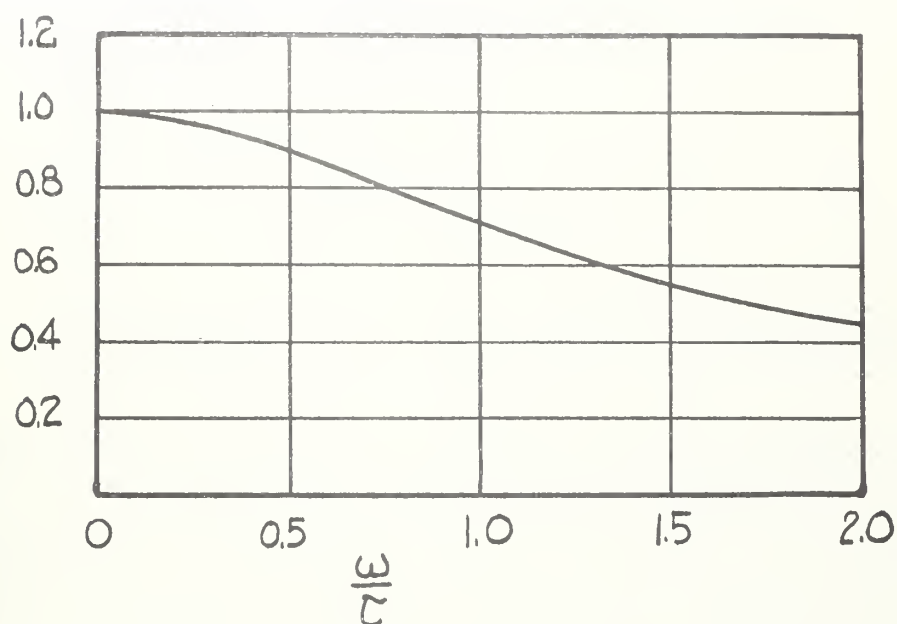
The analytic model considered here will exploit the conclusion found in Section 8A that the lowest natural frequency of a flat circular diaphragm will probably be high with respect to frequencies of interest in experiments visualized in this type work. We will now

assume that the lowest natural frequency of the diaphragm is also high with respect to the acoustic effects of the tube, cavity and resilient diaphragm. This assumption enables us to "uncouple" the dynamic response of the diaphragm, which accounts for diaphragm mass and elasticity, from the response of tube, cavity, and elastic (mass-less) diaphragm. Thus we expect dynamic behavior of the tube, cavity and elastic diaphragm to be of interest at frequencies low enough to consider the diaphragm to be stiffness-controlled.

The problem is to consider the attenuation of oscillatory pressure fluctuations in a viscous fluid traveling through a connecting tube to an instrument cavity terminated with an elastic but mass-less diaphragm. This analysis is reported in Appendix C. Sinusoidal gauge-pressure fluctuations of frequency ω are assumed at the entry port of the connecting tube of radius r . The pressure fluctuation at the diaphragm is assumed to be equal to the pressure at the cavity-end of the tube. The diaphragm elasticity and cavity volume provide a condition on fluid continuity. The result is presented as a complex ratio of the indicated- to external-pressure fluctuation p_i/p_o . The magnitude of the ratio is the amplitude response normalized with respect to hydrostatic response, and the argument of the ratio is the phase lag of diaphragm sinusoidal response.

The response p_i/p_o is characterized by the value of the dimensionless parameter $\omega a^2/\nu$. This parameter also characterizes the velocity profile in the tube. (See L. Loitsyanskii [1957], Section 86; H. Schlichting [1955], Chap. XI.)

For values of $\omega a^2/\nu$ less than one, viscous forces are predominant



FRACTIONAL RESPONSE AND
PHASE LAG OF INDICATED PRESSURE,
VISCOUS REGIME.

FIGURE 40.

and inertial forces negligible. In this case

$$\frac{p_i}{p_o} = \frac{1}{1 + j\omega\tau}$$

where

$$\tau = 8/\omega_n^2 a^2$$

$$\omega_n^2 = \text{a characteristic frequency constant for a given fluid, tube, and cavity, and diaphragm elasticity.}$$

This result is also derived directly with a model assuming uniform Poiseuille flow throughout the tube and neglecting inertia effects. The relative response is down 29 percent at the cutoff frequency $\omega_c = 1/\tau$ and the phase error is 45 degrees lag. The cutoff frequency is decreased with increased diaphragm elasticity (sensitivity).

For values of $\omega a^2/\nu$ of about four inertial effects are significant. A convenient approximation is to present the system response in the form

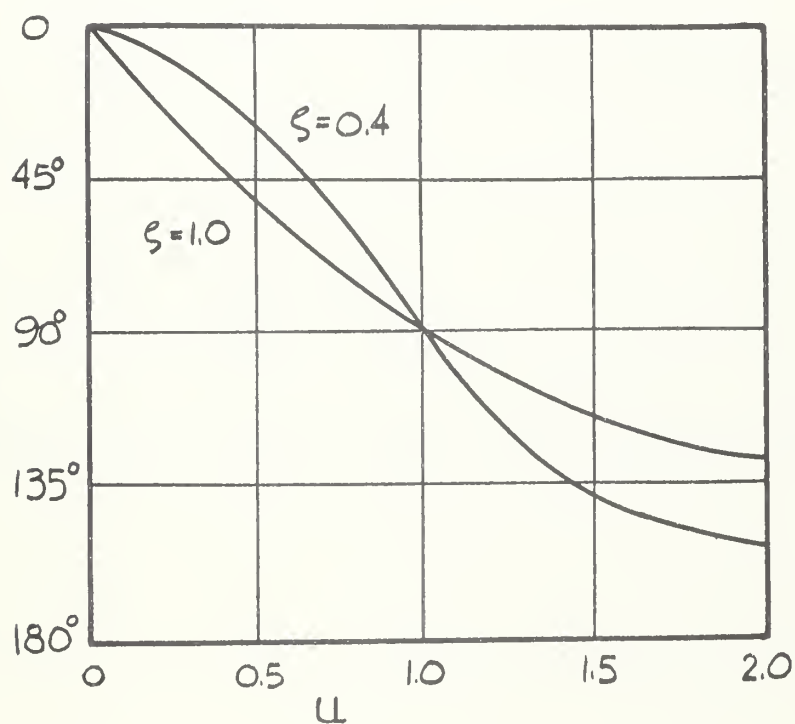
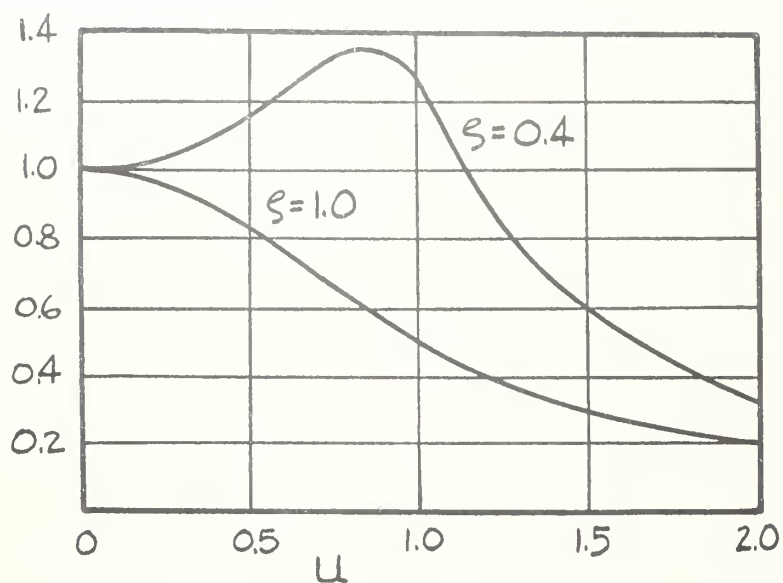
$$\frac{p_i}{p_o} = \frac{1}{(1 - u^2) + ju2\zeta}$$

Here u is the normalized frequency ratio ω/ω_o , where ω_o is a characteristic frequency analogous to the resonant frequency of a moderately damped spring-mass system. For $\omega = \omega_o$ the indicated pressure lags the driving source 90 degrees. The damping ratio is ζ .

For large values of $\omega a^2/\nu$ the response ratio tends to

$$\frac{p_i}{p_o} = \frac{1}{1 - (\omega/\omega_n)^2}$$

This is useful in showing the undamped (non-viscous) nature of the



FRACTIONAL RESPONSE AND PHASE
LAG OF INDICATED PRESSURE,
MODERATE DAMPING

FIGURE 41.

acoustic response and also alerts one to the fact that strong acoustic resonance is predicted which might damage a sensitive diaphragm.

The most general expression is

$$\frac{p_i}{p_o} = \frac{aL}{aL \cosh aL + bL \sinh aL}$$

where

$$aL = j 2\pi(L/\lambda) \sqrt{1/(1-J)}$$

$$bL = - (\omega/\omega_n)^2 / (1-J)$$

$$J = 2J_1(ka)/(ka)J_2(ka)$$

$$(ka)^2 = j\omega a^2/\nu .$$

For tube lengths L small with respect to the acoustic wavelength in the tube λ , this tends to

$$\frac{p_i}{p_o} = \frac{1}{1 - \left(\frac{\omega}{\omega_n}\right)^2 \frac{1}{1-J}}$$

and approximations for $1/(1-J)$ give the reductions cited above.

ACKNOWLEDGMENT

I wish to acknowledge that the Department of the Navy made possible the period of study during which this work was done and sponsored the research.

I was introduced to this problem by Professor John V. Wehausen and I particularly express my thanks for the opportunity to study and to work under his direction.

I wish to express my appreciation to Professors J. Randolph Paulling, Jr., and Edmund Pinney for their review of this work.

An observation that often a candidate devotedly acknowledges the encouragement and understanding of his wife is certainly valid in this case.

References

Colby, M.Y.

Sound waves and acoustics. H. Holt and Co., New York, 1939. v + 356 pp.

Dimpker, August

Über schwingende Körper an der Oberfläche des Wassers. Werft, Reederei, Hafen 15 (1934), 15-19.

Föppl, A.; Föppl, L.

Vorlesungen über technische Mechanik, Bd.V., B.G. Teubner, Leipzig, 1907. xii + 391 pp.

Drang und Zwang, Bd.I., R. Oldenbourg, Munich, Berlin, 1924. xi + 359 pp.

Gerritsma, J.

Experimental determination of damping, added mass and added mass moment of inertia of a ship model. Intl. Shipbuilding Prog. 3 (1957), 505-519 = Netherlands' Research Centre T.N.O. for Shipbuilding and Navigation, Report 25S, (1957) = Delft Shipbuilding Laboratory, Publication No. 8.

Golovato, P.

The force and moment on a heaving surface ship. J. Ship Res. 1 (1) (1957), 19-26, 54-55 = The David W. Taylor Model Basin, Washington, D.C., Rep 1074 (1956) 44 pp.

Griffith, A. A.

The theory of pressure capsules. Aero. Res. Comm. (Great Britain), Rep. and Memo. 1136 (1927). 14 pp + 1 pl.

Grim, Otto

Berechnung der durch Schwingungen eines Schiffskörpers erzeugten hydrodynamischen Kräfte. Jbuch schiffbautech. Ges. 47 (1953), 277-296; Orörterung, 296-299.

Hencky, H.

Über den Spannungszustand in kreisrunden Platten mit verschwindender Biegungsteifigkeit. Z. Math. Phys. 63 (1915), 311-317.

Holstein, Horst

Untersuchungen an einem Tauchschwingungen ausführenden Quader. Werft, Reederei, Hafen 23 (1936), 385-389.

Iberall, A. S.

Attenuation of oscillatory pressures in instrument lines. Research Paper RP2115, J. Res. Natl. Bu. Stds. 45 (1950), 85-108.

Landweber, L.; and Macagno, Matilde

Added mass of a three-parameter family of two-dimensional forms oscillating in a free surface. J. Ship Res. 2 (4) (1949), 36-48.

Added mass of two-dimensional forms oscillating in a free surface. J. Ship Res. 1 (3) (1957), 20-30.

Lewis, F. M.

The inertia of the water surrounding a vibrating ship. Trans. Soc. Naval Arch. Marine Engrs. 37 (1929) 1-17; Discussion 18-20.

Lilly, J. C.; Legallis, V.; Cherry, R.

A variable capacitor for measurements of pressure and mechanical displacements; a theoretical analysis and its experimental evaluation. J. Appl. Phys. 18 (1947), 613-628.

Loitsyanskii, L. G.

Mekhanika zhidkosti i gaza. [Mechanics of fluids and gases.] Gos. Izdat. Tekhn.-Teoret. Lit., Moscow, 1957, 784 pp.

Nadai, A.

Die elastische Platten. Springer Verlag, Berlin, 1925.

Mason, W. P.

Electromechanical transducers and wave filters. D. Van Nostrand Company, New York, 1942.

Patterson, J. L.

A miniature electrical pressure gage utilizing a stretched flat diaphragm. NACA Tech. Note 2659, (1952) 47 pp.

Prohaska, C. W.

Vibrations verticales du navire. Bull. L'Assoc. Tech. Maritime et Aeronautique. (1947) 171-215.

Schlichting, H.

Boundary layer theory, Pergamon Press, New York, 1955, 535 pp.

Schuler, M.

Erzeugung von Oberflächenwellen durch schwingende Körper. Z. angew. Math. Mech. 16 (1936), 65-72.

Stoker, J. J.

Water waves. The mathematical theory with applications. Interscience Publishers, New York, 1957.

Tasai, Fukuzo

On the damping force and added mass of ships heaving and pitching. (Japanese) J. Zôsen Kyôkai 105 (1959), 47-56. Translated in Institute of Engineering Research, University of California, Berkeley, Report, Series 82, Issue 15 (1960).

Thorne, R. C.

Multipole expansions in the theory of surface waves. Proc. Cambridge Philos. Soc. 49 (1953), 707-716.

Timoshenko, S.

Theory of plates and shells. McGraw-Hill Book Co., New York, 1940.

Ursell, F.

On the heaving motion of a circular cylinder on the surface of a fluid. Quart. J. Mech. Appl. Math. 2 (1949), 218-231.

Short surface waves due to an oscillating immersed body. Proc. Roy. Soc. London. Ser. A. 220 (1953), 90-103.

On the rolling motion of cylinders in the surface of a fluid. Quart. J. Mech. Appl. Math. 2 (1949), 335-353.

On the virtual mass and damping of floating bodies at zero speed ahead. Proceedings, Symposium on the behaviour of ships in a seaway, Wageningen, 1957.

Water waves generated by oscillating bodies. Quart. J. Mech. Appl. Math. 7 (1954), 427-437.

Way, S.

Bending of circular plates with large deflection. Am Soc. Mech. Engrs. Trans. 56 (1934), 627-636.

Wehausen, J. V.

Surface Waves. Handbuch der Physik, Vol. IX, Springer Verlag, Berlin, 1960.

Yu, Yun-Sheng

Surface waves generated by an oscillating circular cylinder in shallow water. Dissertation, Massachusetts Institute of Technology, Cambridge, 1960, vi + 93 pp.

APPENDIX A

Mathematical Notes Referenced in the Text

- A-1 Asymptotic Behavior of $\varphi_{2m}''(x,y,h)$ for
 $|x| \rightarrow \infty, y = 0.$
- A-2 Asymptotic Behavior of $\varphi_s(K,h)$ for
 $|x| \rightarrow \infty, y = 0.$
- A-3 Expanded Forms Useful in Numerical Calculation
of Certain Definite Integrals.
 - A-3.1 The Coefficients of $p_{2m}(\delta), q_{2m}(\delta)$ in
Expansion Equations for the Method of Integration.
 - A-3.2 Two Special Forms.
 - A-3.3 Expressions in the Right-Hand Side of the
 $p_{2m}(\delta)$ Expansion Equations.
 - A-3.4 Alternate Forms for $\varphi_{sa}(\delta,\theta), \gamma_{sa}(\delta,\theta).$
 - A-3.5 Expressions in the Right-Hand Side of the
 $q_{2m}(\delta)$ Expansion Equations.

APPENDIX A

A-1 Asymptotic Behavior of $\varphi_{2m}''(x, y, h)$ for $|x| \rightarrow \infty$, $y = 0$.

The asymptotic behavior of the function

$$\varphi_{2m}''(x, y, h) = \oint_0^{\infty} L(k) \varepsilon^{-kh} \frac{K \sinh ky - k \cosh ky}{K \cosh kh - k \sinh kh} \cos kx \, dk$$

for $|x| \rightarrow \infty$, $y = 0$ as required in Section 3.32 may be determined by considering the complex contour integral

$$\oint L(k) \frac{K \sinh ky - k \cosh ky}{K \cosh kh - k \sinh kh} \varepsilon^{-kh} \varepsilon^{ikx} \, dk = \oint F(k) \varepsilon^{ikx} \, dk,$$

where the variable k is considered complex, temporarily. The integrand of φ_{2m}'' is an even function of x so that we may use $|x|$ in the following. It is understood that $h > 0$. The contour of integration consists of $R \geq \operatorname{Re} k \geq 0$, indented above the singularity defined by the positive real value of K_0 satisfying

$$K \cosh K_0 h - K_0 \sinh K_0 h = 0$$

for given $K = \omega^2/g$ and $h > 0$, the part of the imaginary axis

$R \geq \operatorname{Im} k \geq 0$, and the arc $|k| = R$, $\operatorname{Re} k > 0$, $\operatorname{Im} k > 0$. Here $R > K_0$; this is no restriction since we finally shall let $R \rightarrow \infty$.

Integration around this contour yields

$$\int_{\rightarrow\rightarrow} F(k) \varepsilon^{ikx} \, dk + \int_{\curvearrowleft} F(k) \varepsilon^{ikx} \, dk + \int_{\downarrow} F(k) \varepsilon^{ikx} \, dk + \int_{\sim} F(k) \varepsilon^{ikx} \, dk = 0,$$

with symbols indicating segments of the path. With the contour as defined,

$$\int F(k) \epsilon^{ikx} dk \rightarrow 0 \quad \text{as } R \rightarrow \infty .$$

Therefore after letting $R \rightarrow \infty$ and the radius of the indentation $\rightarrow 0$, we have

$$\int F(k) \epsilon^{ikx} dk = \pi i R_s + \int F(k) \epsilon^{ik|x|} dk ,$$

and, after taking the real part,

$$\varphi_{2m}''(x, y, h) = \text{Re } \pi i R_s + \int_0^{\infty} [\text{Re } iF(ik)] \epsilon^{-k|x|} dk$$

where k is now a real variable and R_s is the residue evaluated below.

The residue R_s is

$$R_s = \lim_{k \rightarrow K_0} (k - K_0) L \epsilon^{-kh} \frac{K \sinh ky - k \cosh ky}{K \cosh kh - k \sinh kh} \epsilon^{ik|x|} .$$

The limiting operation is executed after the substitution

$$K = K_0 \sinh K_0 h / \cosh K_0 h$$

and manipulation of the terms

$$\frac{(k - K_0)}{k \cosh kh - k \sinh kh} = - \frac{(k - K_0) \cosh K_0 h}{K_0 \sinh (k - K_0)h + (k - K_0) \sinh kh \cosh K_0 h} .$$

With this substitution, the residue simplifies to

$$R_s = L(K_0) \epsilon^{-K_0 h} \epsilon^{iK_0 |x|} K_0 \cosh K_0 (h - y) .$$

$$\cdot \lim_{k \rightarrow K_0} \frac{(k - K_0)}{K_0 \sinh (k - K_0)h + (k - K_0) \sinh kh \cosh K_0 h} ,$$

or, after evaluating the limit,

$$\operatorname{Re} \pi i R_S = -K_0 L(K_0) \varepsilon^{-K_0 h} \frac{2\pi}{2K_0 h + \sinh 2K_0 h} \cosh K_0 (h-y) \sin K_0 |x|.$$

We find

$$K_0 L(K_0) \varepsilon^{-K_0 h} = \frac{K_0^{2m} a^{2m}}{(2m-1)! \cosh K_0 h} + \sum_{n=0}^N (-1)^n \frac{a_{2n+1}}{(2s-1)!} \frac{K_0^{2s} a^{2s}}{\cosh K_0 h}$$

by using the definition of $L(k)$ in Section 3.31(c) and substituting

$K = K_0 \sinh K_0 h / \cosh K_0 h$ as well as evaluating the expression for $k = K_0$.

With this expression we may write

$$\operatorname{Re} \pi i R_S = -E_{2m}(K_0 a, K_0 h) \frac{\cosh K_0 (h-y)}{\cosh K_0 h} \sin K_0 |x|$$

where

$$E_{2m}(K_0 a, K_0 h) = \frac{2\pi}{2K_0 h + \sinh 2K_0 h} \left[\frac{K_0^{2m} a^{2m}}{(2m-1)!} + \sum_{n=0}^N (-1)^n \frac{a_{2n+1} K_0^{2s} a^{2s}}{(2s-1)!} \right].$$

The result for $\operatorname{Re} \pi i R_S$ is identified as the asymptotic behavior of $\varphi_{2m}''(x, y, h)$ for $|x| \rightarrow \infty$. On the surface $y = 0$,

$$\varphi_{2m}''(x, 0, h) \sim -E_{2m} \sin K_0 |x| \quad \text{as} \quad |x| \rightarrow \infty.$$

We note that $E_{2m} \rightarrow 0$ as $h \rightarrow \infty$.

A-2 Asymptotic Behavior of $\varphi_S(K, h)$.

The asymptotic behavior of the function

$$\varphi_S(K, h) = \oint_0^{\infty} \frac{\cosh k(h-y) \cos kx}{K \cosh kh - k \sinh kh} dk$$

for $|x| \rightarrow \infty$ as required in Section 3.34 is found by following the procedure of Appendix A-1.

The contour integral to be considered is

$$\oint \frac{\cosh k(h-y) e^{ik|x|}}{K \cosh kh - k \sinh kh} dk.$$

The contour is taken to be the same as in Appendix A-1. After following the procedure outlined there, one finds

$$\varphi_S(K, h) = \operatorname{Re} \pi i R'_S + \int_0^{\infty} [\operatorname{Re} i F'(ik)] e^{-k|x|} dk.$$

Thus the $\operatorname{Re} \pi i R'_S$ gives the first term in the asymptotic expression for $\varphi_S(K, h)$ as $|x| \rightarrow \infty$; that is,

$$\varphi_S(K, h) \sim \frac{2\pi}{2K_0 h + \sinh 2K_0 h} \cosh K_0 h \cosh K_0(h-y) \sin K_0 |x|.$$

On the surface $y = 0$, as $|x| \rightarrow \infty$,

$$\varphi_S(K, h)_{y=0} \sim E_S(K_0 h) \sin K_0 |x|$$

where

$$E_S(K_0 h) = \frac{2\pi (\cosh K_0 h)^2}{2K_0 h + \sinh 2K_0 h}.$$

We note that $E_S(K_0 h) \sim \pi$ as $h \rightarrow \infty$.

A-3 Expanded Forms Useful in Numerical Calculation of Certain Definite Integrals.

A-3.1 The Coefficients of $p_{2m}(\delta)$, $q_{2m}(\delta)$ in Expansion Equations for the Method of Integration.

Coefficients $a_{2m,k}$ and $b_{2m,j}$ are defined for use in solving the expansion equations by the method of integration (Section 5.12).

$$\int_0^{\pi/2} f_{2m}(\theta) \sin k\theta d\theta = a_{2m,k}$$

$$= \begin{cases} k \text{ odd: } \frac{2m(-1)^{\frac{(2m+k-1)}{2}}}{4m^2 - k^2} \\ k \text{ even: } k = 2m: -\pi/4 \\ \quad k \neq 2m: 0 \end{cases} - \frac{\delta}{2m-1} \cdot \begin{cases} k \text{ odd: } \begin{aligned} k = m = 1: & 0 \\ k = 1 \neq m: & (-1)^m \pi/4 \\ k = 2m-1 \neq 1: & + \pi/4 \\ \text{otherwise:} & 0 \end{aligned} \\ k \text{ even: } \frac{k}{k^2 - 1} \frac{2m(2m-2)(-1)^{\frac{(2m+k-2)}{2}}}{(2m-1)^2 - k^2} \end{cases}$$

$$\int_0^{\pi/2} f_{2m}(\theta) \cos j\theta d\theta = b_{2m,j}$$

$$= \begin{cases} j \text{ odd: } \frac{2m}{4m^2 - j^2} + \frac{\delta}{2m-1} (-1)^m \cdot \begin{cases} \frac{j+1}{2} \text{ even: } \frac{1}{1-j} \\ \frac{j+1}{2} \text{ odd: } \frac{1}{1+j} \end{cases} \\ \quad + \frac{\delta}{2m-1} \cdot \begin{cases} \frac{j+2m-1}{2} \text{ even: } \frac{1}{2m-1-j} \\ \frac{j+2m-1}{2} \text{ odd: } \frac{1}{2m-1+j} \end{cases} \\ j \text{ even: } \frac{\delta}{2m-1} \left\{ \frac{2m-1}{(2m-1)^2 - j^2} + (-1)^m \frac{1}{1-j^2} \right\} + \begin{cases} \frac{j+2m}{2} \text{ even: } 0 \\ \frac{j+2m}{2} \text{ odd: } \frac{4m}{4m^2 - j^2} \end{cases} \end{cases}$$

(zero is treated as an even number.)

A-3.2 Two Special Forms.

The following definitions are used for convenience of notation in later integral expansions.

$$I_2(k, n) = \int_0^{\pi/2} \sin k\theta \sin n\theta d\theta$$

$$= \begin{cases} 0 & \text{if } k \text{ or } n \text{ are zero.} \\ + \frac{\pi}{4} & \text{for } n = k \neq 0. \\ \text{for other } k, n: \\ \quad (n+k) \text{ even: } 0 \\ \quad (n+k) \text{ odd:} \\ \qquad \text{if } k \text{ even: } (-1)^{(n+k+3)/2} k/(n^2 - k^2) \\ \qquad \text{if } k \text{ odd: } (-1)^{(n+k+1)/2} n/(n^2 - k^2). \end{cases}$$

$$I_1(n, k) = \int_0^{\pi/2} \cos n\theta \sin k\theta d\theta$$

$$= \begin{cases} 0 & \text{for } k = 0 \\ \text{for other } k, n: \end{cases}$$

If $(n+k)$ even, and if $(n+k)/2$ even, then

$$\begin{aligned} \text{if } k \text{ even: } & 0 \\ k \text{ odd: } & 1/(k-n) \end{aligned}$$

if $(n+k)/2$ odd, then

$$\begin{aligned} \text{if } k \text{ even: } & 2k/(k^2 - n^2) \\ k \text{ odd: } & 1/(k+n) \end{aligned}$$

If $(n+k)$ odd: $\frac{k}{k^2 - n^2}$

A-3.3 Expressions in the Right-Hand Side of the $p_{2m}(\delta)$ Expansion Equations.

$$\int_0^{\pi/2} \gamma_{ca}(\delta, \theta) \frac{\sin k\theta}{\cos j\theta} d\theta = \pi \sum_{p=0}^{\infty} (-1)^{p+1} \frac{\delta^p}{p!} \frac{I_2(k, p)}{I_1(j, p)}$$

$$\int_0^{\pi/2} \gamma_{ca}(\delta, \pi/2) \frac{\sin k\theta}{\cos j\theta} d\theta = \pi \sin \delta \frac{I_2(k, 1)}{I_1(j, 1)}.$$

A-3.4 Alternate Forms for $\varphi_{sa}(\delta, \theta)$, $\gamma_{sa}(\delta, \theta)$.

The form of the quantities $\gamma_{sa}(\delta, \theta)$ and $\varphi_{sa}(\delta, \theta)$ used in the $q_{2m}(\delta)$ expansion equation (Section 5.12) and in the calculation of $M(\delta, \theta)$ (Section 5.22), respectively, are derived from the Cauchy Principal Value integral

$$\oint_0^{\infty} \frac{\varepsilon^{-ky} \varepsilon^{+ikx}}{K - k} dk = \varepsilon^{-K(y-ix)} E_1[K(y-ix)]$$

$$= \varepsilon^{-Ky} [\cos Kx + i \sin Kx] [\underline{\gamma} + \log_{\varepsilon} r - i\theta + \sum_{n=1}^{\infty} \frac{r^n \varepsilon^{-in\theta}}{n!n}].$$

Here $E_1(-iz)$ designates the exponential integral of a complex argument [Tables of the Exponential Integral for Complex Arguments, National Bureau of Standards Applied Mathematics Series 51, May 1958]. Euler's constant 0.57721... is designated $\underline{\gamma}$ and $\theta = \arctan x/y$. The real part of this expression represents a source in the free surface of fluid of infinite depth (Section 3.33) and the imaginary part represents the conjugate stream function. Contour integration leads to the real and imaginary parts given in Section 4.2, but the right-hand side of the above expression is one suitable to numerical

calculations. Evaluating this,

$$\varphi_{sa}(\delta, \theta) = \varepsilon^{-\delta \cos \theta} [Q(\theta) \cos(\delta \sin \theta) + S(\theta) \sin(\delta \sin \theta)]$$

$$\gamma_{sa}(\delta, \theta) = \varepsilon^{-\delta \cos \theta} [Q(\theta) \sin(\delta \sin \theta) - S(\theta) \cos(\delta \sin \theta)]$$

where

$$S(\theta) = \theta + \sum_{n=1}^{\infty} \frac{\delta^n}{n!n} \sin n\theta$$

$$Q(\theta) = \underline{\gamma} + \log_{\varepsilon} \delta + \sum_{n=1}^{\infty} \frac{\delta^n}{n!n} \cos n\theta.$$

It is noted that

$$S(\pi/2) = \pi/2 - \text{Si}(\delta)$$

$$Q(\pi/2) = \text{Ci}(\delta),$$

where $\text{Si}(\delta)$ and $\text{Ci}(\delta)$ are the sine and cosine integrals.

A-3.5 Expressions in the Right-Hand Side of the $q_{2m}(\delta)$ Expansion Equation.

The following integrals appear in Section 5.12.

$$\begin{aligned} \int_0^{\pi/2} \gamma_{sa}(\delta, \theta) \sin \theta \, d\theta &= \int_0^{\pi/2} \varepsilon^{-\delta \cos \theta} Q(\theta) \sin(\delta \sin \theta) \sin \theta \frac{\sin k\theta}{\cos j\theta} \, d\theta - \\ &\quad - \int_0^{\pi/2} \varepsilon^{-\delta \cos \theta} S(\theta) \cos(\delta \sin \theta) \sin \theta \frac{\sin k\theta}{\cos j\theta} \, d\theta \\ &= (\underline{\gamma} + \log_{\varepsilon} \delta) \sum_{p=0}^{\infty} (-1)^{p+1} \frac{\delta^p}{p!} \frac{I_2(k, p)}{I_1(j, p)} + \sum_{n=1}^{\infty} \frac{\delta^n}{n!n} \sum_{p=0}^{\infty} (-1)^{p+1} \frac{\delta^p}{p!} \frac{I_2(k, p+n)}{I_1(j, p+n)} + \\ &\quad + \sum_{p=0}^{\infty} (-1)^{p+1} \frac{\delta^p}{p!} \frac{I_4(k, p)}{I_3(j, p)}. \end{aligned}$$

The quantities not previously defined in this appendix are

$$I_3(j, p) = \frac{1}{2} [A(|p-j|) + A(|p+j|)],$$

where

$$A(|x|) = \begin{cases} \frac{1}{2} \left(\frac{\pi}{2}\right)^2 & \text{for } |x| = 0, \\ \frac{1}{x^2} [-1 + (-1)^{x/2}] & \text{for } |x| \text{ even,} \\ -\frac{1}{x^2} - \frac{\pi}{2x} (-1)^{(x+1)/2} & \text{for } |x| \text{ odd;} \end{cases}$$

and

$$I_4(k, p) = \frac{1}{2} [B(|p+k|) + (\text{signum } k-p) B(|p-k|)], \quad k \neq 0$$

$$= 0 \quad \text{for } k = 0$$

where

$$B(|x|) = \begin{cases} 0 & \text{for } |x| = 0, \\ \frac{\pi}{2x} (-1)^{(x+2)/2} & \text{for } |x| \text{ even,} \\ \frac{1}{x^2} (-1)^{(x-1)/2} & \text{for } |x| \text{ odd.} \end{cases}$$

$$\int_0^{\pi/2} \gamma_{sa}(\delta, \pi/2) \sin \theta \frac{\sin k\theta}{\cos j\theta} d\theta = \pi \cos \delta \int_0^{\pi/2} \sin \theta \frac{\sin k\theta}{\cos j\theta} d\theta$$

$$+ \int_0^{\infty} \frac{\delta e^{-x}}{\delta^2 + x^2} \int_0^{\pi/2} \sin \theta \frac{\sin k\theta}{\cos j\theta} dx d\theta$$

$$= - \left[\left(\frac{\pi}{2} + \text{Si } \delta \right) \cos \delta - \text{Ci } \delta \sin \delta \right] \frac{I_2(k, 1)}{I_1(j, 1)}.$$

This form is found directly from the expanded form of $\gamma_{sa}(\delta, \pi/2)$ given in Section 5.11, and the identity

$$\int_0^{\infty} \frac{\delta e^{-x}}{\delta^2 + x^2} dx = [\pi/2 - \text{Si}(\delta)] \cos(\delta) + \text{Ci}(\delta) \sin(\delta)$$

[Lamb, Hydrodynamics, Art 244 (37)]. Here $\text{Si}(\delta)$ and $\text{Ci}(\delta)$ are the sine and cosine integrals and are available in tabulated or series form. Alternately, the same result for $\gamma_{sa}(\delta, \pi/2)$ may be found in Appendix A-3.4 above where a series form suitable for computation is given.

APPENDIX B

The Finite Deflection of Circular Plates with Initial Tension.

- B-1 Introduction.
- B-2 Governing Differential Equations.
- B-3 Series Assumed for Solution.
- B-4 Evaluation of Coefficients b_{2n} in Terms of b_0
and Definition of the Function c_1 .
- B-5 Evaluation of Coefficients a_{2n} in Terms of b_0
and Definition of the Function c_2 .
- B-6 Evaluation of b_0 by the Boundary Condition.
- B-7 Graphical Solution.
- B-8 Special Cases.
 - a. Zero Initial Strain. (The Solution of Hencky).
 - b. Lightly Loaded Plates.
 - c. Comparison with the Membrane Solution.

APPENDIX B

The Finite Deflection of Circular Plates with Initial Tension.

B-1 Introduction.

Consider a circular plate of homogeneous material obeying Hooke's law which is initially flat until uniformly pressure-loaded on one side. The edge is clamped. The only widely-published solution of the simplified equations of equilibrium including a given initial-tension boundary condition is the membrane solution. The membrane solution assumes vanishing bending stiffness, small deflections, and that the initial tension is large compared to developed material stresses.

In order to maximize pressure sensitivity of a diaphragm-type pressure gauge, one is led to thin diaphragms of vanishing bending stiffness and to reduce the initial tension to the minimum. Application of the membrane solution is not wholly satisfactory when initial tension is small because material stresses become appreciable at moderate loads, and because deflections may not be infinitesimal and because the solution gives no hint of departure from linearity. The exact solution of Hencky assumes zero initial tension and the infinite deflection derivative at zero load is not physically appropriate to stable diaphragms of finite pressure sensitivity.

This appendix presents an exact solution to the equations of equilibrium for this type plate subject to arbitrary initial tension. For zero tension the solution of Hencky is recovered. For large initial tension the membrane solution is approached asymptotically. For

lightly loaded plates the solution always tends to that of the membrane. The initial deflection derivative is limited by the initial tension, physically appropriate to the case of a lightly loaded, thin, stable diaphragm.

The radial and tangential stresses, as well as deflection, are given in this solution.

The membrane solution (large initial tension) is valid only for infinitesimal deflections. This solution is not so limited. The deflection pressure relation of the membrane solution is linear. This solution reveals the nonlinear solution, tending toward a Hencky-type solution as the developed stresses increase relative to initial stresses.

B-2 Governing Differential Equations.

The equations of equilibrium and stress compatibility for an initially flat circular plate with clamped edges were given by A. Föppl [1907] and are repeated by H. Hencky [1915] and S. Way [1934] among others.

We repeat the equations expressing horizontal equilibrium,

$$\frac{d}{dr} (\sigma_r r) - \sigma_t = 0 ,$$

and compatibility,

$$r \frac{d}{dr} (\sigma_r + \sigma_t) + \frac{E}{2} \left(\frac{d\delta}{dr} \right)^2 = 0 ,$$

using σ_r and σ_t as radial and tangential stresses and δ as deflection.

The equation expressing vertical equilibrium,

$$\frac{E}{1 - \mu^2} \frac{t^3}{12} \frac{d}{dr} \left(\frac{1}{r} \frac{d}{dr} \left(r \frac{d\delta}{dr} \right) \right) = \frac{pr}{2} + t\sigma_r \frac{d\delta}{dr} ,$$

is simplified in the case $t^3 \ll t$,

$$0 = \frac{pr}{2} + t\sigma_r \frac{d\delta}{dr} .$$

This is the case of vanishing bending stiffness. For extended argument see, for example, Föppl or Hencky [loc cit] or A. Föppl [1924]. We deal here only with the case of vanishing bending stiffness.

B-3 Series Assumed for Solution.

A power series form is assumed for the dimensionless radial stress ratio (σ_r/E) . The corresponding series for the tangential stress ratio (σ_t/E) is derived with aid of the equation expressing horizontal equilibrium. That differential equation is thereby satisfied.

$$\frac{\sigma_r}{E} = c_1 \sum_{n=0}^{\infty} b_{2n} \left(\frac{r}{a} \right)^{2n} .$$

The stress is made non-dimensional by Young's Modulus E ; the radius r , by the plate radius a . The dimensionless coefficients b_{2n} are to be determined and c_1 is a dimensionless function of the uniform pressure load found later to be

$$c_1^3 = \frac{1}{64} \left(\frac{pa}{Et} \right)^2 .$$

From horizontal equilibrium, the series form for σ_t/E is

$$\begin{aligned}\frac{\sigma_t}{E} &= r \frac{d}{dr} \left(\frac{\sigma_r}{E} \right) + \frac{\sigma_r}{E} \\ &= c_1 \sum_{n=0}^{\infty} (2n+1) b_{2n} \left(\frac{r}{a} \right)^{2n}.\end{aligned}$$

A series form is assumed for the dimensionless deflection (δ/a) compatible with the condition $\delta = 0$ at $r = a$.

$$\frac{\delta}{a} = c_2 \left[\sum_{n=0}^{\infty} a_{2n} - \sum_{n=0}^{\infty} a_{2n} \left(\frac{r}{a} \right)^{2n} \right].$$

The dimensionless coefficients a_{2n} are to be determined and c_2 is a dimensionless function of the uniform pressure load, later found to be

$$c_2^2 = 4c_1.$$

The center deflection at $r = 0$ is

$$\delta(0) = (ac_2) \sum_{n=0}^{\infty} a_{2n}.$$

B-4 Evaluation of Coefficients b_{2n} in Terms of b_0 and Definition of the Function c_1 .

With aid of the equations of compatibility and vertical equilibrium we are able to express b_{2n} in terms of b_0 after making a suitable choice of definition of c_1 .

The nonlinear equation of compatibility in the form

$$\left(\frac{\sigma_r}{E} \right)^2 r \frac{d}{dr} \left(\frac{\sigma_r}{E} + \frac{\sigma_t}{E} \right) + \frac{1}{2} \left(\frac{\sigma_r}{E} \frac{d\delta}{dr} \right)^2 = 0$$

with the equation of vertical equilibrium

$$\frac{\sigma_r}{E} \frac{d\delta}{dr} = - \frac{1}{2} \frac{pr}{Et}$$

takes the form

$$\frac{\sigma_r}{E} r \frac{d}{dr} \left(\frac{\sigma_r}{E} + \frac{\sigma_t}{E} \right) + \frac{1}{8} \left(\frac{pr}{Et} \right)^2 = 0 .$$

The first term of this expression is rewritten as the product of two appropriate series, using for one factor

$$\begin{aligned} r \frac{d}{dr} \left(\frac{\sigma_r}{E} + \frac{\sigma_t}{E} \right) &= c_1 r \frac{d}{dr} \left[\sum_{n=0}^{\infty} b_n \left(\frac{r}{a} \right)^{2n} + \sum_{n=0}^{\infty} (2n+1) b_{2n} \left(\frac{r}{a} \right)^{2n} \right] \\ &= c_1 \left(\frac{r}{a} \right)^2 \sum_{n=1}^{\infty} (2n+2)(2n) b_{2n} \left(\frac{r}{a} \right)^{2n-2} , \end{aligned}$$

so that

$$c_1^3 \left(\frac{r}{a} \right)^2 \left[\sum_{n=0}^{\infty} b_{2n} \left(\frac{r}{a} \right)^{2n} \right]^2 \left[\sum_{n=1}^{\infty} (2n+2)(2n) b_{2n} \left(\frac{r}{a} \right)^{2n-2} \right] + \frac{1}{8} \left(\frac{pr}{Et} \right)^2 = 0 .$$

It is appropriate to define

$$c_1^3 = \frac{1}{64} \left(\frac{pa}{Et} \right)^2$$

in order to leave a non-dimensional expression which is used below to generate recursion formulae for b_{2n} .

$$\left[\sum_{n=0}^{\infty} b_{2n} \left(\frac{r}{a} \right)^{2n} \right]^2 \left[\sum_{n=1}^{\infty} (2n+2)(2n) b_{2n} \left(\frac{r}{a} \right)^{2n-2} \right] + 8 = 0 .$$

This series is expanded and coefficients of powers of r/a are set to zero individually, the first reads conveniently

$$8 b_2 b_0 + 8 = 0 \quad \text{or} \quad b_2 b_0 + 1 = 0 .$$

The succeeding equations for the next higher powers of r/a are

$$3b_4b_0^2 + 2b_0b_2^2 ,$$

$$6b_6b_0^2 + 8b_4b_2b_0 + b_2^3 = 0 , \text{ etc.}$$

Solving these in succession, all succeeding coefficients b_{2n} are expressible in terms of b_0 . The first five are

b_0 , to be determined from boundary condition

$$b_2 = -1/b_0^2$$

$$b_4 = -2/3b_0^5$$

$$b_6 = -13/18b_0^8$$

$$b_8 = -17/18b_0^{11}$$

$$b_{10} = -37/27b_0^{14} .$$

B-5 Evaluation of Coefficients a_{2n} in Terms of b_0 and Definition of the Function c_2 .

With use of the equation expressing vertical equilibrium we are able to find all coefficients a_{2n} in terms of b_0 after making a suitable definition of the function c_2 .

The form of the equation of equilibrium

$$\frac{\sigma_r}{E} \frac{d\delta}{dr} + \frac{1}{2} \frac{pr}{Et} = 0$$

with the series for σ_r/E after using

$$\frac{d\delta}{dr} = -c_2 \sum_{n=0}^{\infty} (2n+2)a_{2n} \left(\frac{r}{a}\right)^{2n+1} = -2c_2 \frac{r}{a} \sum_{n=0}^{\infty} (n+1) a_{2n} \left(\frac{r}{a}\right)^{2n} ,$$

is

$$2c_1 c_2 \sum_{n=0}^{\infty} b_{2n} \left(\frac{r}{a}\right)^{2n} \sum_{n=0}^{\infty} (n+1) a_{2n} \left(\frac{r}{a}\right)^{2n} + \frac{1}{2} \frac{pr}{Et} = 0 .$$

Substitute the previously selected definition of c_1 and define

$$c_2 = \frac{1}{4} \frac{pa}{Et} \frac{1}{c_1} = \sqrt[3]{\frac{pa}{Et}}$$

in order to leave a dimensionless expression which can be solved successively for a_{2n} :

$$\sum_{n=0}^{\infty} b_{2n} \left(\frac{r}{a}\right)^{2n} \sum_{n=0}^{\infty} (n+1) a_{2n} \left(\frac{r}{a}\right)^{2n} - 1 = 0 .$$

When this series is expanded and the coefficients of powers of r/a set equal to zero individually, one has a series of equations

$$0 = a_0 b_0 - 1$$

$$0 = 2a_2 b_0 + a_0 b_2$$

$$0 = 3a_4 b_0 + 2a_2 b_2 + a_0 b_4 , \text{ etc.}$$

Substituting for b_{2n} in terms of b_0 and solving successive equations yield for the first six a_{2n}

$$a_0 = + 1/b_0$$

$$a_2 = + 1/2 b_0^4$$

$$a_4 = + 5/9 b_0^7$$

$$a_6 = + 55/72 b_0^{10}$$

$$a_8 = + 105/90 b_0^{13}$$

$$a_{10} = + 205/108 b_0^{16} .$$

B-6 Evaluation of b_o by the Boundary Condition.

The unit strain ϵ in terms of the in-plane stresses is

$$\sigma_t - \mu\sigma_r = E\epsilon .$$

The edge $r = a$ of the plate is rigidly clamped. If the plate is not initially strained, $\epsilon = 0$ at $r = a$ and must remain zero because of clamp action. If the plate is initially strained and then clamped at $r = a$, the strain $\epsilon = \epsilon_o$ at $r = a$ and by clamp action must remain ϵ_o . The boundary condition is

$$\sigma_t - \mu\sigma_r = E\epsilon_o \Big|_{r=a} ,$$

$$\epsilon_o = \text{initial strain.}$$

The series form for σ_t/E and σ_r/E at $r = a$ are

$$\sigma_t \Big|_{r=a} = c_1 E \sum_{n=0}^{\infty} (2n+1) b_{2n}$$

$$\sigma_r \Big|_{r=a} = c_1 E \sum_{n=0}^{\infty} b_{2n} .$$

The boundary condition in series form is

$$\sum_{n=0}^{\infty} (2n+1 - \mu) b_{2n} = \epsilon_o / c_1$$

or, expanded,

$$b_o + \frac{3-\mu}{1-\mu} b_2 + \frac{5-\mu}{1-\mu} b_4 + \frac{7-\mu}{1-\mu} b_6 + \dots = \epsilon_o / c_1 (1-\mu)$$

and in terms of b_o

$$b_o - \frac{(3-\mu)}{(1-\mu)} \frac{1}{b_o^2} - \frac{2}{3} \frac{(5-\mu)}{(1-\mu)} \frac{1}{b_o^5} - \frac{13}{18} \frac{(7-\mu)}{(1-\mu)} \frac{1}{b_o^8} - \dots = \epsilon_o / c_1 (1-\mu) .$$

For given material and load this equation can be solved for a numerical value of b_o and the problem is solved.

B-7 Graphical Solution.

A convenient procedure for evaluating b_o from the boundary condition equation and the deflection coefficient $K = \sum_{n=0}^{\infty} a_{2n}$ is a graphical one.

The left-hand side of the boundary condition equation, including terms up to the n -power in b_o , is designated $f_n(b_o)$ so that with sufficiently large n and $b_o > 1$ it is nearly true that

$$f_n(b_o) = \epsilon_o / c_1 (1 - \mu) .$$

Values of b_o were assumed in the range $1 < b_o < 10$ and n was taken as 17. The numerical values of $f_{17}(b_o)$ are plotted in the figure to enable graphical solution of the inverse problem: given an initial strain ϵ_o the quantity $\epsilon_o / c_1 (1 - \mu)$ is computed and the corresponding b_o may be determined graphically.

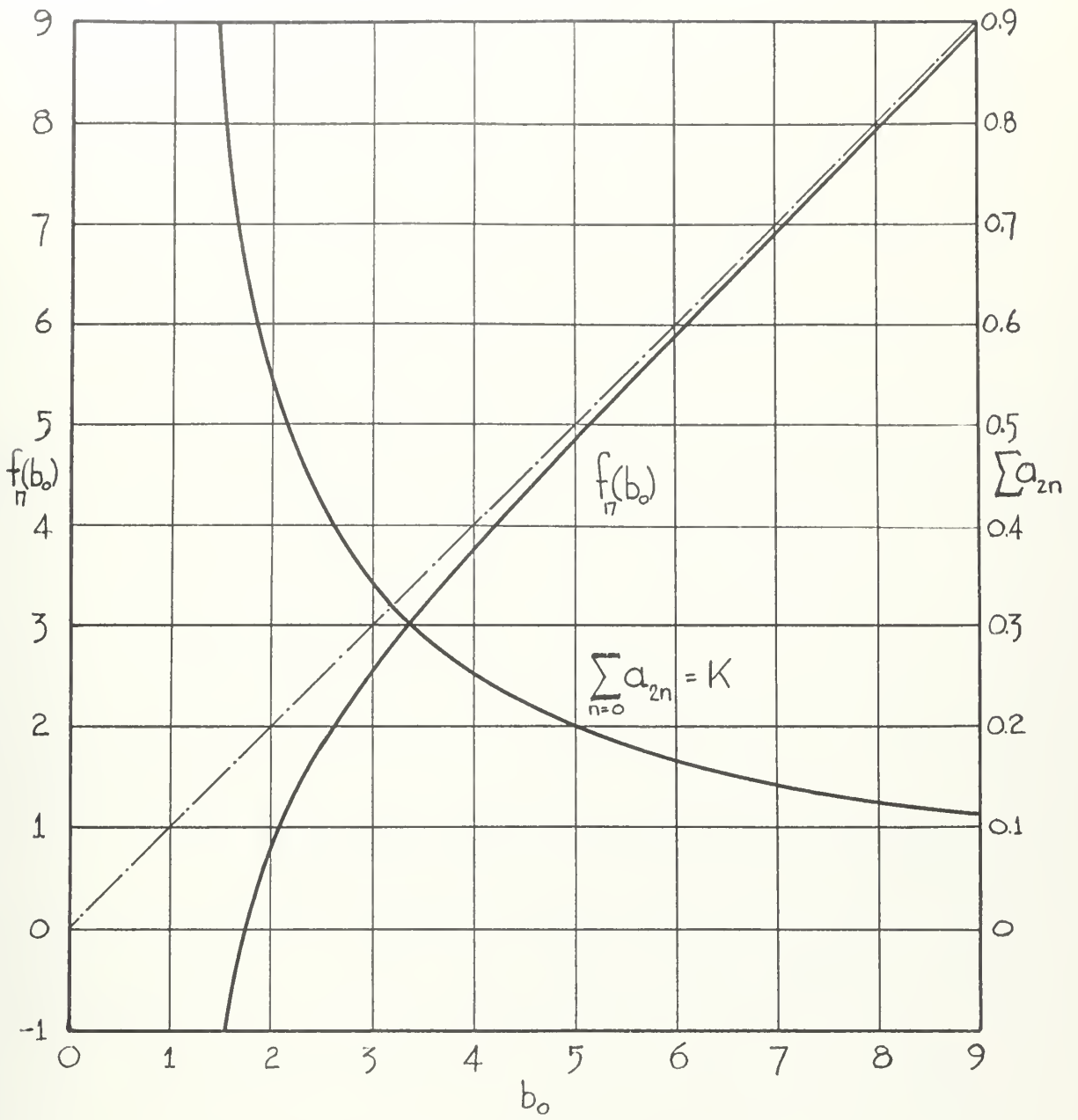
The center deflection is

$$\delta(0) = (ac_2) \sum_{n=0}^{\infty} a_{2n} = K \sqrt[3]{\frac{pa^4}{Et}}$$

where we have introduced K , defined by

$$K = \sum_{n=0}^{\infty} a_{2n} = \frac{1}{b_o} + \frac{1}{2b_o^4} + \frac{5}{9b_o^7} + \frac{55}{72b_o^{10}} + \frac{70}{60b_o^{13}} + \frac{205}{108b_o^{16}} + \dots .$$

This summation has been computed for the assumed values of b_o , $1 < b_o < 10$, using these six terms, and the numerical value of K is presented



THE FUNCTIONS $f_{17}(b_0)$ AND $K(b_0)$

FIGURE 42

graphically. As a matter of convenience, the two figures

$$f_{17}(b_o) \text{ vs } b_o$$

$$\sum_{n=0}^{\infty} a_{2n} \text{ vs } b_o$$

are graphically combined to eliminate b_o and present

$$K \text{ vs } \epsilon_o/c_1(1-\mu) .$$

With this graph, one enters with known load and initial strain to find a value for K and with this the center deflection is

$$\frac{\delta}{t} = K \sqrt[3]{\frac{pa^4}{Et^4}} .$$

B-8 Special Cases.

a. Zero Initial Strain. (The Solution of Hencky).

If the initial strain is zero, this solution becomes that of Hencky. The series expression $f(b_o)$ is equal to zero. The corresponding value of K is evaluated for the root b_o of $f(b_o) = 0$. Our computed value using $f_{17}(b_o)$ differs by less than one percent from Hencky's value $K = 0.662$ and the difference is no doubt entirely due to numerical procedures.

b. Lightly Loaded Plates.

This special case is appropriate for considering the initial pressure sensitivity and for comparison with the zero-initial tension case which predicts an infinite initial-deflection derivative suggestive of an unstable initial position.

As the pressure load approaches zero, c_1 approaches zero, and $f(b_0)$, proportional to $1/c_1$, is increasingly large. The function $f(b_0)$ approaches its asymptote, b_0 :

$$f(b_0) \Big|_{b_0 \text{ large}} = b_0 - \frac{3-\mu}{1-\mu} \frac{1}{b_0^2} - \dots \approx b_0 .$$

For large values of b_0 , the value of K is

$$K = \sum_{n=0}^{\infty} a_{2n} = \frac{1}{b_0} + \frac{1}{2b_0^4} + \dots \approx \frac{1}{b_0}$$

$$\approx \frac{1}{f(b_0)} .$$

One may substitute for $f(b_0)$ its equivalent in terms of the initial strain, $\epsilon_0/c_1(1-\mu)$, but it is more revealing to make another substitution as follows.

Under the assumed conditions, b_0 is large and therefore all b_{2n} for $n > 0$ are negligible. Therefore, at the edge $r = a$, $\sigma_r = \sigma_t$ and the edge boundary condition may be written

$$\sigma_t - \mu\sigma_r = \sigma(1-\mu) = E\epsilon_0 \Big|_{r=a} .$$

The initial tension $T = \sigma t$, so that one may use for $f(b_0)$ an expression in terms of T : $f(b_0) = \epsilon_0/c_1(1-\mu) = T/c_1 t E$. With this the center deflection coefficient K is $c_1 t E/T$ and the center deflection reduces to

$$\delta(0) = \frac{pa^2}{4T}$$

which is exactly the membrane solution.

Thus the initial deflection of a lightly loaded plate is controlled by the initial tension. It is not considered appropriate to assume zero initial tension for a stable diaphragm of vanishing bending stiffness; the initial deflection derivative is bounded and equivalent to the membrane result $a^2/4T$.

c. Comparison with the Membrane Solution.

The membrane solution may be recovered here by observing that a particular solution to the equation expressing horizontal equilibrium is

$$\sigma_r = \sigma_t = \sigma = \text{constant} = T/t .$$

The equation of compatibility will be satisfied only for infinitesimal deflection in this case, so that $(d\delta/dr)^2$ is negligible. The vertical equilibrium equation is equivalent to the membrane equation,

$$\nabla^2 \delta = - p/T .$$

In terms of our series solution, b_{2n} are zero for $n > 0$ and the result is given in section b above.

The complete series solution given here is not limited to infinitesimal deflection and shows that as the pressure load (deflection) increases, c_1 increases, $f(b_0)$ decreases and the deflection tends to that of Hencky [$f(b_0) = 0$] as the developed stresses become increasingly large compared with the initial stress.

APPENDIX C

The Attenuation of Oscillatory Pressure Fluctuations Travelling
in a Viscous Fluid Through a Connecting Tube to an Instrument
Cavity with Resilient Walls.

- C-1 Description.
- C-2 The Navier-Stokes (Momentum) Equations.
- C-3 The Equation of Continuity.
- C-4 The Equation of State and Effect on Tube
Wall Elasticity.
- C-5 Boundary Conditions and the Effect of
Diaphragm Elasticity.
- C-6 Solution of the Governing Equation.
- C-7 The Short Tube Approximations.
- C-8 Approximation Valid for Small Values of $\omega^2 a / \nu$.
- C-9 Approximation Valid for Moderate Damping Values.
- C-10 Approximation Valid for Small Damping Values.

APPENDIX C

The Attenuation of Oscillatory Pressure Fluctuations Travelling
in a Viscous Fluid Through a Connecting Tube to an Instrument
Cavity with Resilient Walls.

C-1 Description.

The required diameter of a diaphragm-type pressure gauge may be controlled by the sensitivity desired. This diameter may exceed the allowable diameter on the surface where pressures are to be measured. The apparent diameter can be reduced by communicating the pressure through a port of allowable diameter to a cavity whose one wall is the required diaphragm.

The apparent diaphragm diameter is reduced, but there may be a penalty in degradation of the dynamic response of the system tube-cavity-diaphragm compared to that of the diaphragm alone.

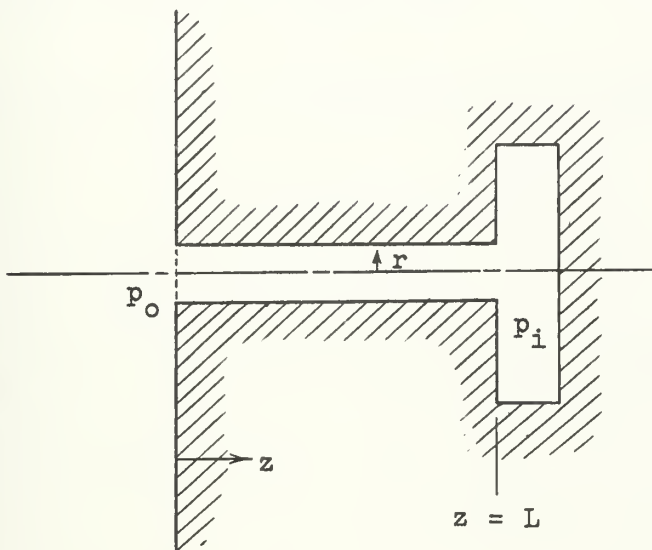
This appendix reports an analysis of the attenuation of oscillatory pressure fluctuations travelling in a viscous fluid from an entry port through a connecting tube to an instrument cavity. The instrument cavity is expected to have a resilient wall, the diaphragm of a pressure gauge in our application. Related work is known in the literature but is usually concerned with long tube lengths, compressible gases, or does not include the effect of a resilient wall.

The present analysis concentrates on the arrangements expected in measurements of small pressure fluctuations on the surface of small bodies oscillating in a fluid. The slight compressibility of a fluid and the high flexibility of a sensitive diaphragm contrast

with the more usual situation of gas compressibility and relative cavity rigidity reported in acoustics. Diaphragm elasticity plays an important role. It may in fact be the limiting factor in dynamic measurements of this type.

C-2 The Momentum (Navier-Stokes) Equation Yields Particle Displacement and Volume Rate of Flow.

The momentum equation for a fluid element in the tube is the Navier-Stokes equation for the axial velocity component w . We assume radial symmetry.



$$\frac{\partial w}{\partial t} + w \frac{\partial w}{\partial z} = - \frac{g}{\rho} \frac{\partial p}{\partial z} + \nu \left(\frac{\partial^2 w}{\partial r^2} + \frac{1}{r} \frac{\partial w}{\partial r} + \frac{\partial^2 w}{\partial z^2} \right) .$$

Assume that $\partial w / \partial z$ is negligible compared to $\partial w / \partial t$ and $\partial w / \partial r$.

Assume also that the particle displacement is harmonic in time. Then

$$\delta(r, t) = \delta(r) e^{j\omega t} ,$$

$$w(r) e^{j\omega t} = \frac{\partial \delta}{\partial t} = j\omega \delta(r) e^{j\omega t} ,$$

$$- \frac{\partial w}{\partial t} + \nu \left(\frac{\partial^2 w}{\partial r^2} + \frac{1}{r} \frac{\partial w}{\partial r} \right) = \frac{g}{\rho} \frac{\partial p}{\partial z} ,$$

$$\frac{d^2 \delta}{dr^2} + \frac{1}{r} \frac{d\delta}{dr} + \frac{\omega \delta}{j\nu} = \frac{g}{j\omega \mu} \frac{\partial p}{\partial z} .$$

A particular solution of this equation, assuming p not a function of r , is

$$\delta = \left(\frac{\partial p}{\partial z} \right) g / \omega^2 \rho .$$

A homogeneous solution of this equation, finite at $r = 0$, is

$$\delta = J_0(kr)$$

$$k^2 = - j\omega / \nu .$$

Combining these solutions with a constant c ,

$$\delta = \left(\partial p / \partial z \right) g / \omega^2 \rho + c J_0(kr) .$$

The constant is evaluated by the no-slip condition that $\delta = 0$ for $r = a$.

$$\delta = \frac{\left(\frac{\partial p}{\partial z} \right) g}{\omega^2 \rho} \left[1 - \frac{J_0(kr)}{J_0(ka)} \right] .$$

It is noted that the radial derivative of particle displacement, $\partial\delta/\partial r$, vanishes at the centerline $r = 0$ as it should.

The volume rate of flow through a given section is found by integrating the area-velocity product over the tube radius at that section.

$$\begin{aligned} dV &= \frac{\partial\delta}{\partial t} 2\pi r dr = \frac{j2\pi g(\partial p/\partial z)}{\rho\omega} \left[r dr - \frac{J_0(kr) r dr}{J_0(ka)} \right] \\ V &= \int_0^a dV \\ &= \frac{j2\pi g(\partial p/\partial z)}{\rho\omega} \left[\frac{a^2}{2} - \frac{1}{k^2 J_0(ka)} \int_0^{ka} kr J_0(kr) d(kr) \right] \\ &= \frac{j\pi a^2 g(\partial p/\partial z)}{\rho\omega} \left[1 - \frac{2J_1(ka)}{kaJ_0(ka)} \right] . \end{aligned}$$

For simplicity we use notation

$$J = 2J_1(ka)/kaJ_0(ka)$$

$$V = - \beta(\partial p/\partial z)$$

$$\beta = \pi a^2 g(1-J)/j\rho\omega .$$

It may be observed that for small (ka)

$$1 - J \rightarrow (ka)^2/8 .$$

Substituting this in the expression for the volume rate of flow,

$$V = - \pi a^4 g(\partial p/\partial z)/8\mu ,$$

the known volume-rate of Poiseuille pipe flow in which inertia forces are negligible. That is, for ω/ν vanishingly small this solution recovers the Poiseuille solution.

C-3 The Equation of Continuity.

The equation of continuity of fluid in a thin section of a tube of area A and flowing with radial symmetry is

$$\frac{\partial \rho A}{\partial t} + \frac{\partial (\rho w A)}{\partial z} = 0 .$$

We will substitute the previous result

$$V = wA = - \beta (\partial p / \partial z)$$

and change variables from the actual local pressure p to the fractional overpressure φ . The overpressure φ , or pressure signal, is normalized with respect to the amplitude p_0 of the sinusoidal pressure assumed to exist at the tube entry. The forcing pressure p_0 is assumed to be independent of r .

$$\varphi = (p - p_0) / p_0$$

$$\frac{\partial p}{\partial z} = p_0 \frac{\partial \varphi}{\partial z}$$

$$\frac{\partial \rho A}{\partial t} + \frac{\partial}{\partial z} \left[- \rho \beta p_0 \frac{\partial \varphi}{\partial z} \right] = 0 .$$

C-4 The Equation of State and Effect of Tube Wall Elasticity.

Introduce now the equation of state of the fluid in the tube in the form of a relation $\rho(p)$. For the small pressure fluctuations expected in this work the density-pressure relation may be expressed by means of a constant bulk modulus of compression B_1 of the liquid:

$$\rho = \rho_0 \left(1 + \frac{p - p_0}{B_1} \right) .$$

Analysis from this point concerns nearly incompressible liquids. For

gases, a similar path would be followed but different equations of state are necessary (A. Iberall [1950]).

The elasticity of the tube walls may not be negligible in comparison with the slight compressibility of the liquid. In this case the cross-section area A is a function of pressure and might be written as approximately

$$A = A_o \left(1 + f \frac{p - p_o}{E} \right)$$

where E = Young's Modulus of wall material,

f = a geometric function of wall thickness and nominal form. For a thin-wall circular tube $f = a/t$,

A_o = cross-section area at $p = p_o$.

[For a table of f for ordinary shapes see I.P. Ginsberg, Prikladnaya Gidrogazodinamika, Leningrad University, 1958, p. 106.]

Combining these results to define an apparent bulk modulus in the tube, we find

$$\rho A = \rho_o \left(1 + \frac{p - p_o}{B_1} \right) A_o \left(1 + \frac{f(p - p_o)}{E} \right)$$

$$\cong \rho_o A_o \left(1 + \frac{p - p_o}{B} \right),$$

$$\frac{1}{B} = \frac{1}{B_1} + \frac{f}{E}.$$

Whether this apparent modulus B differs from B_1 is a measure of the effect of tube wall elasticity. Using the above expression for (ρA) , we obtain

$$\frac{\partial \rho A}{\partial t} = \frac{\rho_o A_o p_o}{B} \frac{\partial \varphi}{\partial t}.$$

With this result, the equation of continuity is

$$\frac{\rho_o A_o}{B} \frac{\partial \varphi}{\partial t} - \rho \beta \frac{\partial^2 \varphi}{\partial z^2} = 0 .$$

Here we have required that the product $\rho \beta$ be independent of z . It is noted this product is independent of density, so that we have not assumed density independent of z but we have assumed that the kinematic viscosity is sensibly independent of z .

C-5 Boundary Conditions and the Effect of Diaphragm Elasticity.

The boundary conditions are these.

(i) The pressure fluctuation at the tube entry is specified.

$$\varphi = \varphi_o \varepsilon^{j\omega t} \Big|_{z=0} .$$

(ii) The mass rate of discharge from the tube equals the accession of liquid in the cavity. This augment to the contained fluid is accommodated by elasticity of the diaphragm and compressibility.

The second boundary condition is expressed analytically as follows.

The fluid mass in the cavity is ρV_o so that the mass augment is

$$\rho_o \frac{dV_o}{dt} + V_o \frac{d\rho}{dt} .$$

From the previous relation $\rho(\varphi)$ we derive

$$\frac{d\rho}{dt} = \frac{\rho_o}{B_1} \frac{dp}{dt} .$$

To determine the rate of change of instrument cavity volume we introduce the volume sensitivity, s , of the diaphragm,

$$\frac{dV_o}{dp} = s .$$

The volume sensitivity is geometrically related to the pressure sensitivity σ of the diaphragm, a measure of the change in center deflection per unit change in pressure. For a membrane diaphragm deflecting to a paraboloid of revolution,

$$s = \sigma \pi r^2 / 2 .$$

With the volume sensitivity defined as above, we find

$$\frac{dV_o}{dt} = s \frac{dp}{dt} .$$

The mass influx into the cavity is

$$\frac{V_o \rho_o}{B_1} \frac{dp}{dt} + \rho_o s \frac{dp}{dt} = \frac{\rho_o}{B_1} (V_o + s B_1) \frac{dp}{dt} .$$

The expression $(V_o + s B_1)$ represents an equivalent cavity volume \bar{V} corrected for the resilient diaphragm. The term ρ_o / B_1 is equal to g/c^2 , the squared velocity of acoustic propagation in the volume. With these notations the mass influx

$$\frac{g \bar{V}}{c} \frac{dp}{dt} = j \omega \rho_o \bar{V} / c^2$$

is equated to the mass flux at the end of the tube,

$$\rho V \Big|_{z=L} = - \rho \beta \left[\frac{\partial p}{\partial z} \right]_{z=L} = - \rho \beta p_o \left[\frac{\partial \varphi}{\partial z} \right]_{z=L} .$$

The second boundary condition is

$$\left[\frac{\partial \varphi}{\partial z} \right]_{z=L} = - \frac{j \omega g \bar{V}}{\rho \beta c^2} \varphi = - b \varphi ,$$

where

$$b = j\omega g \bar{V}/\rho\beta c^2 .$$

C-6 The Solution of the Governing Equation.

The differential equation from Section 3, after combining the equations expressing momentum conservation, continuity, and the apparent equation of state, is

$$\frac{\partial^2 \varphi}{\partial z^2} = \frac{A_o \rho_o}{\rho\beta B} \frac{\partial \varphi}{\partial t} .$$

The solution is

$$\varphi = (c_1 \epsilon^{\alpha z} + c_2 \epsilon^{-\alpha z}) \epsilon^{j\omega t}$$

where

$$\alpha^2 = j\omega A_o \rho_o / \rho\beta B .$$

The desired form of the result is φ/φ_o which is

$$\left[\frac{c_1}{c_2} \epsilon^{\alpha z} + \epsilon^{-\alpha z} \right] / \left[\frac{c_1}{c_2} + 1 \right] .$$

The ratio c_1/c_2 is evaluated by means of the boundary condition of continuity at the cavity, $\varphi_z + b\varphi = 0$ at $z = L$, so that

$$\frac{c_1}{c_2} = \frac{(\alpha - b)\epsilon^{-\alpha L}}{(\alpha + b)\epsilon^{+\alpha L}} .$$

Finally, evaluating the pressure-signal ratio at $z = L$,

$$\frac{\varphi_L}{\varphi_o} = \frac{(\alpha L)}{(\alpha L) \cosh(\alpha L) + (bL) \sinh(\alpha L)} .$$

The ratio φ_L/φ_o is the pressure fluctuation in the cavity per unit fluctuation at the tube entry. This ratio is called p_i/p_o in the text. The products αL and bL are as follows.

$$\alpha L = \frac{j\omega L}{c_t} \frac{1}{\sqrt{1-J}}.$$

Here c_t^2 , the apparent sound velocity in the tube, is ρ_o/Bg , determined by the apparent modulus B rather than the fluid modulus alone as in the cavity. The ratio ω/c_t is the fluctuation wavelength in the tube, i.e.

$$\alpha L = j 2\pi \frac{L}{\lambda} \frac{1}{\sqrt{1-J}}.$$

Similarly, for bL we have

$$bL = -\omega^2 \frac{\bar{V}L}{c_A^2} \frac{1}{1-J}.$$

The quantity $c_A^2/\bar{V}L$ is the square of a characteristic frequency,

$$\omega_n^2 = c_A^2/\bar{V}L,$$

so that

$$bL = \frac{\omega^2}{\omega_n^2} \frac{1}{1-J}.$$

It should be noted that αL and bL are, in general, not real variables, as J is the ratio of a complex quantity and Bessel functions of a complex argument.

The natural frequency ω_n is lowered by increasing diaphragm sensitivity through the effective volume \bar{V} .

C-7 The Short Tube Approximation.

If the tube length L is a small part of the pressure fluctuation wavelength in the tube, the product αL is small and

$$\frac{p_i}{p_o} = \frac{\alpha L}{(\alpha L) \cosh(\alpha L) + (bL) \sinh(\alpha L)}$$

$$\approx \frac{1}{1 + bL} = \frac{1}{1 - \left(\frac{\omega}{\omega_n}\right)^2 \frac{1}{1 - J}} .$$

This is the form discussed in the text.

C-8 Approximation Valid for Small Values of $\omega a^2/\nu$.

The value of

$$J = \frac{2}{ka} \frac{J_1(ka)}{J_0(ka)}$$

for small values of the argument

$$(ka)^2 = -j\omega a^2/\nu$$

is approximately

$$J \approx 1 + \frac{(ka)^2}{8}$$

so that

$$\frac{1}{1 - J} \approx -\frac{j8\nu}{\omega a^2} .$$

The response ratio for this case is

$$\frac{p_i}{p_o} = \frac{1}{1 + j\omega\tau} , \quad \tau = 8\nu/\omega_n^2 a^2 .$$

This result is identical with the one obtained by assuming uniform Poiseuille flow and constant pressure gradient. If the Poiseuille flow mass rate,

$$Q = \rho V = - \frac{\pi a^4 g}{8} \left(\frac{\partial p}{\partial z} \right) ,$$

with constant pressure gradient,

$$\frac{\partial p}{\partial z} = \frac{p_i - p_o}{L} ,$$

is equated to the instrument-cavity mass rate

$$\frac{g\bar{V}}{c^2} \frac{dp_i}{dt} ,$$

the governing ordinary differential equation is

$$\tau \frac{dp_i}{dt} + p_i = p_o(t) .$$

Assuming periodic flow yields the result given above.

The time constant τ is increased by increasing diaphragm sensitivity or decreasing the entry port diameter, for

$$\tau = 8\sqrt{L\bar{V}}/\pi a^4 c^2 .$$

C-9 Approximation Valid for Moderate Damping Values.

The identity

$$\frac{1}{1 - J} = - \frac{J_o(ka)}{J_2(ka)}$$

is, for moderate values of the argument, approximately

$$\frac{4}{3} - j \frac{8}{(\omega a^2/\nu)} .$$

The corresponding response ratio is

$$\frac{p_i}{p_o} = \frac{1}{(1-u^2) + ju^2\zeta} ,$$

where we have used the notation

$$u^2 = \frac{4\omega^2}{3\omega_n^2} , \quad \zeta = \frac{\sqrt{3}}{4} \tau .$$

This form is motivated by analogy to that for the response of a moderately damped spring-mass system. This system responds with 90 degree phase lag at a dimensionless frequency $u = 1.0$ with an amplitude ratio $1/2\zeta$.

This form is also analogous to the classical Helmholtz Resonator results, but the present more-detailed analysis predicts a lower resonant frequency of 90 degree phase lag and generally greater phase lag at frequencies near resonance.

To clarify the differences in the results, compare the above with the following. We recall from section 8 the ordinary differential equation

$$\tau \frac{dp_i}{dt} + p_i = p_o .$$

Multiplying by the tube area makes more evident that this is a force balance of pressure force and Poiseuille tube-wall friction considered to be constant along the tube length:

$$A\tau \frac{dp_i}{dt} = 2\pi a \cdot L \cdot \frac{4\eta Q}{\pi a^3 g} = A(p_o - p_i) ,$$

where $(4\eta Q/\pi a^3 g)$ is recognized as the constant Poiseuille-flow tube-wall friction per unit area. Add to this force balance an inertia term

$$\frac{L}{g} \frac{dQ}{dt} = \frac{L\bar{V}}{c^2} \frac{d^2 p_i}{dt^2}$$

and the force balance may be written

$$\frac{d^2 p_i}{dt^2} + \frac{c^2 A}{L\bar{V}} \tau \frac{dp_i}{dt} + \frac{c^2 A}{L\bar{V}} p_i = \frac{c^2 A}{L\bar{V}} p_o .$$

The steady-state solution, assuming periodic pressure fluctuations of frequency ω , is

$$\frac{p_i}{p_o} = \frac{1}{1 - \left(\frac{\omega}{\omega_n}\right)^2 + j2 \frac{\omega}{\omega_n}} ,$$

where

$$\omega_n^2 = \frac{c^2 A}{L\bar{V}}$$

as before and

$$\zeta_o = \omega_n^2 \tau/2 = 4\eta/a^2 \omega_n .$$

This is the result given by Rayleigh and generally observed to predict resonant frequencies that are higher than measured values (M. Colby [1939] p. 220; J. Patterson [1952] p. 9).

The more detailed analysis, admitting longitudinal variation of pressure gradient and a more general radial velocity profile, predicts acoustic resonance at a frequency about 14 percent lower. This further lowers the expected range of frequencies free of acoustic effects. It is observed that in either case the effective instrument cavity volume is used in calculating ω_n .

C-10 Approximation Valid for Cases with Small Damping.

The identity

$$\frac{1}{1 - J} = - \frac{J_0(ka)}{J_2(ka)}$$

tends to unity for large values of the argument. The response ratio is therefore

$$\frac{p_i}{p_o} = \frac{1}{1 - \frac{\omega^2}{\omega_n^2}} .$$

The value of this approximation lies in the fact that it emphasizes the tendency toward undamped acoustic resonance.



THE SHEAR'S
PRESSBOARD
ESTD 1912

COVER
No. R129

MANUFACTURED BY
THE SHEAR MANUFACTURING COMPANY, NEW YORK, N.Y.

thesP748

Pressure distributions, added-mass, and



3 2768 001 92342 8

DUDLEY KNOX LIBRARY